Title

Substrate binding, heme accessibility, and active site residues control heme reactivity in horseradish peroxidase

Author

Newmyer, Sherri L.

Publication Date

1996

Peer reviewed|Thesis/dissertation

Substrate Binding, Heme Accessibility, and Active Site Residues Control Heme Reactivity in Horseradish Peroxidase

by

Sherri L. Newmyer

DISSERTATION

Submitted in partial satisfaction of the requirements for the degree of

DOCTOR OF PHILOSOPHY

in

Pharmaceutical Chemistry

in the

GRADUATE DIVISION

of the

UNIVERSITY OF CALIFORNIA

San Francisco

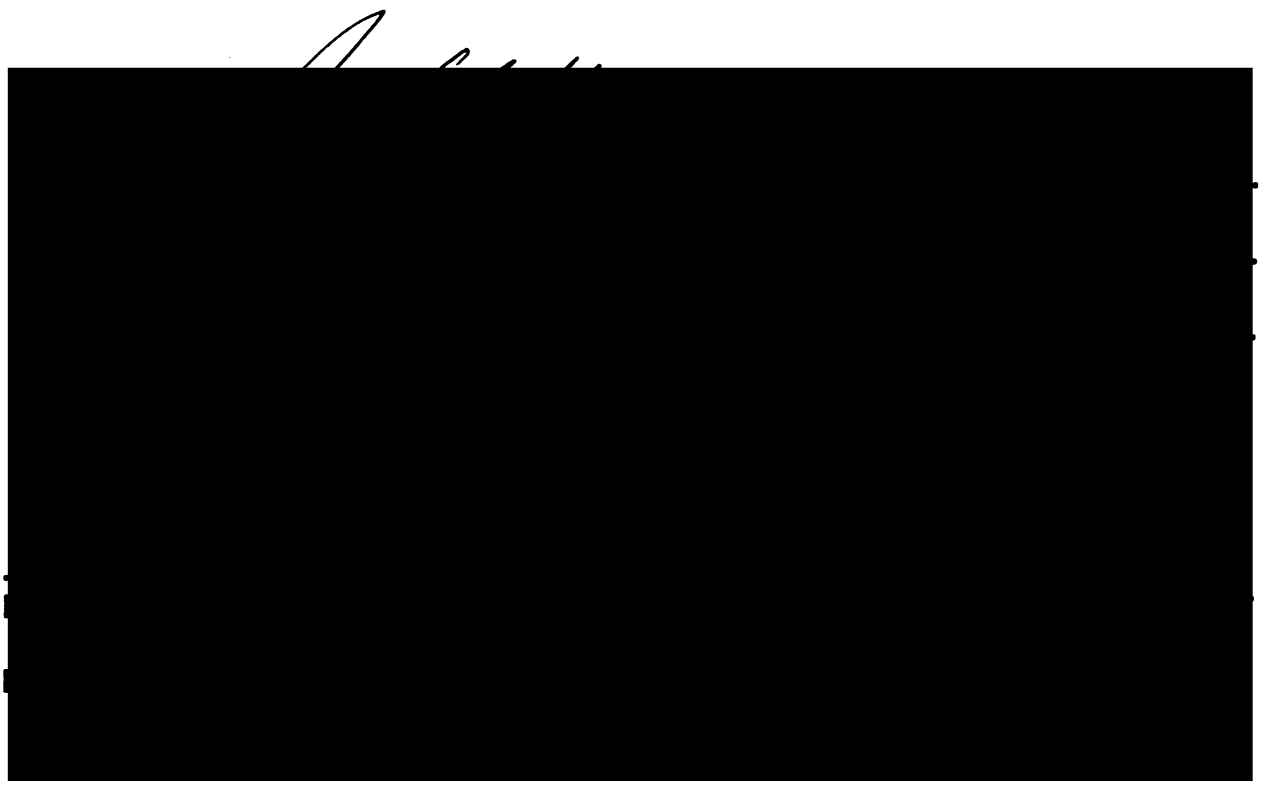

To my Mother,

for her encouragement, love, and friendship

Acknowledgments

I am glad to have this opportunity to acknowledge the people who have helped me to reach this stage of my career. I would like to thank Dr. Ralph Yount at Washington State University who sparked my interest in enzymology. Thanks to him, I managed to find my way to the University of California, San Franscisco, where I have been surrounded by a diverse group of talented people who have helped in cultivating my scientific way of thinking. I'd especially like to thank Dr. Charles Craik and Dr. George Kenyon for their editing of this manuscript and for their helpful comments throughout my graduate studies. I will miss my coworkers--both old and new--in the POM lab who contributed to my project in immeasurable ways and who provided a great research environment. Special thanks are given to Christa Hartmann, for initially expressing HRP which allowed me to do my mutagenesis studies; Robert Harris, who was like a big brother during those initial graduate years; and Angela Wilks, for her friendship and endless support. I would also like to thank my friends at UCSF--Eric Pettersen, Chris and Melanie Schafmeister, and Marcelo Guitierrez. Life in San Francisco was never dull with these guys around. My family deserves a big thank you for their support and encouragement. I would especially like to thank my mother and sister, whose friendship I will always treasure no matter how absorbed I am in my work. I should also probably mention my sweetheart, Daniel. One of the more momentous events of my graduate career was falling in love with him. Fortunately, I get to take him with me. Lastly and most sincerely, I thank my advisor, Dr. Paul Ortiz de Montellano, for his advice and for my graduate training.

Substrate Binding, Heme Accessibility, and Active Site Residues Control Heme Reactivity in Horseradish Peroxidase

Sherri L. Newmyer

Abstract

Conserved heme pocket residues distinguish classes of hemoproteins and are postulated to promote hemoprotein function by modulating heme reactivity. Horseradish peroxidase (HRP), a prototypic and well-characterized peroxidase, was employed in the following studies to characterize the factors that control peroxidase heme reactivity.

To investigate HRP-catalyzed substrate oxidation, the oxidation of iodide was compared to that of guaiacol and thioanisole, substrates which are oxidized by the δ-*meso* heme edge and the Compound I ferryl oxygen, respectively. Iodide, like guaiacol, is oxidized by electron transfer to the δ-*meso* heme edge. Binding studies reveal that iodide, guaiacol, and thioanisole are bound at different sites within HRP. These studies suggest that the protein differentially binds substrates in a manner that favors oxidation by either the heme edge or the ferryl oxygen of Compound I.

The conserved distal peroxidase residues of HRP--His 42, Phe 41, and Arg 38--represent the primary barrier that hinders substrate access to the heme iron. F41A-, H42A-, and H42V-HRP were therefore generated in an attempt to improve accessibility to the heme iron. These mutants display significantly improved rates of thioanisole sulfoxidation and styrene epoxidation, reactions which are mediated by transfer of the Compound I ferryl oxygen to the substrate. The putative general acid/base catalytic role of His 42 was also examined. The distal histidine mutants exhibit weak peroxidase activity that is limited by slow Compound I formation. Exogenous imidazole binds to the distal cavity created by the H42A mutation and rescues H42A HRP Compound I formation by deprotonating peroxide.

The proximal histidine was mutated to an alanine residue to investigate its role in peroxidase catalysis. The resulting H170A HRP mutant exhibits a decreased rate of Compound I formation. Exogenous imidazole coordinates to the heme iron on the proximal heme face and partially restores native-like Compound I formation. This suggests that heterolytic cleavage of the dioxygen bond of the ferric peroxide complex is promoted by the electron density that is donated to the heme iron by the proximal imidazole ligand. H170A HRP is predominantly six coordinate in the absence and presence of imidazole, suggesting that a critical role of the tethered histidine ligand is to maintain the heme in a five-coordinate state.

These mutagenesis studies demonstrate that peroxidase heme reactivity is predominantly determined by (a) the inaccessibility of the heme iron to substrates and (b) the invariant distal and proximal histidines, both of which promote rapid Compound I formation.

Table of Contents

List of Tables

List of Figures

List of Abbreviations

ABTS	2,2'-Azinobis(3-ethylbenzothiazoline-6-sulfonic Acid
AcOH	Acetic Acid
ARP	*Arthromyces ramosus* Peroxidase
AXP	Pea Ascorbate Peroxidase
BRC	Biomolecular Research Center, UCSF
BSA	Bovine Serum Albumin
CCP	Cytochrome c Peroxidase
DMSO	Dimethylsulfoxide
DNA	Deoxyribonucleic Acid
E. coli	*Escherichia coli*
EDTA	Ethylenediamine Tetraacetic Acid
EPR	Electron Paramagnetic Resonance
ESR	Electron Spin Resonance
EXAFS	Extended Absorption X-ray Fine Structure
Glc	Glucose
GlcNAc	N-Acetylglucose
HPLC	High Performance Liquid Chromatography
HRP	Horseradish Peroxidase
Imid	Imidazole
LIP	Lignin Peroxidase
LPO	Lactoperoxidase
Man	Mannose
Mb	Myoglobin
mCPBA	*Meta*-chloroperoxybenzoic Acid

MeOH	Methanol
MnP	Manganese Peroxidase
MOI	Multiplicity of Infection
MPO	Myeloperoxidase
Ni(II)NTA	Nickel(II) Nitrilotriacetic Acid
NMR	Nuclear magnetic Resonance
P450	Cytochrome P450
PCR	Polymerase Chain Reaction
PeP	Peanut Peroxidase
rWT HRP	Recombinant Wild-Type Horseradish Peroxidase
Sf9	*Spodoptera frugiperda*
T. ni	*Trichoplusia ni*

Chapter 1: Introduction

The peroxidases are an intriguing class of hemoproteins which catalyze the peroxide-mediated oxidation of a variety of substrates, including phenols, anilines, aromatic amines, and halides. Members of this class include proteins of varying origins: bacterial, fungal, plant, and animal (Table 1.1). The fungal, and plant peroxidases are

Table 1.1: Peroxidases representative of fungal, plant, and mammalian origins.

Genetic Origin	Peroxidase	Source
Fungal	Cytochrome c Peroxidase (CCP)[a]	yeast mitochondria
	Lignin Peroxidase (LIP)[b]	*Phanerochaete chrysosporium*
	Arthromyces Ramosus Peroxidase (ARP)[c]	*Arthromyces ramosus*
Plant	Pea Ascorbate Peroxidase (AXP)[d]	pea chloroplast and cytosol
	Peanut Peroxidase (PeP)[e]	peanut
	Horseradish peroxidase (HRP)[f]	horseradish
Mammalian	Myeloperoxidase (MPO)[g]	polymorphous leukocytes
	Lactoperoxidase (LPO)[h]	bovine milk

[a](Bosshard *et al.*, 1991), [b](Gold *et al.*, 1989), [c](Kunishima *et al.*, 1994), [d](Mittler and Zilinskas, 1991), [e](van Huystee, 1991), [f](Dunford, 1991), [g](Klebanoff, 1991), [h](Thomas *et al.*, 1991).

similar in size. HRP and CCP are monomeric proteins of 42 kDa and 35 kDa molecular weight, respectively (Dunford, 1991; Bosshard *et al.*, 1991). Based on sequence similarity, these peroxidases are grouped into a superfamily of three classes (Welinder,

1992a). Class I consists of peroxidases of prokaryotic origins, including cytochrome c and pea ascorbate peroxidases which are respectively found in mitochondria and chloroplasts. Class II encompasses extracellular fungal peroxidases like LIP and ARP. Class III includes the plant peroxidases, which are also secreted. HRP and PeP are representatives of the class III peroxidase and are ~50% identical with one another (Buffard *et al.*, 1990). Both the class II and class III sequences encode an N terminal secretion leader sequence. Collectively, these three classes of peroxidases display nine invariant and 21 nearly invariant residues (Welinder, 1992a). The mammalian peroxidases are larger and often more complex proteins. LPO is a 78 kDa monomeric protein (Thomas *et al.*, 1991), and MPO is a 150 kDa tetrameric protein (Johnson and Nauseef, 1991). Genetically the mammalian peroxidases are more distantly related, and consequently, are classified as a separate peroxidase family. The mammalian peroxidases display ~45-70% sequence identity with each another (Zeng and Fenna, 1992).

Peroxidase substrates The function of these peroxidases is equally broad and includes the scavenging of peroxide, the biosynthesis of plant cell wall components, the metabolism of hormones, and a cytotoxic role against invading pathogens (Dalton, 1991; Fry, 1983 and 1986; Campa, 1991; Klebanoff, 1991). Classic peroxidase substrates are aromatic molecules, including anilines and phenols. In the oxidation of these substrates, one electron is abstracted and the resulting radical species usually enters into nonenzymatic recombination and polymerization reactions. The plant peroxidases, including HRP, oxidize these molecules with high specific activity and have been implicated in crosslinking cell wall components which are chemically similar (Fry 1983; Fry 1986). For example, crosslinking may occur through the oxidation of ferulate, which is a component of the cell wall matrix and is oxidized by HRP with high specific activity (Figure 1.1). HRP has also been postulated to function in metabolizing plant hormones (Campa, 1991). HRP has been

shown to oxidize indole-3-acetic acid, a plant hormone that stimulates cell growth. Plant peroxidases have also been proposed to oxidize 1-aminocyclopropane-1-carboxylic acid in

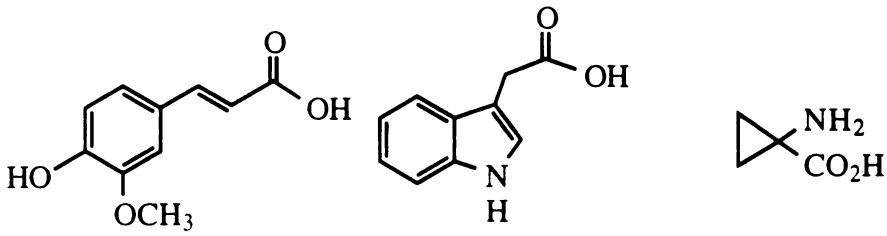

Ferulic acid | Indole-3-acetic acid | 1-Aminocyclopropane-1-carboxylic acid

Figure 1.1: Proposed physiological substrates for HRP.

the biosynthesis of ethylene, a hormone involved in plant growth and development. These molecules and a wide range of aromatic compounds are oxidized by HRP with high specific activity. This promiscuous behavior is characteristic of the plant peroxidases.

The physiological role of the mammalian peroxidases is thought to involve the oxidation of chloride and thiocyanate; however, these enzymes can also oxidize classic peroxidase substrates (Hurst, 1991; Thomas *et al.*, 1991). Myeloperoxidase functions in leukocytes, oxidizing Cl^- to hypochlorous acid (HOCl). This reactive molecule is proposed to act as an antimicrobial agent. Fungal and plant peroxidases can also oxidize halides, but the reduction potential for some peroxidases often limits their oxidative abilities. For example, HRP is only able to oxidize I^- and Br^- (Roman and Dunford, 1972; Ashley and Griffin, 1981).

Classic peroxidase cycle The classic peroxidase cycle involves the three irreversible steps illustrated below (Figure 1.2). The ferric resting state enzyme is oxidized by hydroperoxides, including hydrogen-, alkyl-, and acyl-hydroperoxides, to generate the two electron-oxidized Compound I species. In the formation of Compound I, one electron is taken from the iron, oxidizing Fe^{III} to Fe^{IV} (Moss *et al.*, 1969), and the second electron is

typically taken from the porphyrin, generating a porphyrin cation radical (Dolphin et al., 1974). One peroxide-derived oxygen atom is retained by the Compound I species in the form of a ferryl oxygen, Fe^{IV}=O (Schonbaum and Lo, 1972; Adediran and Dunford, 1983). In the Compound I species of CCP, in lieu of a porphyrin radical cation, one oxidative equivalent is associated with the protein in the form of a protein radical (Yonetani,

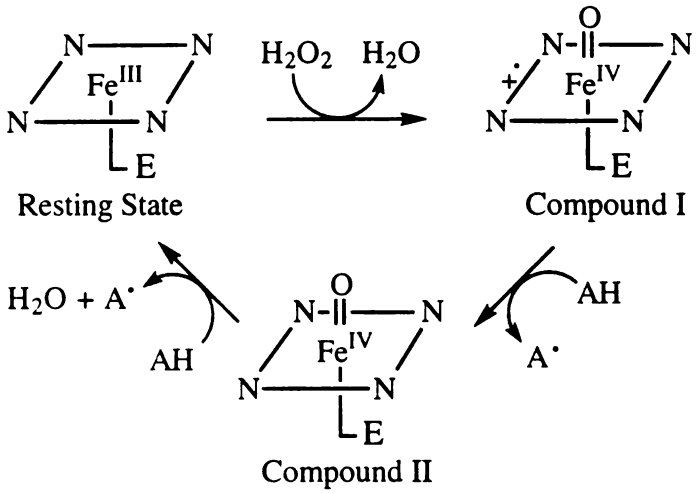

Figure 1.2: A schematic representation of the peroxidase cycle. The heme is depicted by a square of nitrogens surrounding the iron center, and the structure (+·) denotes the porphyrin radical cation species of Compound I.

1976). A combination of ENDOR spectroscopy and CCP mutagenesis studies assigned Trp 191 as the site of the radical (Sivaraja *et al.*, 1989). More recently the anomalous EPR signal exhibited by the protein radical was linked to coupling between the oxyferryl moiety $(Fe{=}O)^{2+}$ and the tryptophan radical of CCP Compound I (Houseman *et al.*, 1993). Both Compound I species are reduced back to the resting state via two sequential electron abstraction steps. The first electron neutralizes the porphyrin radical cation (or protein radical), reducing Compound I to a one electron-oxidized Compound II species. The second electron reduces the iron of Compound II, regenerating the resting state with the concomitant loss of the ferryl oxygen as a water molecule.

Peroxidase history Peroxidase activity was first described in 1810 when the field of enzymology was relatively young. In this study, blue coloring was obtained when plant extracts, including that of horseradish, were treated with peroxide and resin from the guaiacum tree. Early HRP studies were complicated by the existence of multiple peroxidase isoforms which are now known to be characteristic of peroxidase expression in plants. Thirty peroxidase isoforms have been isolated from horseradish (Welinder, 1985). Some of these forms merely represent differences in glycosylation; however, others represent unique gene products. Nine novel peroxidase sequences, displaying 50-95% identity with each other, were obtained from isolated horseradish genes and gene products (Welinder, 1992b). The purpose of expressing multiple isozymes in the plant is not known; however, different isozymes have been found to display varying substrate specificity and varying cellular distribution (Ishida *et al.*, 1985). This suggests that the isozymes may have unique functions. HRP isozyme c is the most abundant and well-characterized peroxidase isozyme in horseradish. For simplicity, the discussion of HRP that follows will only regard this isozyme.

The early isolation of HRP, along with the abundant availability of the protein provided by the plant, has facilitated a long history of HRP studies (Bach and Chodat, 1903). Numerous physico-chemical studies have characterized the electronic states of the resting state, Compound I, and Compound II species of HRP. These species are spectrally distinct, allowing the kinetics for each step of the peroxidase cycle to be advantageously investigated. These studies have contributed significantly to our present understanding of peroxidase and general hemoprotein catalysis.

More recently, the solution of the CCP crystal structure has vastly expanded our understanding of peroxidase catalysis by identifying active site residues (Poulos *et al.*, 1980; Finzel *et al.*, 1984). Two helices, labeled B & F, were found to sandwich the heme and form the majority of the contacts between the protein and the heme molecule. The

sequences corresponding to these helices represent the two most conserved sequences among the bacterial, fungal, and plant peroxidases (Welinder, 1992a). For this reason, the CCP crystal structure has been used widely as a structural peroxidase model. The recently obtained crystal structures of representatives of the fungal and plant peroxidases, LIP (Piontek *et al.*, 1993; Poulos *et al.*, 1993), ARP (Kunishima *et al.*, 1994), MnP (Sundaramoorthy *et al.*, 1994) and PeP (Poulos, unpublished result), show the C_α backbones of these proteins superimpose upon that of the CCP structure (Figure 1.3). Thus it appears that the overall protein fold has been conserved throughout these species, and we expect all the representative peroxidases to display similar tertiary structures. This information has been used to build a 3-D structure model of HRP (Loew *et al.*, 1995).

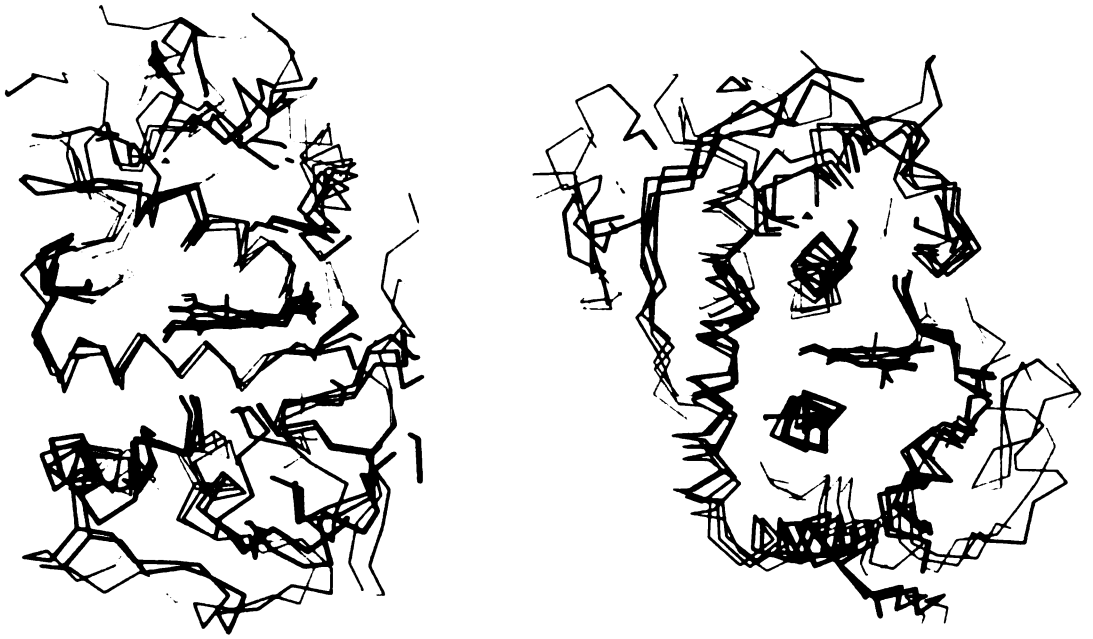

Figure 1.3: Crystallographic structures of CCP, ARP, LIP, and PeP. The C_α backbones of these structures are overlaid with one another to show the conserved tertiary fold among the bacterial, fungal, and plant peroxidases. The illustrations show a cut away version of the structure to reveal the distal B (top) and proximal F (bottom) helices which sandwich the heme. These structures are oriented so that the δ-*meso*- (left) and α-*meso*-heme edges (right) are directed out of the page.

HRP versus CCP HRP and CCP represent the best characterized peroxidases; however, CCP significantly deviates from typical peroxidases in exhibiting an aberrant Compound I species and in preferentially oxidizing cytochrome c, a 12 kDa protein that differs significantly from classic aromatic substrates. As stated earlier, a protein radical is observed in the Compound I species of CCP, instead of a porphyrin radical cation (Yonetani *et al.*, 1966). It is speculated that within CCP the stabilization of one oxidizing equivalent on Trp 191 is attributed to the positioning of this oxidizable residue in the vicinity of the heme (Figure 1.4). In support of this theory, mutagenesis of Trp 191 to an alanine affords a Compound I species containing a transient porphyrin radical cation (Miller *et al.*, 1995a). Even though the half life of this species is short (14 ms), it is relatively

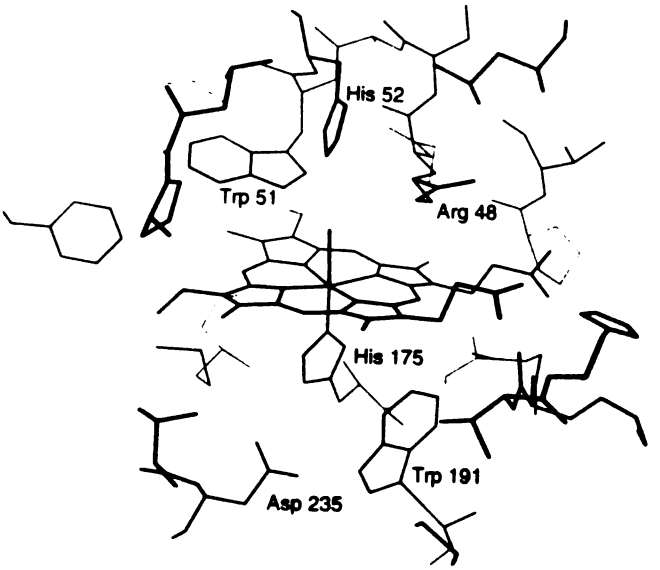

Figure 1.4: Heme pocket of CCP as revealed by its crystal structure. The proximal (Trp 191) and distal (Trp 51) residues that are unique to the class I peroxidases are labeled.

stable when considering that a porphyrin radical cation has never been observed with the native enzyme. The oxidative equivalent associated with the porphyrin in W191A CCP is subsequently transferred to the protein in the form of a protein radical, demonstrating that

removal of Trp 191 only partially stabilizes the porphyrin radical cation. The latter electron transfer to the protein may be mediated by Trp 51, an additional tryptophan that is found adjacent to the heme and that is unique to CCP (Figure 1.4). The presence of an oxidizable residue does not guarantee that a protein radical will be observed in the Compound I species. This is supported by the finding that AXP has a porphyrin radical cation Compound I species despite having a tryptophan positioned in a similar manner to Trp 191 in CCP (Patterson *et al.*, 1995). The proximal tryptophan in AXP is postulated to be difficult to oxidize due to the presence of a neighboring cation (presumably K^+) (Patterson and Poulos, 1995). Thus, it appears that the environment of the oxidizable residue contributes to the ability of the residue to carry an oxidative equivalent. In HRP, the reverse experiment was performed, positioning an oxidizable residue proximal to the heme (Miller *et al.*, 1995b). Phe 172, located near the heme in HRP, was mutated to a tyrosine and the resulting mutant afforded a Compound I species that initially displayed a porphyrin radical cation which rapidly decayed to a Compound I species displaying a protein radical. Presumably this EPR detected radical was carried by Tyr 172.

The unique nature of the Compound I species of CCP appears to bestow upon this enzyme the ability to oxidize its physiological substrate, cytochrome c, with high specific activity. CCP has been linked to aerobic metabolism in yeast and may act to scavenge H_2O_2 generated in respiring mitochondria (Chance *et al.*, 1970; Pettigrew and Moore, 1987). Cytochrome c is a small 12 kDa protein that mediates electron transfer between cytochrome c reductase and cytochrome oxidase. Other peroxidases only display a limited ability to oxidize cytochrome c (Chance, 1950; Nicholls, 1962). The efficiency of the CCP/cytochrome c reaction appears to be governed by Trp 191, the site of the Compound I protein radical in CCP. Several pathways likely facilitate the transfer of electrons from cytochrome c to CCP; however, Trp 191 seems to provide the major branch point for electron transfer. W191F CCP exhibits a dramatically reduced cytochrome c oxidation

activity that is 10^4-10^5 slower than that of the native enzyme (Miller *et al.*, 1995a). This mode of electron transfer differs significantly from that exhibited by peroxidases in the oxidation of classic substrates, which characteristically occurs through the δ-*meso* heme edge. Reconstitution of HRP with δ-*meso*-ethylheme significantly suppresses guaiacol (2-methoxyphenol) peroxidation, presumably by deterring electron transfer through the heme edge (Ator *et al.*, 1989). Similar treatment of CCP also suppresses guaiacol activity (4% of native activity), but only mildly influences cytochrome c oxidation (59% of native activity) (DePillis *et al.*, 1991). The crystal structures have been solved for the complexes of CCP with both yeast and horse cytochrome c (Pelletier and Kraut, 1992). These structures show yeast and horse cytochrome c to bind at similar sites at the surface of the CCP protein. These authors argue that a single cytochrome c binding site exists for cytochrome c, as suggested by earlier kinetic studies (Kim *et al.*, 1990). However, Brownian dynamics simulations and kinetic studies have suggested that multiple cytochrome c binding sites exist (Northrup *et al.*, 1988; Hoffman, *et al.*, 1991; McLendon, 1991). Regardless of the nature or number of cytochrome c binding sites, CCP is distinguished from other peroxidases by the important role played by Trp 191 and the unimportance of the δ-*meso* heme edge in cytochrome c oxidation.

Cytochrome c is vastly different from classic aromatic peroxidase substrates. CCP oxidizes classic peroxidase substrates, but the specific activity is reduced relative to that of most peroxidases. For example, pyrogallol is oxidized greater than 300 fold slower by CCP than by HRP (Yonetani and Ray, 1965). The weaker classic peroxidase activity displayed by CCP appears to be partially due to the distal tryptophan, Trp 51 (Figure 1.4). W51F CCP exhibits accelerated rates of oxidation for cytochrome c (~2 fold), aniline (~100 fold), and 4-aminophenol (~9 fold) relative to native CCP (Goodin *et al.*, 1991; Roe and Goodin, 1993). The hyperactivity of W51F CCP was attributed to a more reactive oxyferryl heme. The weaker activity of native CCP was postulated to arise through

stabilization of the oxyferryl heme by hydrogen bonding between the indole nitrogen atom of Trp 51 and the ferryl oxygen (Figure 1.4). The residue corresponding to Trp 51 in the fungal and plant peroxidases is a phenylalanine (Phe 41 in HRP). Thus, the improved classic peroxidase activity displayed by these peroxidases relative to CCP may be partially attributed to their lack of a hydrogen bond donating distal tryptophan residue. Conversely, the deviating behavior displayed by CCP relative to other peroxidases appears to stem from the presence of the two tryptophans in the heme pocket.

The peroxidase active site: proximal heme face In order for the various classes of hemoproteins to display such a broad range of functions, the reactivity of the heme prosthetic group must be controlled by the protein. Ergo the active site accommodating the heme molecule is expected to distinguish each class of hemoproteins. In the peroxidases, identification of amino acids in the peroxidase active site began with identification of the fifth heme (proximal) ligand. The first experiments to suggest that the fifth heme ligand in HRP was a histidine demonstrated that a transition associated with the iron-imidazole bond in the absorption difference spectrum of myoglobin (low spin cyano-met Mb versus high spin free met Mb) was also found in the difference spectrum of HRP (low spin Compound II species versus high spin resting state HRP) (Brill and Sandberg, 1968). Sequencing the full length of the HRP gene also highlighted a sequence that contained a histidine and was homologous to the imidazole-containing proximal helix of myoglobin (Table 1.2). In a photolabeling study, photooxidation of myoglobin apoenzyme reconstituted with protoporphyrin IX modified the proximal histidine ligand (Mauk and Girotti, 1973). It was surmised that photolabeling caused by the attack of excited oxygen would modify residues in the vicinity of the porphyrin molecule. In accord with this expectation, photolabeling of HRP modified His 170 (Mauk and Girotti, 1974), the residue postulated to be the proximal histidine based on the comparison between the HRP and myoglobin sequences. A comparison of HRP and 4 turnip peroxidase sequences showed this histidine to be an

invariant residue contained within one of two highly conserved regions (Welinder, 1977). Solution of the 2.5-Å resolution crystal structure of CCP revealed His 175 to be the proximal heme ligand in CCP (Poulos *et al.*, 1980). Alignment of the CCP and plant peroxidase sequences suggested that His 170 was the proximal ligand in HRP (Welinder, 1985) (Table 1.2). ESR studies demonstrated that this ligand differed in electronegativity

Table 1.2: Sequence alignment of peroxidase and sperm whale Mb proximal helices.

Enzyme	Proximal Residues (His* refers to the proximal histidine)												
CCP[a]	Glu	Val	Val	Ala	Leu	Met	Gly	Ala	His*	Ala	Leu	Gly	Lys
LIP[a]	Glu	Leu	Val	Trp	Met	Leu	Ser	Ala	His*	Ser	Val	Ala	Ala
ARP[b]	Glu	Val	Val	Asp	Leu	Leu	Ala	Ala	His*	Ser	Leu	Ala	Ser
PeP[c]	Glu	Leu	Val	Thr	Leu	Ser	Gly	Ala	His*	Thr	Ile	Gly	Gln
HRP[a]	Asp	Leu	Val	Ala	Leu	Ser	Gly	Gly	His*	Thr	Phe	Gly	Lys
Mb[d]	Glu	Leu	Lys	Pro	Leu	Ala	Gln	Ser	His*	Ala	Thr	Lys	His

[a](Welinder, 1992a), [b](Baunsgaard *et al.*, 1993), [c](Buffard et al., 1990), and [d](Edmundson, 1965).

from that found in myoglobin, hemoglobin, and cytochrome c (Peisach and Blumberg, 1972). An interpretation of these data suggested that the fifth heme ligand displayed imidazolate character and that partial or complete deprotonation of the imidazole group could arise through hydrogen bonding interactions with other residues in the active site. A weak hydrogen bond occurs between the $N_{\delta 1}$ nitrogen atom of the proximal histidine and a backbone carbonyl in the globins (Ladner *et al.*, 1977; Bolton and Perutz, 1970). Further refinement of the CCP crystal structure to 1.7-Å resolution positioned Asp 235, a strong hydrogen bond accepting group, in close proximity to the proximal histidine ligand, His

175 (Finzel *et al.*, 1984) (Figure 1.5). The $N_{\delta 1}$ nitrogen atom of His 175 lies 2.9 Å away from the carboxylate of Asp 235. This distance along with the buried nature of the aspartate group provides strong evidence for the existence of a relatively strong hydrogen bond. The highly conserved nature of this aspartic acid (Welinder, 1992a) and its similar positioning in the more recently solved peroxidase crystal structures suggests that this hydrogen bond is essential to peroxidase catalysis (Poulos *et al.*, 1993; Kunishima *et al.*, 1994, Patterson and Poulos, 1995).

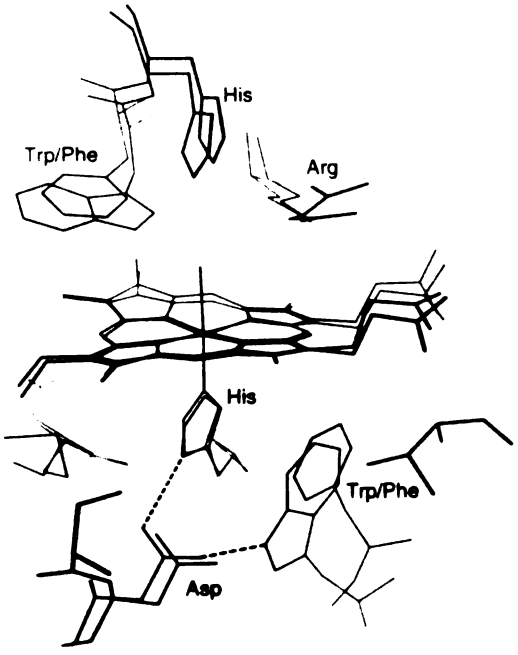

Figure 1.5: CCP and PeP heme pocket residues as revealed by their respective crystal structures. Key active site residues include the proximal histidines, the hydrogen bonding aspartates, CCP Trp 191, and PeP Phe 213. In CCP the aspartate also hydrogen bonds to the nitrogen atom of the tryptophan indole ring. The crystal structure of PeP is shown because the sequence of this enzyme is ~50% identical to that of HRP, and correspondingly, the PeP structure is deemed more representative of the structure of HRP (Buffard, 1990).

The CCP crystal structure also identified Trp 191 as a residue that lies adjacent to the proximal histidine. The tryptophan indole ring π stacks against the imidazole ring of the histidine side chain. One of the carboxylate oxygen atoms of Asp 235 forms a hydrogen bond with the NH proton of the tryptophan indole ring. As discussed above, this tryptophan is the site of the protein radical of the CCP Compound I species. Sequence alignments comparing CCP with representatives of the class II and class III peroxidases (Welinder, 1992a) suggest, as confirmed by the crystal structures of ARP, LIP, and PeP, that an analogous tryptophan to that of CCP Trp 191 does not exist in these proteins. In the class II fungal peroxidases, the residue corresponding to Trp 191 is a phenylalanine. Like Trp 191 in CCP, this phenylalanine π stacks with the proximal histidine. In the plant peroxidases, the amino acid corresponding to Trp 191 appears to vary since sequence alignments show several residues at this position, including phenylalanine and leucine residues. As in the ARP and LIP structures, the PeP crystal structure positions a phenylalanine residue next to the proximal histidine. The 3D HRP model based on the CCP, LIP, and ARP crystal structures predicts Phe 221 to be similarly positioned.

The distal heme face Assignment of the distal histidine began with modification studies in which acetic anhydride was proposed to modify a functional distal histidine residue (Schonbaum *et al.*, 1971). In alignment studies comparing HRP and globin sequences, a region within HRP contained two histidines and was speculated to be a distal peptide analogous to the distal helix of myoglobin which contains a histidine (Table 1.3). Later alignment studies comparing HRP and 4 isozymes of turnip peroxidase revealed this region to display high homology among the five sequences (Welinder *et al.*, 1977). The conservation of the two histidines among these peroxidase sequences (His 40 and His 42 in HRP) further supported the existence of a histidine at the distal heme face of peroxidases. The 2.5 Å resolution CCP crystal structure identified His 52 as the distal histidine in CCP (Poulos, 1980). His 52 sits directly over the heme iron with the $N_{\varepsilon 2}$ nitrogen atom

pointing towards the heme iron. Arg 48 and Trp 51 were identified as residues that neighbor the distal histidine. The 1.7 Å resolution CCP crystal structure suggested that the $N_{\delta 1}H$ proton of the distal histidine hydrogen bonds with the side chain oxygen atom of Asn 82 (Figure 1.6) (Finzel *et al.*, 1984). In the sequence alignment of bacterial, fungal, and plant peroxidases, Arg 48, His 52, and Asn 82 are invariant residues that correspond to Arg 38, His 42, and Asn 70 in HRP.

Table 1.3: Sequence alignments of peroxidase and sperm whale Mb distal helices.

Enzyme	Distal residues (His* refers to the distal histidine)											
CCP[a]	Val	Leu	Val	Arg	Leu	Ala	Trp	His*	Thr	Ser	Gly	Thr
LIP[a]	Glu	Ser	Ile	Arg	Leu	Val	Phe	His*	Asp	Ser	Ile	Ala
ARP[b]	Lys	Ile	Leu	Arg	Ile	Val	Phe	His*	Asp	Ala	Ile	Gly
PeP[c]	Ser	Leu	Leu	Arg	Leu	His	Phe	His*	Asp	Cys	Phe	Val
HRP[a]	Ser	Ile	Leu	Arg	Leu	His	Phe	His*	Asp	Cys	Phe	Val
Mb[d]	Ala	Ser	Glu	Asp	Leu	Lys	Lys	His*	Gly	Val	Thr	Val

[a](Welinder, 1992a), [b](Baunsgaard *et al.*, 1993), [c](Buffard *et al.*, 1990), and [d](Edmundson, 1965).

The distal histidine, asparagine, and arginine residues are invariant throughout the bacterial, fungal, and plant peroxidases (Welinder, 1992a). The class II and class III peroxidase crystal structures show these distal residues, along with the proximal histidine and aspartate residues, to be essentially superimposed with the corresponding residues found in the CCP crystal structure. The distal tryptophan in CCP is replaced by a phenylalanine in the sequences of the class II and class III peroxidases. The distal tryptophan and phenylalanine side chains are similarly positioned in the peroxidase crystal

structures, and the corresponding indole and phenyl groups π stack with the heme (Figure 1.6). NMR studies on cyanide-bound HRP also demonstrate that the conserved distal residues are positioned in the same manner as they are found in LIP. The accumulated structural data suggest that the integrity of the peroxidase active site is highly conserved among the bacterial, fungal and plant peroxidases. This is further supported by the conservation of the heme pocket residues -Arg 38, Phe 41 (Trp), His 42, Asn 70, His 170, and Asp 235 (numbering based on the HRP sequence)- which represent one highly conserved aromatic residue and five invariant residues found within this peroxidase superfamily. Thus the events that direct peroxidase catalysis are likely to be coordinated by these residues.

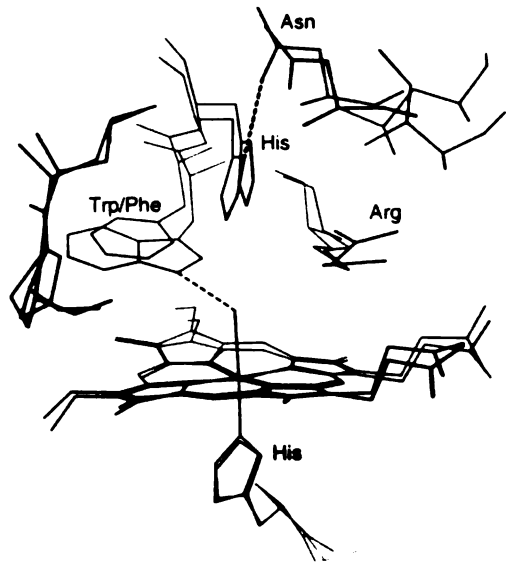

Figure 1.6: The conserved positioning of the distal peroxidase residues as revealed by the superimposed crystal structures of CCP and PeP. The hydrogen bond between CCP His 52 and Asn 82 is illustrated with the dashed line. The hydrogen bond between the indole ring of CCP Trp 51 and a water molecule bound to the sixth heme coordination site is also shown.

Substrate accessibility In addition to the conservation of peroxidase active site residues, similar accessibility of substrates to the heme molecule is found among the peroxidases and is also likely to influence heme reactivity. Restricted accessibility to the peroxidase heme molecule has become increasingly evident with chemical modification and NMR studies and with crystallographic structures which collectively support the δ-*meso* heme edge as the only region accessible to substrates. In chemical modification studies, reaction of alkyl- and aryl-hydrazines with a range of hemoproteins affords heme or protein modification that reveals the regions accessible to the substrate. Interestingly, the resulting modifications distinguish among established classes of hemoproteins. Peroxidases are predominantly modified at the heme edge (Ator and Ortiz de Montellano, 1987; DePillis and Ortiz de Montellano, 1989), whereas cytochrome P450s form iron-aryl complexes (Raag *et al.*, 1990; Ortiz de Montellano, 1995). Given that peroxidases typically abstract electrons to reduce the ferryl oxygen, and that P450s typically transfer the ferryl oxygen to substrates, these findings suggest that ferryl accessibility plays a role in determining heme reactivity (Ortiz de Montellano, 1987).

Modification of peroxidases by aryl- and alkyl-hydrazines specifically modifies the δ-*meso* heme edge (Figure 1.7) (Ator *et al.*, 1987). Reconstitution of the apoenzymes of HRP and CCP with δ-*meso*-ethyl heme significantly suppresses the classic peroxidase activity of both peroxidases, decreasing their guaiacol activities to ~5% of that of the native enzymes (Ator *et al.*, 1989; DePillis *et al.*, 1991). Thus, the region of the heme that is susceptible to modification appears to be the site of substrate oxidation.

NMR has been used to look at substrate binding to the resting state species of a range of peroxidases. The interactions between numerous substrates and the heme-containing active site of HRP have been monitored through relaxation methods and transferred nuclear Overhauser effects. These techniques have been used to estimate the positioning and kinetics of substrate binding. In agreement with the chemical modification

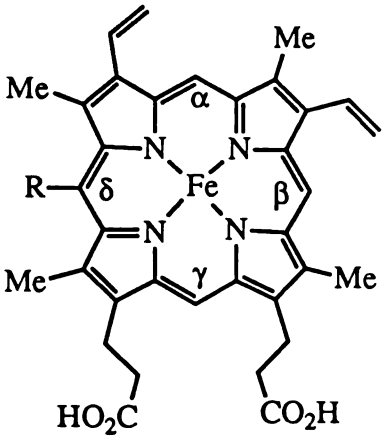

δ-meso heme modification

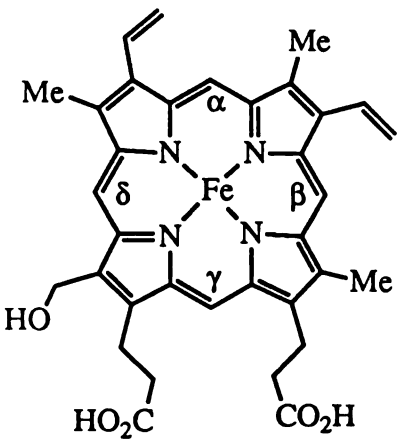

8-hydroxymethyl-heme

Figure 1.7: Heme modifications brought about by the reaction of HRP with aryl- and alkyl-hydrazines. Treatment with methyl-, ethyl-, and phenyl-hydrazine produce δ-*meso* heme adducts where R = methyl, ethyl, and phenyl, respectively. Treatment with phenylhydrazine also generates 8-hydroxymethyl-heme.

studies, aromatic substrates like resorcinol (3-hydroxyphenol) (Paul and Ohlsson, 1978; Sakurada *et al.*, 1986), ferulic acid (Veitch, 1995), and benzhydroxamic acid (Schonbaum, 1973; La Mar *et al.*, 1992) have been shown to bind exclusively at the δ-*meso* heme edge within 5 Å of the 8-methyl group. NMR and optical difference spectroscopy studies, performed on cyanide-ligated HRP, demonstrate that similar substrate binding occurs to this six coordinate species, based on the finding of similar distances and binding affinities (Hosoya *et al.*, 1989; Morishima and Ogawa, 1979). The cyanide-ligated species mimics the six coordinate nature of Compound I and Compound II. These NMR findings suggest that movement of the iron into the plane of the heme with the formation of a six coordinate species, akin to Compound I and Compound II, does not drastically influence substrate binding.

Accessibility of the δ-*meso* heme edge is also revealed in the peroxidase crystal structures which show a solvent accessible channel that exposes the δ-*meso* heme edge (Figure 1.8) (Finzel *et al.*, 1984; Poulos *et al.*, 1993; Kunishima *et al.*, 1994; Patterson and Poulos, 1995). The width and height of the channel vary slightly among the crystal structures of CCP, LIP, ARP, and PeP. However, in all these structures the three distal

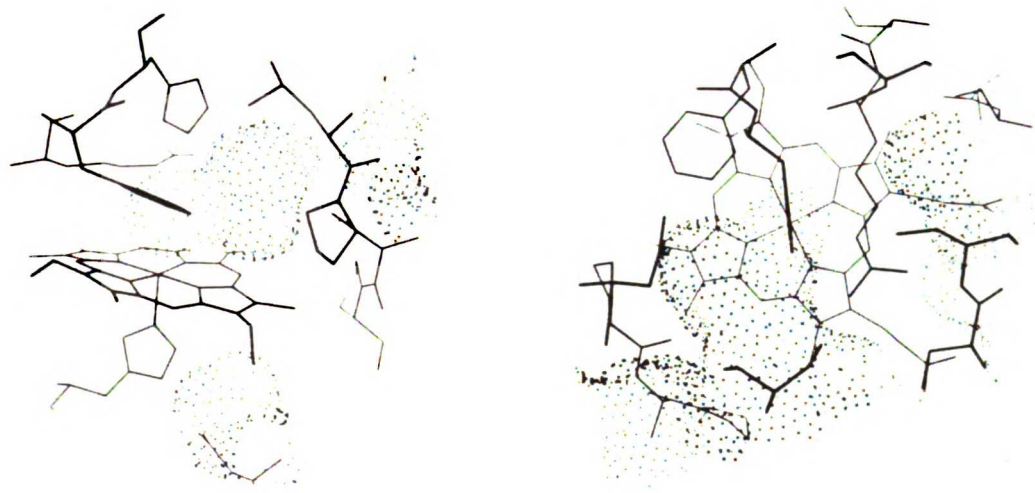

Figure 1.8: Solvent accessible surface for PeP. The dotted surface represents the solvent accessible surface. The structure to the right is oriented so that the reader is looking down at the distal heme face. The structure to the left is seen when looking at the α-*meso* heme edge.

residues (Arg 38, Phe 41, and His 42 in PeP and HRP) largely shape the channel as it approaches the heme molecule. The end of the channel is met by the distal phenylalanine (tryptophan) residue, and the ceiling of the channel is formed by the distal histidine and arginine residues. As elucidated through spectral changes, small molecules (including cyanide, azide, and carbon monoxide) have access to the heme iron and coordinate to the sixth coordination site (Keilin and Hartree, 1951; Blumberg *et al.*, 1968). However, the

distal residues form a barrier to larger molecules, such as imidazole, which do not coordinate to the sixth heme position at concentrations higher than 1 M. These peroxidase crystal structures reflect the conformation of the resting state enzyme which may vary from the structures of the Compound I and Compound II species. However, crystallographic analysis of the fluoride-ligated CCP, which mimics the six coordinate nature of the Compound I and Compound II species, shows little perturbation of heme accessibility from that in the native enzyme (Edwards, 1984).

The structural characterization of the peroxidases has elucidated several features that distinguish the peroxidases as a class of hemoproteins. These features include 1) a proximal imidazolate ligand, 2) a hydrogen-bonded distal histidine, 3) a polar heme pocket containing His 42, Arg 38, and Asp 247 (HRP numbering), and 4) restricted heme accessibility, where only the δ-meso heme edge is accessible to substrates. The active site of the peroxidase has been slowly pieced together, bringing us to an exciting stage where we can begin to ask questions regarding the specific mechanism of peroxidase action and the manner in which substrates interact with Compound I.

HRP reaction cycle The accepted catalytic cycle for HRP was first proposed by George long before any details were known about the active site (George, 1952):

$$\text{HRP} + \text{H}_2\text{O}_2 \xrightarrow{k_1} \text{Compound I} + \text{H}_2\text{O}$$

$$\text{Compound I} + \text{AH}_2 \xrightarrow{k_2} \text{Compound II} + \text{AH}^{\cdot}$$

$$\text{Compound II} + \text{AH}_2 \xrightarrow{k_3} \text{HRP} + \text{AH}^{\cdot} + \text{H}_2\text{O}$$

The peroxide-generated green and red colored species corresponding to Compound I and Compound II were discovered over 50 years ago. Spectra of the Soret region of these species were first reported in 1949 (Chance, 1949a; and Chance, 1949b) and were extended to the visible region in 1952 (Chance, 1952). The spectra of the ferric, Compound I, and Compound II species are distinct from one another (Table 1.4 and Figure

1.9). This has offered an advantageous means of monitoring each species during the course of peroxidase cycling.

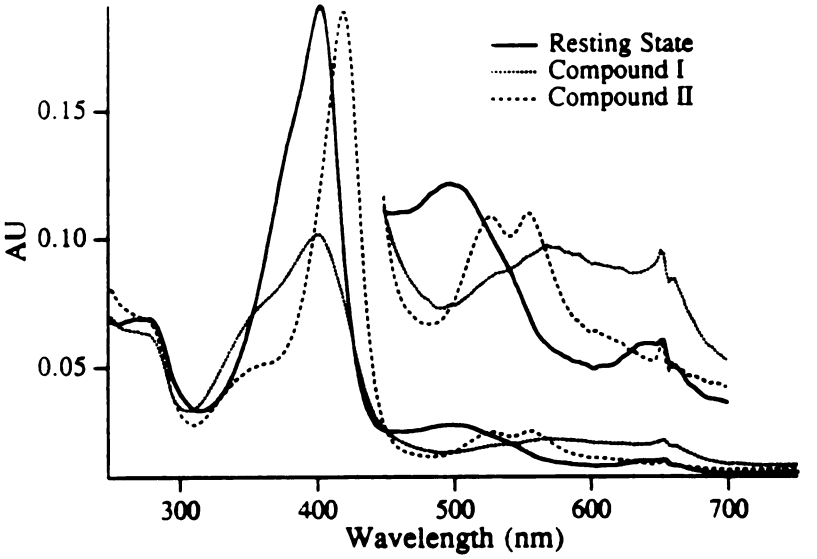

Figure 1.9: Spectrally distinct resting state, Compound I, and Compound II species of HRP.

Table 1.4: Absorption λ_{max} values for the ferric, Compound I, and Compound II species of HRP in the Soret and visible regions.

Enzymic species	Soret (nm)[a]	Visible (nm)[a]
Ferric	403	498, 640
Compound I	400	577, 622, 651
Compound II	420	527, 554

[a](Schonbaum and Lo, 1972; Roman and Dunford, 1972)

Ferric resting state The ferric resting state has been characterized extensively by physico-chemical methods. The iron is five-coordinate as determined through NMR, ESR,

and resonance Raman studies (Vuk-Pavlovic and Siderer, 1977; Maltempo *et al.*, 1979; Teraoka and Kitagawa, 1981). The resting state species displays a mixture of spin states (S = 3/2 and S = 5/2). This is distinct from myoglobin, which has a water occupying the sixth coordination site and is predominantly high spin (Morikis et al., 1990). The five-coordinate nature of HRP is promoted by displacement of the iron away from the plane of the heme. This is postulated to be partially due to the strongly hydrogen bonding proximal aspartate (Asp 247 in HRP), which is replaced in myoglobin by a backbone carbonyl. The strength of this hydrogen bond in myoglobin and several peroxidases has been correlated with an increased reduction potential (Fe^{3+}/Fe^{2+}) (Banci *et al.*, 1993). These findings support the ability of hydrogen bonding, by the proximal histidine ligand, to influence the strength and, therefore, the length of the Fe-N bond. The positioning of the iron with respect to the plane of the heme can also be modulated by the tethering action of the protein ligand.

Compound I formation The peroxidases are unique in their ability to react rapidly with hydroperoxides -including H_2O_2, alkyl hydroperoxides, and acyl hydroperoxides. The rate of reaction of HRP with H_2O_2 is 1.8×10^7 $M^{-1}s^{-1}$ (Dunford *et al.*, 1978). The resulting two electron-oxidized species, Compound I, has been characterized by spectral techniques and has been shown to consist of a porphyrin π-cation radical and an oxyferryl group ($Fe^{IV} = O$) (Dolphin *et al.*, 1971; Moss *et al.*, 1969; Ogura and Kitigawa, 1987). EXAFS experiments assert that the distance between the iron and the ferryl oxygen is 1.54 Å (Penner-Hahn *et al.*, 1986).

The mechanism of Compound I formation is postulated to involve a push-pull mechanism, in which the proximal ligand and distal residues work cooperatively (Figure 1.10). The distal histidine and arginine residues provide the "pull" and are proposed to deprotonate and polarize the peroxide molecule. These actions are postulated to accelerate

the formation of a ferric peroxide complex and promote heterolytic cleavage of the ferric peroxide dioxygen bond (Poulos and Kraut, 1980). The distal histidine is postulated to

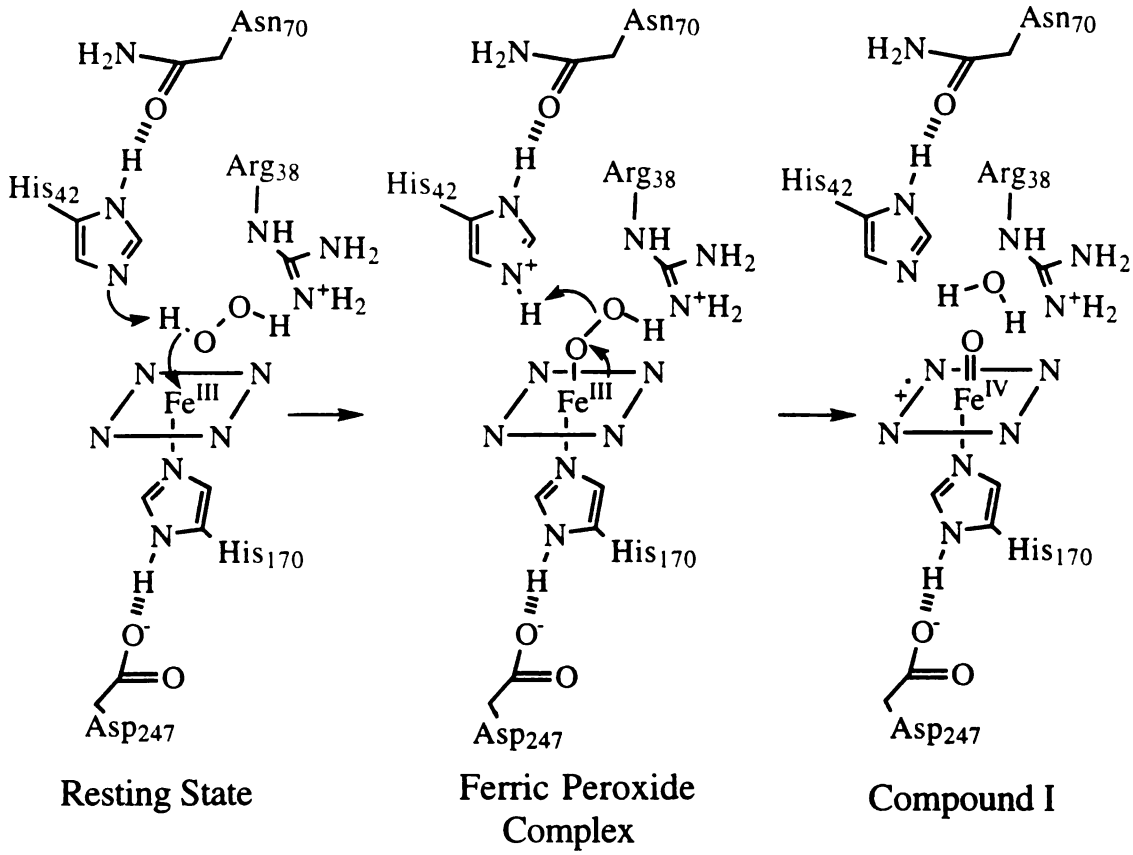

Figure 1.10: Proposed mechanism of Compound I formation. The numbering of the residues refers to the HRP sequence.

initiate Compound I formation by deprotonating the peroxide molecule which generates the nucleophilic peroxide anion that can attack the heme iron. The need for a basic distal residue, like histidine, is evident in light of the high pKa value of hydrogen peroxide (pKa 11.6) (Everett and Minkoff, 1953). In the CCP crystal structure, the distal histidine sits directly over the heme iron. This positioning is optimal for deprotonating the peroxide molecule proximal to the sixth coordinating site of the iron. In support of this role for the distal histidine, model studies have shown that the heme propionates and exogenous collidine (2,4,6-trimethylpyridine) can mimic the distal histidine and accelerate the

peroxide-generated formation of a Compound I-like species (Traylor and Popovitz-Biro, 1988). Additionally mutagenesis studies show that removing the distal histidine of CCP (H52L) decreases the rate of Compound I formation by five orders of magnitude (3.2×10^7 $M^{-1}s^{-1}$ to 2.9×10^2 $M^{-1}s^{-1}$) (Erman and Vitello, 1992).

Asn 82 in CCP is an additional invariant peroxidase distal residue that accepts a hydrogen bond from the $N_{\delta 1}H$ proton of the distal histidine. This residue corresponds to Asn 70 in HRP. This hydrogen bond is likely to influence the basicity of the distal histidine and probably also restricts rotation of the imidazole ring so that the $N_{\varepsilon 1}$ nitrogen atom is positioned next to the iron atom. Mutagenesis of Asn 70 to a valine residue within HRP removes this hydrogen bond and produces a 25 fold reduction in the rate of Compound I formation (Nagano *et al.*, 1995), demonstrating that this residue also plays a role in peroxidase catalysis.

After deprotonating the peroxide molecule, the distal histidine is proposed to donate the abstracted proton to the distal oxygen, promoting heterolytic cleavage of the O-O bond. Dioxygen bond scission is known to occur through heterolytic cleavage since two oxidative equivalents remain with the heme after the peroxidase is treated with one equivalent of H_2O_2. Additionally it has been shown that the reaction of HRP with alkyl hydroperoxides results in the release of ROH (Schonbaum and Lo, 1972), and the reaction of HRP with *p*-nitroperbenzoic acid results in the release of *p*-nitrobenzoic acid (Adediran and Dunford, 1983).

The distal arginine has also been incorporated into the mechanism of Compound I formation, due to its invariant nature and conspicuous positioning next to the distal histidine. This residue is proposed to assist heterolytic cleavage of the dioxygen bond by polarizing the peroxide molecule. In the CCP crystal structure, peroxide binding was proposed to occur with the distal oxygen equidistant from the N_ε and the NH_2 nitrogen atoms of arginine (Poulos and Kraut, 1980). This positioning is ideal for stabilizing the

negative charge that would develop on the distal oxygen during O-O bond scission. Consistent with this role, replacing the arginine in CCP with a lysine causes only a 2 fold reduction in the rate of Compound I formation (Erman and Vitello, 1992). Surprisingly, a similar mutation in HRP lowers the rate of Compound I formation 840 fold (Smith *et al.*, 1992a). The sensitivity of HRP to mutation of the distal arginine may stem from alteration of the coordination state of the mutant relative to native HRP. R38K HRP demonstrates a five to six coordinate transition that is modulated by an unidentified ionizable group with a pKa of 7.5 (Sanders *et al.*, 1994). Thus, peroxide activation leading to the formation of Compound I may be inhibited in R38K HRP by steric blocking of the sixth coordination site. In CCP, replacing the charged side chain of Arg 38 to that of a neutral leucine residue caused the rate of Compound I formation to decrease 100 fold from that of the native enzyme (Erman and Vitello, 1992). Thus, the putative role of the distal arginine is to provide a positive charge at the site of peroxide activation.

The push-pull mechanism of Compound I formation also enlists the participation of the proximal ligand. The imidazolate ligand is a distinguishing feature of the peroxidases. In model compounds, resonance Raman indicates that the imidazolate ligand has a stronger Fe-N bond relative to the neutral imidazole (Stein *et al.*, 1980). The resulting increased electron density at the heme iron is postulated to provide "push" in heterolytically cleaving the O-O bond of the ferric peroxide species in the generation of Compound I. Model studies have shown that, relative to neutral imidazole, the imidazolate ligand accelerates both the formation of a Compound I-like species and peroxidase activity (Traylor and Popovitz-Biro, 1988). Contrary to these model studies, mutating the proximal histidine to a glutamine or glutamate does not appreciably influence the rate of Compound I formation (Choudhury *et al.*, 1994). H175E CCP was estimated to form Compound I as fast or faster than native CCP, and the measured rate of H175Q CCP Compound I formation was only three fold reduced from that of native CCP. Hence, the chemical nature of the

proximal ligand appears to have little influence on the rate of Compound I formation. These studies suggest that the imidazolate ligand plays a minor role in the heterolytic cleavage of the dioxygen bond. The conserved nature of the proximal histidine and aspartate residues suggests, therefore, that these amino acids serve another purpose. In CCP, Asp 235 was mutated to an asparagine. The resulting mutant was 4-5 fold less effective in the formation of Compound I (Vitello *et al.*, 1992). This decrease in peroxide activation could result from decreased O-O bond scission. However, this mutant was also predominantly six coordinate at pH values greater than six and was suggested to contain either a hydroxyl group or the distal histidine at the distal axial heme position. Filling the sixth heme coordination site would sterically inhibit peroxide attack on the iron. These findings suggested that the imidazolate ligand assists in the maintenance of a 5 coordinate species. This would be facilitated by the shortened nature of the iron-nitrogen bond displayed by the imidazolate ligand relative to the neutral imidazole ligand, as this would better displace the iron from the plane of the heme, deterring coordination at the distal axial position.

Collectively, several active site residues are thought to contribute to the efficient formation of Compound I. These residues and their postulated roles are summarized in the following scheme (Figure 1.11). Mutagenesis studies on CCP demonstrate that the distal histidine is a crucial residue in promoting Compound I formation; however, the other residues, notably Arg 38, Asn 70, and Asp 247 (numbering for HRP), also contribute. Myoglobin also contains proximal and distal histidines, but lacks residues which are analogous to the proximal aspartate and distal arginine and asparagine residues found in the peroxidases. Correspondingly, the reaction of hydroperoxide with myoglobin deviates significantly from that with the peroxidases. The rate at which myoglobin reduces peroxide is 10^5-times slower than the rate of HRP Compound I formation (McCarthy and White, 1983; George and Irvine, 1955). Cleavage of the dioxygen bond of the resulting

myoglobin ferric-peroxide complex predominantly occurs via homolytic scission and yields a Compound II species (Fe^{IV}=O) with a protein radical (Wilks and Ortiz de Montellano, 1992; Rao *et al.*, 1993; Allentoff *et al.*, 1992). The distinguishing peroxidase residues, Arg 38, Asn 70, and Asp 247 (in HRP), thus appear to play a part in deprotonating the peroxide and in promoting heterolytic cleavage.

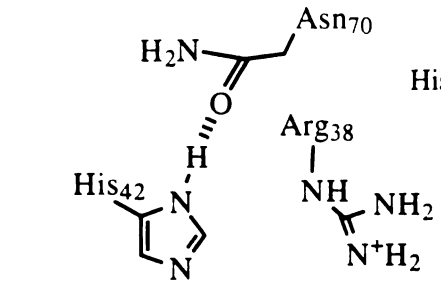

His 42: Deprotonate peroxide in Compound I formation
Protonate distal oxygen of ferric peroxide complex

Asn 70: Influence basicity of His 42
Restrict rotation of His 42 imidazole ring

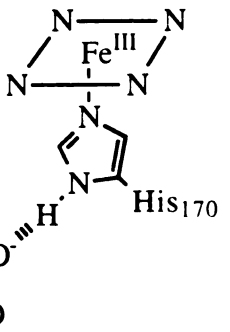

Arg 38: Polarize O-O bond of ferric peroxide complex

His 170: Donate electron density to heme iron

Asp 247: Hydrogen bonding to proximal imidazole
donates more electron density to the heme iron
Assists in maintenance of 5 coordinate species

Figure 1.11: Peroxidase active site residues and their proposed roles. Numbering of residues is based on the HRP sequence.

Reduction of Compound I to Compound II In the one electron reduction of Compound I to Compound II, the porphyrin cation radical (or the protein radical) is neutralized. This leaves an Fe^{IV}=O low spin (S=1) structure. The length of the Fe-O bond increases to 1.93 Å from 1.54 Å found in Compound I (Chance *et al.*, 1984). A proton is taken up by the protein (Yamada and Yamazaki, 1974), and a new hydrogen bond appears between the ferryl oxygen and a distal residue, presumably the distal histidine (Sitter *et al.*, 1985). Deprotonation of an active site group of pKa ~5.1 yields optimal reduction of Compound I (Marnett *et al.*, 1986). This pKa value is proposed to be that of the distal

histidine, the neutral imidazole of which is postulated to abstract a proton from the substrate (Figure 1.12). In the HRP-catalyzed oxidation of phenols and aromatic amines, free energy relationships suggest that these substrates simultaneously lose an electron and a proton in the reaction with either Compound I or Compound II (Job and Dunford, 1976). The lost proton may be directly or indirectly taken up by the distal histidine. A more recent interpretation of these data argues that only the electron is abstracted in the development of the transition state (Colclough and Smith, 1994). These authors postulate that proton transfer from the substrate follows (Figure 1.12).

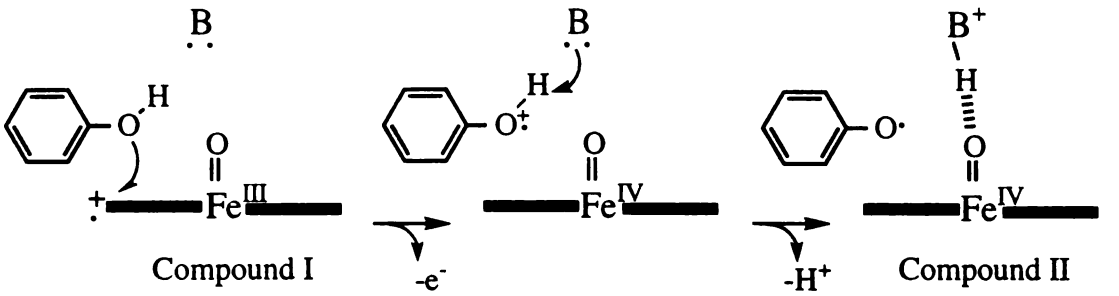

Figure 1.12: Proposed mechanism of peroxidase-catalyzed oxidation of aromatic molecules, including phenols and aromatic amines. The rate-limiting abstraction of an electron by HRP gives the radical cation species of the substrate. Proton transfer from the substrate to the protein follows. The ionizable distal residue, B, is postulated to be the distal histidine.

Reduction of Compound II to the ferric resting state In the reduction of Compound II to the resting state, Fe(IV) is reduced to Fe(III) with the release of the ferryl oxygen as a water molecule. Compound II is inactivated upon deprotonation of an ionizable group of pKa 8.6 (Dunford and Stillman, 1976). Since the hydrogen bond to the ferryl oxygen is lost in conjunction with inactivation, the ionizable group is speculated to be His 42 in HRP (Sitter, *et al.*, 1985: Hashimoto *et al.*, 1986; Makino *et al.*, 1986). The proton carried by

the distal histidine is likely to be donated to the ferryl oxygen in the generation of a water molecule. Inactivation at alkaline conditions may reflect a decrease in the reduction potential of the oxyferryl heme caused by removal of this hydrogen bond. The proposed mechanism for the reduction of Compound II is similar to the mechanism invoked for the oxidation of classic substrates by Compound I. The reduction of Compound II is initiated by electron abstraction from the substrate and is followed by the transfer of a proton to the enzyme (Figure 1.13) (Dunford and Adeniran, 1986; Colclough and Smith, 1994).

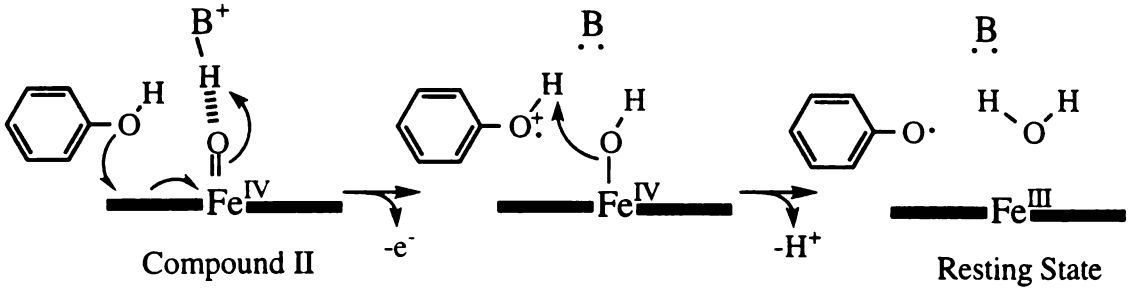

Figure 1.13: Proposed mechanism for the oxidation of classic peroxidase substrates by Compound II. Electron abstraction by HRP is speculated to occur in the formation of the transition state. Proton transfer to the protein follows. The ionizable distal residue, B, is postulated to be the distal histidine.

The reduction of Compound II usually represents the slowest step in the peroxidase cycle, and consequently, the spectrum of Compound II is typically observed in the steady state turnover of most substrates. The reactions of a range of substrates with Compound I and Compound II have been measured independently. The majority of these substrates, including phenols and $K_4Fe(CN)_6$, reduce Compound II ~40 fold more slowly than they reduce Compound I (Marnett *et al.*, 1986). For example, guaiacol is oxidized by Compound I at a rate of 9×10^6 $M^{-1}s^{-1}$ for Compound I and 3×10^5 $M^{-1}s^{-1}$ for Compound II (Yamazaki and Yakota, 1973).

The kinetics of the peroxidase cycle can be represented by a modified version of ping pong kinetics as described by the following equation ($v = -d[AH_2]/dt$) (Dunford, 1991). Since the reduction of Compound II (k_3) is commonly slower than that of Compound I (k_2), equation 1.1 typically simplifies to equation 1.2.

$$2[HRP]_o/v = ((k_2+k_3)/(k_2k_3))(1/[AH_2]) + (1/k_1)(1/[H_2O_2]) \quad (1.1)$$

$$2[HRP]_o/v = (1/k_3)(1/[AH_2]) + (1/k_1)(1/[H_2O_2]) \quad (1.2)$$

<u>One electron-oxidized versus two electron-oxidized peroxidase substrates</u> Classic peroxidase substrates are oxidized by one electron, generating a free radical product. There also exists a small group of peroxidase substrates that are thought to be oxidized by two electrons. Reaction of peroxidases with these substrates differs markedly from that with one electron-oxidized substrates in that Compound I is observed in the steady state turnover of the two electron-oxidized substrates. These substrates include halides (I^-, Br^-, and Cl^-) (Roman and Dunford, 1972; Morrison and Schonbaum, 1976), sulfite (Araiso *et al.*, 1976), thiocyanate (Modi *et al.*, 1991), and thioanisoles (Kobayashi *et al.*, 1986; and Kobayashi *et al.*, 1987). Among the halides, the oxidation of Cl^- is limited to peroxidases of higher reduction potentials. For example, MPO which displays the highest reduction potential of the peroxidases is able to catalyze chloride oxidation. HRP, however, can only oxidize iodide and bromide (Roman and Dunford, 1972; Ashley and Griffin, 1981). The stoichiometry of the reaction of HRP with iodide was determined to be the following (Roman and Dunford, 1972):

$$2I^- + H_2O_2 + 2H^+ \rightarrow I_2 + 2H_2O$$

Two mechanisms have been invoked to describe the two electron oxidation of I^- (Figure 1.14). The first mechanism is similar to that of classic peroxidase substrates, where two sequential single electron abstraction steps occur and oxidize I^- to I^+. $I^\cdot$ is generated as an intermediate, and the enzymatic product, I^+, reacts with I^- in the solution to

generate I_3^-. In this first mechanism, the second electron abstraction step must be faster than the first abstraction step ($k_3 > k_2$) to be consistent with the observation of Compound I in the steady state turnover of iodide. This is reversed from classic peroxidase kinetics ($k_2 > k_3$).

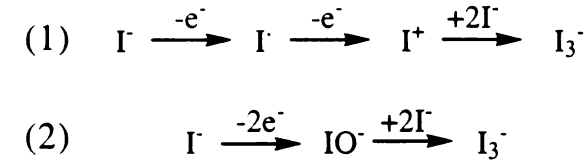

Figure 1.14: Two proposed mechanisms for HRP-catalyzed iodide oxidation.

The second postulated mechanism of iodide oxidation, as catalyzed by HRP, involves the transfer of the Compound I ferryl oxygen to I^-, generating hypoiodous acid (IOH). This enzymatic product would react with I^- in the solution to generate I_3^-. Support for the latter mechanism is drawn from studies of the myeloperoxidase-catalyzed oxidation of chloride, which generates Cl_2. In the oxidation of [Cl^{35}] NaCl by myeloperoxidase, [Cl^{35}] NaOCl was trapped as a product (Harrison and Schultz, 1976). This suggested that the true enzymatic product was hypochlorous acid, a highly reactive compound that would be susceptible to further solution chemistry, especially in the presence of excess chloride ion. Generation of such a product could most easily be afforded through the direct transfer of the ferryl oxygen to the chloride ion, although no direct evidence supports this event. In the sulfoxidation of thioanisole, labeling studies have demonstrated that the peroxide-derived ferryl oxygen of HRP Compound I is incorporated into the thioanisole sulfoxide product (Kobayashi *et al.*, 1986), suggesting that transfer of the Compound I ferryl oxygen of HRP is possible. Thioanisole peroxygenation, however, does not appear to occur through a direct two electron transfer. The mechanism of HRP-catalyzed thioanisole sulfoxidation is thought to involve the initial abstraction of a single electron in a manner that is characteristic of peroxidase chemistry (Figure 1.15). The resulting sulfur cation radical

is then postulated to recombine with the ferryl oxygen of Compound II, yielding the sulfoxide. This is supported by the relationship between the redox potentials of various thioanisoles and their rates of sulfoxidation (Kobayashi *et al.*, 1986; Doerge, 1986) and by the detection of a Compound II species with stopped flow spectrophotometry (Pérez and Dunford, 1990a; Pérez and Dunford, 1990b). Transfer of the ferryl oxygen is characteristic of P450-catalyzed hydroxylation and epoxidation reactions, but is proposed to be deterred in peroxidase catalysis by a protein barrier that prevents substrates from approaching the ferryl oxygen. Consequently, thioanisole is argued to bind near the ferryl oxygen in the Compound I species of HRP in order to afford oxygen transfer.

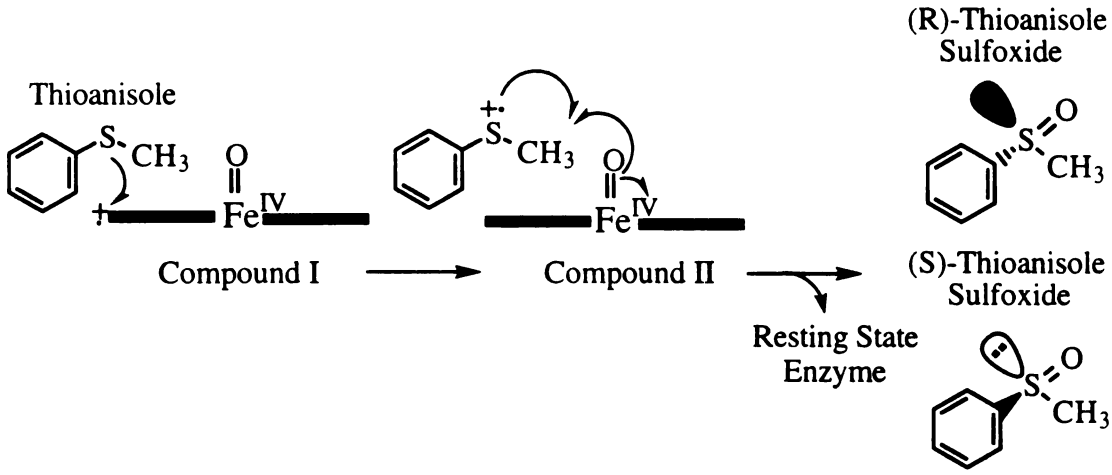

Figure 1.15: Mechanism of HRP-catalyzed thioanisole sulfoxidation.

The kinetics that distinguish the oxidation of one- and two-electron oxidized substrates could be manifested by the differing chemical makeup that exists between these two sets of substrates. The two-electron oxidized substrates contain S or I atoms which are less easily oxidized than guaiacol and, therefore, are probably oxidized less effectively by the δ-*meso* heme edge. Consequently, the oxidation of iodide and thioanisole may require closer positioning of these substrates to the heme edge to promote electron transfer. Such positioning may also allow the transfer of the ferryl oxygen. This reasoning may explain

the significantly different oxidative fates of guaiacol and thioanisole despite their sharing similar conformations. The manner by which these substrates interact with the heme molecule may also be modulated by how these molecules are bound by HRP. The binding of aromatic substrates to the δ-*meso* heme edge of HRP is supported by NMR studies and crystallographic structures. Electron abstraction from these substrates also occurs at the heme edge, as revealed by the decreased guaiacol oxidizing activity exhibited by δ-*meso*-ethylheme-reconstituted HRP (Ator *et al.*, 1987). In contrast, thioanisole sulfoxidation activity is stimulated in δ-*meso*-ethylheme-reconstituted HRP relative to native HRP (Harris *et al.*, 1993). The distinguishing influence that the ethyl group has on these two activities argues that guaiacol and thioanisole react at distinct sites within the Compound I species. Guaiacol and classic substrates are thus oxidized at the heme edge, and thioanisole is presumably oxidized closer to the ferryl oxygen to support oxygen transfer. HRP-catalyzed iodide oxidation may also occur near the ferryl oxygen. Iodide binding has been characterized by NMR studies, which show that iodide binds an equal distance from the 1- and 8-methyl groups and within 10 Å of the heme iron atom (Sakurada *et al.*, 1987). These authors also demonstrated that iodide has no influence over the binding of resorcinol, as indicated by an unchanged K_d for the latter in the presence of iodide. These studies suggest that iodide has a distinct binding site from that of resorcinol, a molecule that like guaiacol binds near the 8-methyl heme group. Thus, the differing binding of iodide relative to that of guaiacol may differentiate its reactivity with Compound I.

THESIS PROPOSAL

The conserved active site residues and heme accessibility exhibited by the peroxidases are postulated to (a) promote the peroxide-mediated formation of Compound I, and (b) limit the oxidation of most substrates to the δ-*meso* heme edge. Thus, heme reactivity is largely determined by these active site residues. The restricted heme accessibility bestowed by the protein is proposed to shelter the heme iron and deter the transfer of the Compound I ferryl oxygen to peroxidase substrates. Correspondingly, the one electron-oxidation of guaiacol, a classic peroxidase substrate, occurs by electron abstraction through the δ-*meso* heme edge. In contrast to the one electron oxidation of these substrates, the two electron oxidation of thioanisole occurs via oxygen transfer to the sulfur atom generating thioanisole sulfoxide. This reaction is proposed to occur proximal to the Compound I ferryl oxygen in order to promote oxygen transfer. Thus, differing reactivity of guaiacol and thioanisole with HRP may be promoted by differing interaction with the heme molecule. Additional two electron oxidized substrates, including iodide, may also undergo similar oxidative mechanisms to that of thioanisole. To further distinguish one electron-oxidized substrates from two electron-oxidized substrates, HRP-catalyzed iodide oxidation is compared to that of guaiacol and thioanisole. Specifically, chemical modification of HRP, that distinguishes thioanisole and guaiacol activities, is performed to characterize iodide oxidation. Difference spectroscopy and inhibition studies are also performed to compare the binding of iodide by HRP to that of guaiacol and thioanisole. In addition to characterizing the mechanism of iodide oxidation, this comparison of peroxidase substrates also probes the mechanism by which hemoproteins control heme reactivity by modulating substrate/heme interactions.

To further explore the determinants of heme reactivity in peroxidase catalysis, mutagenesis studies are performed on HRP to eliminate features that distinguish it as a

prototypic peroxidase. As revealed by the peroxidase crystal structures, the distal histidine, phenylalanine (tryptophan), and arginine residues directly contact the distal face of the heme molecule. Consequently, these residues largely shape the solvent accessible channel as it approaches the heme prosthetic group and also shelter the heme iron. In the present work, the distal residues, Phe 41 and His 42, are mutated to smaller neutral residues (alanine and valine) in an attempt to improve accessibility to the heme iron. Accessibility of the heme iron is probed by modification of the mutant proteins with phenyldiazene. To determine how accessibility to the heme iron influences peroxidase and peroxygenase activities, these mutants are assayed for guaiacol peroxidation, thioanisole sulfoxidation, and styrene epoxidation activities.

Characterization of the H42A- and H42V-HRP mutants is also aimed at elucidating the role played by the distal histidine in peroxidase cycling. This invariant peroxidase residue is proposed to assist in Compound I formation by (a) deprotonating peroxide to promote formation of the ferryl peroxide complex, and (b) donating the abstracted proton to the distal oxygen of the ferryl peroxide complex promoting the heterolytic cleavage of the dioxygen bond. Accordingly, H42A- and H42V-HRP are examined for their ability to form Compound I relative to the native enzyme. The distal histidine also participates in the reduction of Compound I and Compound II and may shuttle protons between substrates and the ferryl oxygen of Compound I. Collectively, Compound I formation and peroxidase and peroxygenase activities, exhibited by H42A- and H42V-HRP, are characterized to further clarify how the distal histidine participates in the three steps that make up the peroxidase cycle.

The role that the proximal histidine plays in peroxidase catalysis is also investigated by removing the imidazole group through mutation of this residue to an alanine. The invariant peroxidase proximal histidine is proposed to largely act in maintaining a five coordinate heme iron by providing a heme tether. Consequently, attempts are made to bind

exogenous imidazole to the cavity created by the H170A mutation. A comparison between imidazole-free versus imidazole-bound H170A HRP is examined to reveal how tethering of the imidazole ligand promotes peroxidase cycling. Specifically, the role that the exogenous imidazole ligand plays in Compound I formation and peroxidase activity is studied.

Chapter 2: Horseradish Peroxidase Mutagenesis, Expression, Purification and Initial Characterization

INTRODUCTION

Native horseradish peroxidase, isolated from the plant, is a secreted, soluble protein containing eight Asn-linked glycosylation sites and four disulfide bonds. Glycosylation does not appear to influence HRP activity, since enzymatic removal of the sugar residues yields active protein (Tams and Welinder, 1995). Additionally, HRP can be expressed in *E. coli*, yielding the unglycosylated protein (Smith *et al.*, 1990). The resulting recombinant protein is found in the form of inclusion bodies but can be refolded to produce the fully active enzyme. This refolding process requires urea and glutathione to solubilize the protein and disrupt incorrectly bridged disulfide bonds. HRP has also been expressed through baculovirus methods in cultured *Spodoptera frugiperda* (Sf9) cells (Hartmann and Ortiz de Montellano, 1992). This expression system advantageously generates a soluble recombinant protein that is properly folded and fully functional. Like the plant enzyme, the baculovirus-expressed protein is glycosylated. However, different oligosaccharide processing between plant and insect species yields recombinant protein from insect cells that displays simpler glycosylation patterns than found in the plant protein.

Insect cells, like plant cells, cotranslationally link $Glc_3Man_9GlcNAc_2$ structures to the side chain nitrogen atom of the asparagine residue found in the sequence Asn-X-Ser/Thr (Kornfeld and Kornfeld, 1985). This event yields the structure $Glc_3Man_9GlcNAc_2$-Asn. Processing of these oligosaccharide structures in plants includes trimming and modification events. Thus, a heterogenous pool of HRP is isolated from the plant, which displays glycosylation that differs in the eight glycosylation sites within and between protein molecules (Harthill and Ashford, 1992; Welinder, 1985). Insect oligosaccharide processing is simpler and only involves trimming events.

Correspondingly, the initial $Glc_3Man_9GlcNAc_2$-Asn structure is typically truncated to $Man_{(3-9)}GlcNAc_2$-Asn (Hsieh and Robbins, 1984; Butters and Hughes, 1981; Butters et al., 1981). Thus, insect cells produce a simpler heterogenous pool of HRP that is characterized by varying degrees of trimming between glycosylation sites.

In order to probe peroxidase activity with mutagenesis studies, baculovirus techniques were used to generate a series of HRP mutants. The baculovirus/insect cell expression system was implemented because this system generated properly folded, soluble, and fully active recombinant wild-type (rWT) protein (Hartmann and Ortiz de Montellano, 1992). In order to facilitate purification of these mutants, a sequence encoding a polyhistidine tag was appended to the 5' end of the HRP gene. The genetic construction, expression, purification and initial characterization of these polyhistidine-tagged mutants are described below.

MATERIALS AND METHODS

Tissue Culture. Sf9 cells were maintained in spinner flasks at 27°C (75 rpm) with 90% Hink's TNM-FH insect cell media supplemented with Grace's media (JRH Biosciences) and 10% fetal calf serum, heat-inactivated, 0.2 μm filtered (UCSF Cell Culture facility). *Trichoplusia ni* cells (*T. ni*) (Invitrogen) were maintained in suspension in Sf900-II SFM (Gibco BRL) in a rotary shaker incubator at 27°C (130 rpm).

Site-Directed Mutagenesis and Subcloning. Plasmids were transformed into and maintained in *E. coli*, strain DH5α, grown in LB. Transformed vectors were selected by ampicillin resistance. Plasmid preparation was afforded through Qiagen mini-preps or Promega Wizard mini-preps. Plasmid fragments from restriction enzyme digests were typically isolated by electrophoresing the digest on an agarose gel and extracting the DNA with a gel extraction kit (USB Glass Beads or Qiagen gel extraction kit). DNA sequencing was carried out with either the sequenase kit, version 2.0 (USB) or was performed by the

Biomolecular Research Center (BRC) at UCSF. The construct pUC-HRP, containing a synthetic version of the HRP gene that is cloned into pUC19 (British Biotechnologies, Ltd.) was used for subcloning and site-directed mutagenesis. To append an N terminal polyhistidine tag-encoding sequence found in the pET-19b vector (Novagen) to the 5' end of the HRP gene, the HRP gene was isolated from pUC-HRP by *Nde I*/*EcoR* I digestion

Polyhistidine tag sequence encoded by the pET-19b vector:

CCATGGGC $(CAT)_9$ CACAGCAGCGGCCATATC $(GAC)_4$ AAGCA
GTACCCG $(GTA)_9$ GTGTCGTCGCCGGTATAG $(CTG)_4$ TTCGTATAC

and subcloned into pET-19b, yielding pET-HRP (Figure 2.1). The polyhistidine tagged HRP-encoding insert was subsequently subcloned into the baculoviral vector, pACGP67B (PharMingen). This vector encoded a sequence for the GP67 leader sequence at the 5' end of the multiple cloning site, targeting the translated HRP gene product for secretion. *Nco* I digestion of the pET-HRP construct yielded a fragment containing the polyhistidine sequence and a portion of the HRP sequence. This fragment was ligated into *Nco* I cut baculoviral vector pACGP67B (Figure 2.1). The isolated plasmid containing the correctly oriented gene fragment (GPhisHRP NcoFragA) was used as the construct for introducing *Sac I*/*EcoR* I cut pUC-HRP, restoring the full length of the HRP gene. *Sac I*/*EcoR* I fragments from mutated pUC-HRP were also ligated into the baculoviral vector in this manner.

pUC-HRP mutants were generated through cassette mutagenesis. Sense and antisense oligonucleotides, corresponding to the region of interest within the HRP gene, were synthesized by the BRC. Individual cassettes were generated for each mutation as outlined in Table 2.1. The annealed cassette was ligated to *Nde I*/*Sac* I or *BspE I*/*BstE* II cut pUC-HRP, and the resulting mutant was subcloned into *Sac I*/*EcoR* I digested GPhisHRP NcoFragA, as outlined above.

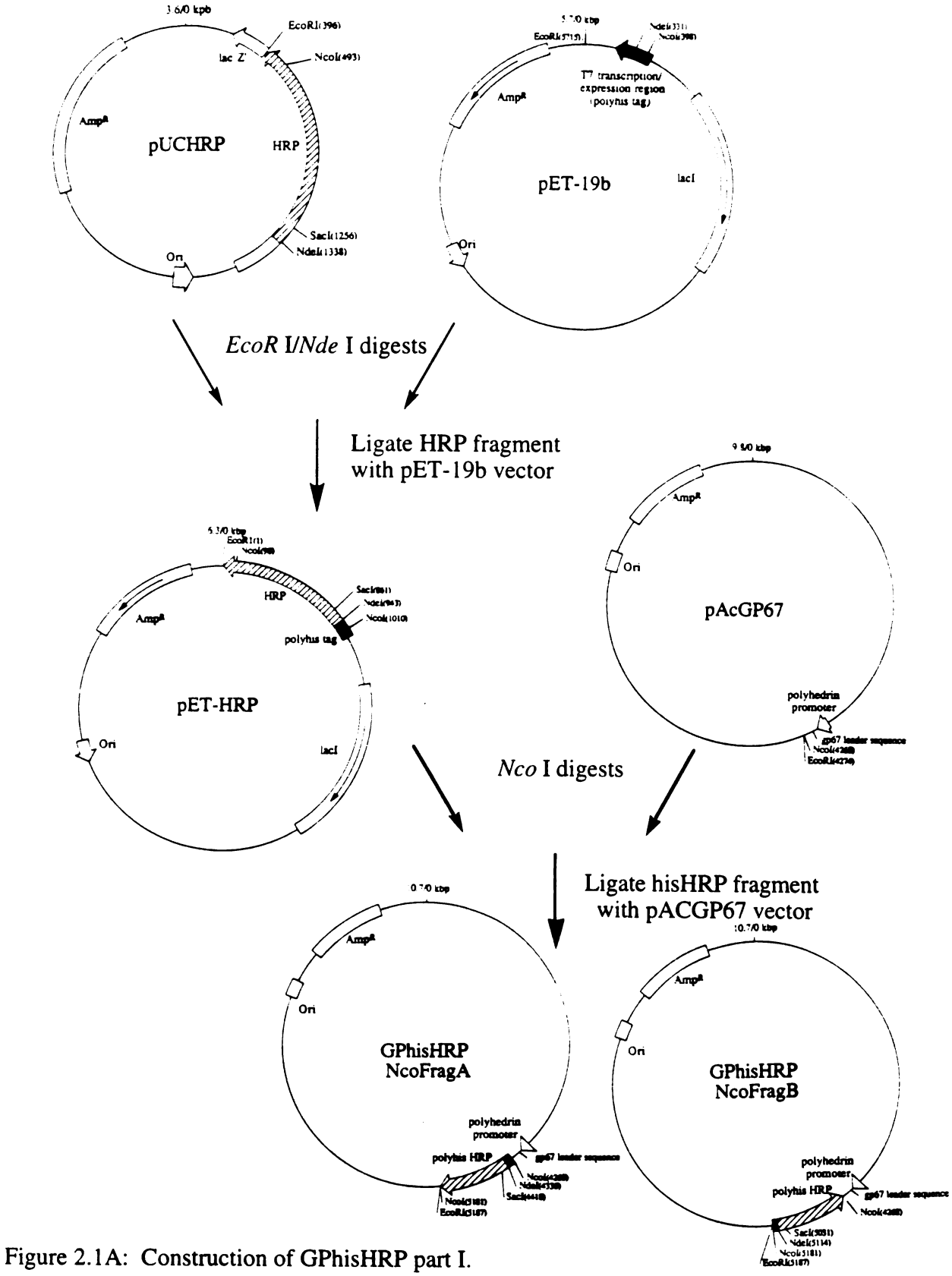

Figure 2.1A: Construction of GPhisHRP part I.

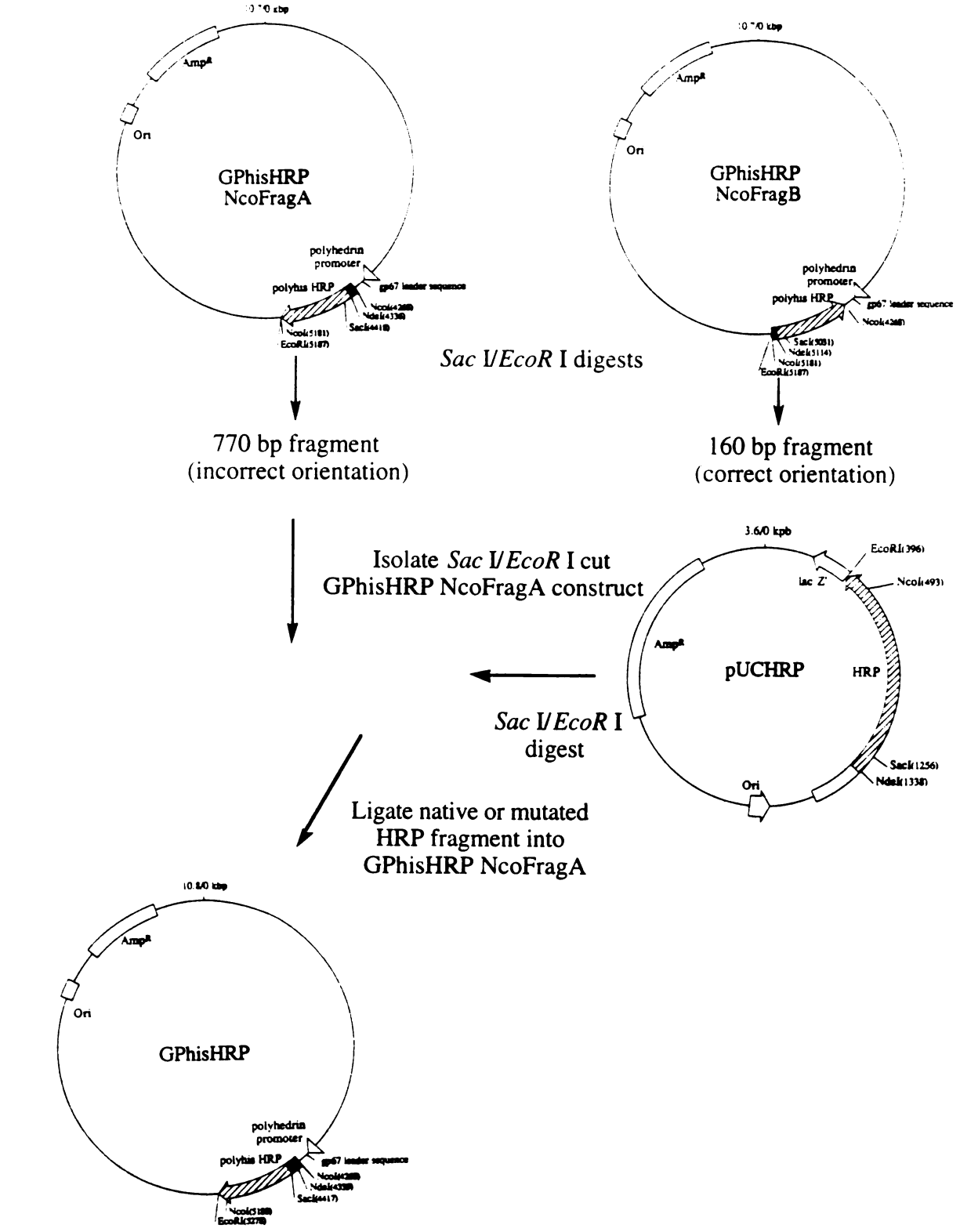

Figure 2.1B: Construction of GPhisHRP part II.

Table 2.1: The oligonucleotides used for cassette mutagenesis contained the indicated mutation-yielding codon and were flanked by the listed restriction sites. Selection of these restriction sites was based on their uniqueness within the pUC-HRP construct.

HRP Mutation	Codon Substitution	Flanking Restriction Sites
H42A	CAT → GCT	*Nde* I/*Sac* I
H42V	CAT → GTT	*Nde* I/*Sac* I
F41A	TTC → GCT	*Nde* I/*Sac* I
H170A	CAC → GCC	*BspE* I/*BstE* II

Production of Recombinant Virus. Recombinant virus production, purification, and amplification were performed in Sf9 cells. The sequence encoding polyhistidine-tagged HRP was introduced into the wild-type virus, *Autographica californica* nuclear polyhedrosis virus, with the Baculogold transfection kit (PharMingen). The resulting transfection media was isolated by centrifugation (1000 x g, 10 min) and subjected to one round of plaque purification. Plaques which represent infection by a single virus particle were individually isolated and mixed with 1 ml complete media. Viral amplification of this initial stock was afforded through successive rounds of infection. To begin amplifying the virus for expression purposes, a 900 µl volume was used to infect a monolayer of Sf9 cells in a 60 mm petri dish (10^6 cells/ml, 3 ml final volume). After 4 days incubation, the media was isolated through centrifugation (5 min, 1,000 x g), and the presence of the HRP insert in the viral DNA was verified by PCR. In a second round of amplification, 250 µl of this viral stock was used to infect a monolayer of Sf9 cells seeded on a 100 mm petri dish (5 x 10^6 cells, 10 ml final volume). After incubating the cells for 4 days, the media were

harvested by centrifugation as above. A final round of amplification used 500 µl of this latter viral stock to infect 100 ml of Sf9 in suspended culture (2 x 10^6 cells/ml). After a three day incubation the media were harvested by centrifugation. This series of amplification steps gave a viral stock with a viral titer of 1-3 x 10^8 pfu/ml. Expression was performed in *T. ni* cells. Typically a 1 L culture of cells (1.5-2 x 10^6 cells/ml) was inoculated with virus (MOI ~1). A 10 ml volume of 0.2 µm filtered hemin/BSA solution (0.24 mM hemin, 0.4 mM BSA, in 75 mM Na_2HPO_4, pH 7.2) was added at the time of inoculation (Tenhunen, 1968). The expression media were harvested after 60-64 hr.

Protein Purification. The expression media were separated from the cells by centrifugation (1000 x g, 10 min). The supernatant was concentrated and ultrafiltrated at room temperature with an Amicon Spiral-Wound Cartridge Concentrator CH2PRS (S1Y10, 10,000 MW cutoff spiral membrane) to a 150-200 ml volume in 20 mM Na_2HPO_4, 500 mM NaCl, pH 8.0 (binding buffer). Particulate material was removed from the ultrafiltrate by centrifugation (17,000 x g, 30 min). The supernatant was stirred with 7.5-10 ml nickel-chelated resin, Ni(II) nitrilotriacetic acid resin (Ni(II)NTA) (Qiagen), at 4°C. This resin is strongly bound by polyhistidine sequences which chelate the Ni(II) atoms associated with the column. After 1.5-2 hr, the resin was collected in a 1.5 cm diameter column support. The resulting column was washed with binding buffer at 75 ml/min until the eluant ran clear. In a similar manner the resin was successively washed with binding buffer adjusted to pH 6.0 and containing 0, 0.1 and 1 M imidazole. The 1 M imidazole wash was dialyzed against 20 mM Na_2HPO_4, pH 8.0. The dialysate was run through a 1.5 cm x 10 cm Pharmacia Sepharose QFF column (flow by gravity). The eluant was dialyzed against 20 mM Na_2HPO_4, pH 7.0. The total amount of protein was measured after each purification step with the Bradford assay (Bio-Rad), using known amounts of bovine serum albumin as the standards (Bradford, 1976).

Guaiacol Assay. Guaiacol activity was measured to monitor the rWT activity during purification. Sample activity was determined spectrophotometrically at 20°C (ε_{470} = 2.76 $cm^{-1}mM^{-1}$). Enzyme (~10 pmol) was mixed with 5.1 mM guaiacol in 20 mM Na_2HPO_4, pH 7.0 (1 ml final volume). H_2O_2 (0.5 mM, final) was added to initiate the reaction.

Thermal Stability of Wild-Type and Mutant Proteins. The wild-type and mutant enzymes were incubated overnight at 4, 37, 40, 45, 50, and 55 °C. Loss of activity was monitored with the guaiacol assay as described above. Changes in the Soret absorbance, reflecting loss of the heme group, were also monitored spectrophotometrically.

pH Profile for Native-, rWT-, and F41A-HRP. Guaiacol activity was assayed as described above, substituting 25 mM buffers of varying pH. Acetate buffer was used for assays at pH 4-5.5 and phosphate buffer for assays at pH 6-8. NaCl was added to maintain constant ionic strength (0.1 M).

RESULTS

Purification of Recombinant, Polyhistidine-Tagged Wild-Type and Mutant HRP Proteins. Recombinant HRP mutants lacking the polyhistidine tag could not be purified by the conventional methods used to purify native and baculovirus-expressed rWT HRP (Shannon *et al.*, 1966; Hartmann and Ortiz de Montellano, 1992). A polyhistidine tag was added at the N terminus of recombinant HRP to facilitate purification. The following specific activities and RZ values were obtained after each purification step. The Ni(II) NTA resin afforded rapid purification of the expressed protein, purifying rWT HRP by a factor of 351 fold. The 0.1 M imidazole wash was necessary to elute contaminants from the column. Unfortunately, a significant amount of HRP also eluted at this imidazole concentration, lowering the yield. In the expression of the HRP mutants, protein loss

Table 2.2: Purification profile for rWT HRP. Harvested media refers to the expression media obtained 60 h post infection and was isolated from the cells through centrifugation. Concentrated media is the ultrafiltrated, harvested media. Ni(II) NTA pertains to the pooled fractions eluted from the Ni(II) NTA column with 1 M imidazole. Sepharose-QFF refers to the pooled fractions that eluted from this resin. Quantitation of protein was achieved through the Bradford assay. The guaiacol assay described in the methods was used to measure activity.

Enzyme	Total mg Protein	Specific Activity ($\mu M\ s^{-1}\ mg^{-1}$)	RZ Value	Activity Yield(%)	Purification Factor
harvested media	420.0	2.0	0.05	100	1x
concentrated media	406.4	12.8	0.23	100	6.4x
Ni(II)NTA	11.1	4496.4	1.94	33	2248x
Sepharose-QFF	5.1	8365.2	2.88	33	4182x

occurred to a lesser extent. The major remaining contaminant, BSA, was removed with the Sepharose QFF column. The overall yields of the expressed proteins ranged between 5 and 20 mg per 1 L of expression media. The RZ value, (A_{403}/A_{280}), compares the absorption of the heme Soret to that of the protein and is used to gauge heme content. One molecule of heme binds to one molecule of apoprotein and good preparations from the plant display RZ values ranging from 3.0 to 3.4. With the exception of the His 170 mutants, the purified mutants were obtained with significant RZ values (~2.5-3.4), indicating that the majority of the purified protein contained heme. N terminal sequencing afforded the

sequence, ADLGS, which corresponds to the beginning of the multiple cloning site of the pACGP67B vector. This indicated that removal of the pACGP67B baculoviral secretion sequence had occurred.

Reconstitution of H170A HRP. H170A HRP was purified to greater than 95% purity on the Ni(II) NTA resin, based on SDS PAGE. However, the spectra of the protein thus obtained showed that the major form isolated was the apoprotein (> 90%). It is difficult to say whether the protein loaded onto the Ni(II) NTA column was fully reconstituted. However, it is likely that some heme was stripped from the protein during purification because heme was observed to leach slowly from the column during the pH 5 wash. The Sepharose QFF column was not used with H170A HRP because the Ni(II) NTA-isolated protein was of sufficient purity. The mutant was reconstituted in Na_2HPO_4 by the addition of 1 equivalent of hemin. The reconstitution was performed at pH 4 to minimize heme binding by the polyhistidine tag. After 30 min, the protein was brought to pH 6.0. The bound heme was judged to be specifically bound to the heme pocket based on the finding that the Soret band of the reconstituted protein was not decreased by running the protein through BSA-bound Sepharose (Bio-Rad). Nonspecifically bound heme would have been removed by binding to BSA and would have resulted in a reduction of the RZ value of the eluted mutant. Heme content was determined using the pyridine hemochromogen assay (Furhop and Smith, 1975). The concentration of H170A HRP indicated in the experiments that follow refers to the level of holoenzyme present. Typical yields of ~20 mg/L of expression media were obtained, based on the Bradford assay (Bradford, 1976). This is characteristic of the yields obtained for the distal mutants. After reconstitution, ~80% of H170A HRP was obtained as the holoenzyme form.

Guaiacol activity of wild-type proteins. rWT HRP displays guaiacol activity that is markedly similar to that of native HRP (Table 2.3). F41A HRP also displays native-like activity, while the distal and proximal histidine mutants display markedly decreased peroxidase activity.

Table 2.3: Guaiacol consumption measured for wild-type and mutant proteins. The assays were performed in duplicate, with the exception of H170A HRP. The reported error represents the deviation obtained upon averaging two measurements.

Enzyme	Guaiacol Activity (mol $s^{-1}mol^{-1}$)
Native	$1.6 \pm 0.6 \times 10^{3}$
rWT	$1.5 \pm 0.4 \times 10^{3}$
F41A	$2.0 \pm 2.0 \times 10^{3}$
H42A	$2.1 \pm 0.0 \times 10^{-2}$
H42V	$2.3 \pm 0.5 \times 10^{-2}$
H170A	3.6×10^{-2}

pH Profiles for Native-, rWT-, and F41A-HRP. Figure 2.2 shows the influence that pH has on native-, rWT-, and F41A-HRP guaiacol activity. rWT HRP behaves in the same manner as native HRP. F41A HRP displays a similar but not identical profile. The pH profiles for the distal and proximal histidine mutants are presented later (Chapters 5 & 6).

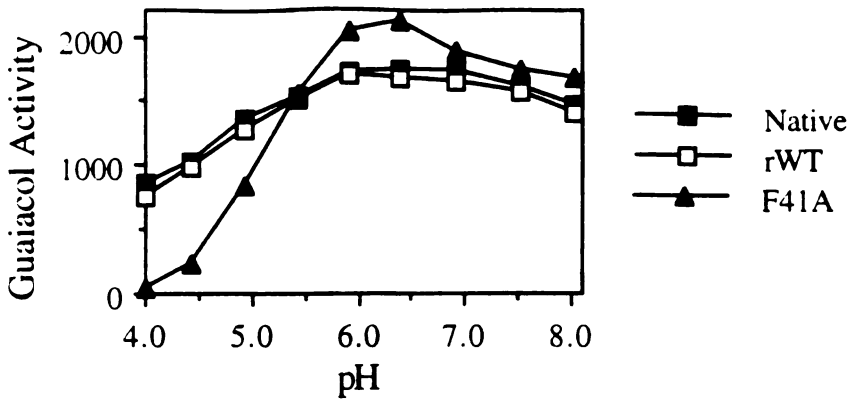

Figure 2.2: pH profile for the peroxidase activity of native-, rWT-, and F41A-HRP (5 nM final enzyme concentration). The units for guaiacol activity are mol s^{-1} mol^{-1}.

Thermal Stability of Wild-Type and Mutant Proteins. Figures 2.3 and 2.4 show the influence of temperature on the expressed proteins. All of the proteins examined displayed similar losses in RZ value at temperatures exceeding 45 °C. In a similar manner, the activities of native-, rWT- and F41A-HRP drop off with increasing temperature. The activities of the distal histidine mutants deviate by actually increasing as the temperature is raised above 45 °C.

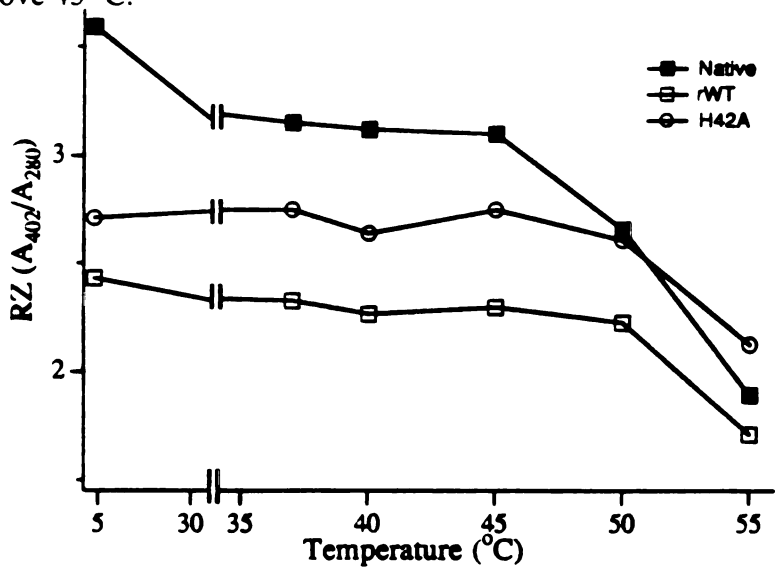

Figure 2.3: Influence of temperature on the RZ values for native-, rWT- and H42A-HRP. F41A- and H42V-HRP are not shown, but display similar loss of heme to that of native- and H42A-HRP, respectively. The spectra were monitored at 20 °C.

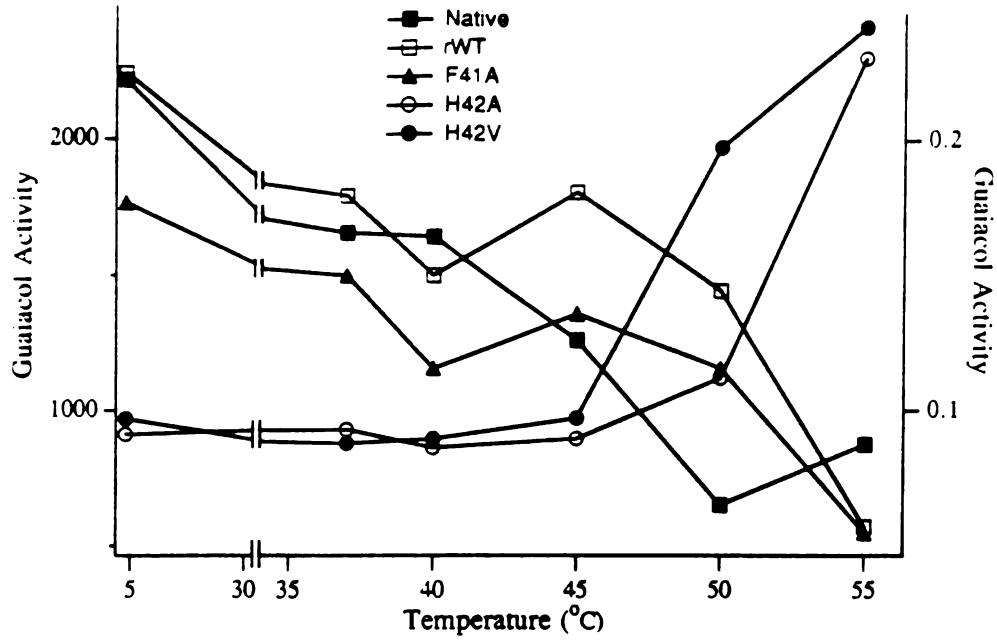

Figure 2.4: Influence of temperature on guaiacol activity of wild-type and mutant HRP proteins. The units for guaiacol activity are mol s^{-1} mol^{-1}. An aliquot of protein incubated at the indicated temperature was assayed for guaiacol activity at 25 °C. The left axis refers to the activities of native-, rWT-, and F41A-HRP activity. The right axis refers to the activities of the distal histidine mutants.

DISCUSSION

rWT HRP exhibited native-like behavior with respect to the oxidation of guaiacol and the pH dependence of guaiacol oxidation. This suggests that rWT peroxidase activity is unaffected by either the N terminal polyhistidine tag or the differing glycosylation pattern resulting from expression in insect cells. Attempts were made to remove the polyhistidine tag through enzymatic digestion at the enterokinase cleavage site encoded by the pET-19b vector. The inability to remove the tag may be due to partial burial of the enterokinase site within HRP which makes it inaccessible. The polyhistidine tag was therefore left intact and did not appear to interfere with the activity of the protein. The activities of the mutant proteins are discussed in Chapters 4, 5, and 6.

The thermal stability of rWT HRP also matched that of native HRP. The decrease in RZ value observed with increasing temperature corresponded to a loss in the Soret absorbance which is indicative of loss of bound heme. The similar profiles observed for the proteins suggest that the affinity for heme is the same for the recombinant and native proteins. This supports the conclusion that the polyhistidine tag and the altered glycosylation pattern do not significantly alter peroxidase behavior. Increasing temperature also causes the activity to drop slowly in a manner that roughly resembles the decrease in RZ value seen with increasing temperature. This is consistent with reduced activity at elevated temperatures arising from generation of the apoenzyme or some other partially denatured inactive species. These findings again show that the native and rWT proteins are functionally identical.

F41A HRP also exhibits native-like peroxidase activity and thermal stability, suggesting that removal of the distal phenyl group does not significantly influence peroxidase function. The pH profile generated for F41A HRP is similar to that of the native protein but demonstrates that the mutant is less stable at lower pH values. A more detailed examination of the F41A mutant is made in Chapter 4.

The RZ values of the expressed proteins ranged from 2.5 to 3.4, indicating that the holoenzyme was the major form isolated (> 75%). The RZ values reported for the recombinant proteins at 4.0 °C are decreased from that of the native enzyme. These lower RZ values could reflect weaker affinity of the recombinant proteins for heme; however, multiple purifications of these proteins have shown that an increased RZ is observed when the recombinant proteins are purified rapidly. Improved RZ values (> 3) were obtained when the recombinant proteins were purified within a 2 day period, starting from harvesting of the expression media and ending with elution of the pure protein from the Sepharose QFF column.

Interestingly the distal histidine mutants display higher activity upon incubation at higher temperatures. It was also found that storing these mutants at pH 8 for two weeks at 4 °C caused a 50 fold improvement in their guaiacol activities. The time-dependent and quantitative stimulation of the activities exhibited by these distal histidine mutants suggests that the originally purified protein may undergo a structural change that promotes peroxidase activity. Deamidation is a frequent degradation event in proteins and offers a possible explanation for the proposed structural change. An asparagine residue found within a Gly-Asn-Ala sequence is positioned adjacent to the distal histidine and arginine residues which contact the distal face of the heme. This asparagine residue, Asn70, forms a hydrogen bond with the distal histidine (see Introduction) (Figure 2.5). Removal of this

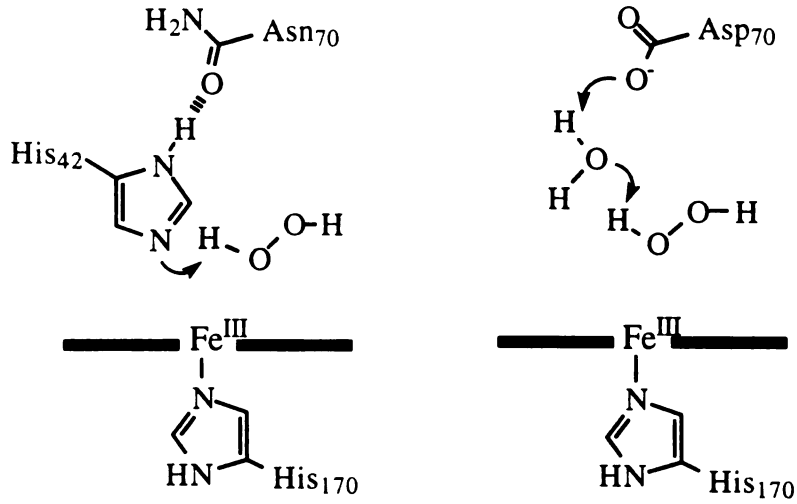

Figure 2.5: Proposed role of deamidated Asn 70 in the generation of Compound I. The resulting carboxylate group could deprotonate the peroxide molecule, generating the peroxide anion in a manner that is similar to the distal histidine in the native protein. This figure shows the deamidated Asn 70 (Asp 70) to deprotonate the peroxide molecule indirectly through a water molecule. The generation of the peroxide anion in the vicinity of the heme iron would promote the formation of Compound I.

hydrogen bond through mutagenesis could feasibly increase the flexibility of the asparagine side chain allowing the cyclization event that leads to deamidation (Aswad, 1994). Several asparagine residues, 27 total, are found throughout the HRP sequence (Welinder, 1992a), but deamidation of Asn 70 is likely to influence activity, given its conspicuous proximity to both the site of the mutation and the heme pocket. This theory could be tested by characterizing the double mutant, H42A/N170D HRP (Figure 2.5).

Regardless of the nature of the activity-influencing changes observed in the distal histidine mutants, the activity level of the initially purified protein could be stabilized by storing these proteins at neutral to slightly acidic conditions. The characterization of the distal histidine mutants, that follows in Chapters 4 and 5, was performed on proteins that were stored at pH 6 or 7.

CONCLUSIONS

Baculovirus-mediated expression of HRP in insect cells is suitable for generating HRP, a heavily glycosylated protein that requires expression in an oxidizing environment to promote disulfide bond formation. Introducing a polyhistidine tag at the N terminus of HRP facilitates rapid purification of the recombinant protein without altering peroxidase activity or stability. The overall yields obtained for the purified recombinant wild-type and mutant proteins range from 5 to 20 mg protein/L expression media. These initial studies also show that F41A HRP demonstrates native-like peroxidase activity and that the distal and proximal histidine mutants display drastically reduced peroxidase activity. The impact of mutating Phe 41, His 42, and His 170 is explored further in the following chapters.

Chapter 3: Characterization of HRP-Catalyzed Oxidation of Iodide: A Comparison of Iodide with Guaiacol and Thioanisole Substrates

INTRODUCTION

Peroxidases as a class of enzymes are remarkable in their ability to oxidize a diverse range of chemically distinct substrates. Classic substrates include phenols and anilines, which are oxidized by one electron. Accordingly, two molecules of these substrates are required to fully reduce Compound I to the resting state, with the generation of Compound II as an intermediate (Figure 3.1). The reduction of Compound II is typically ~40 fold

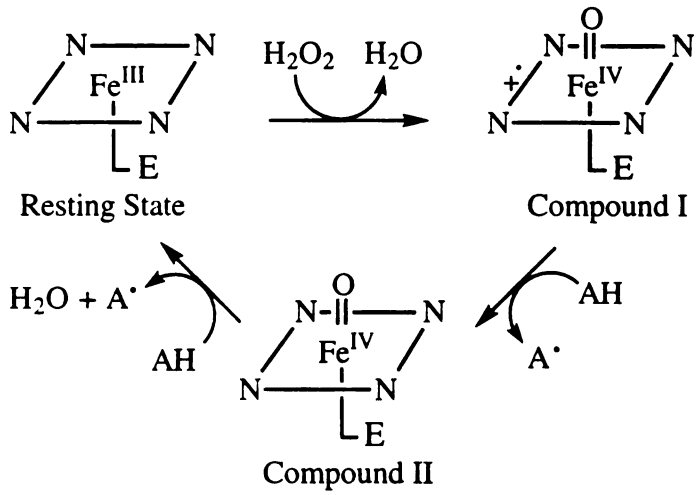

Figure 3.1: The catalytic cycle of HRP in the oxidation of classic aromatic substrates like guaiacol. The resting state enzyme reacts with peroxide in the formation of Compound I. Compound I is reduced to Compound II with the abstraction of an electron from a substrate molecule (AH). Compound II is reduced to the resting state with the abstraction of an electron from a second substrate molecule.

slower than the reduction of Compound I (Marnett *et al.*, 1986). This makes the reduction of Compound II the rate limiting step, and correspondingly, the spectrum of Compound II is observed in the steady state oxidation of classic substrates. Electron abstraction is

postulated to occur at the δ-*meso* heme edge. This is based on mounting evidence that shows aromatic substrates to interact exclusively at this edge. Reaction of HRP with phenylhydrazine produces arylation of the protein as well as two modified hemes, 8-hydroxymethylheme and δ-*meso*-phenylheme (Figure 1.7) (Ator and Ortiz de Montellano, 1987). This outcome deviates significantly from the phenyl-iron complex that is formed upon reaction of phenylhydrazine with myoglobin (Ringe *et al.*, 1984), catalase (Ortiz de Montellano and Kerr, 1983), and cytochrome P450 (Jonen *et al.*, 1982). To reconcile these differences between HRP and the other hemoproteins, the heme iron within the peroxidases was speculated to be inaccessible to modifying reagents and substrates. The finding that modification was restricted to the δ-*meso* heme edge suggested that this was the site where electron abstraction and phenylhydrazine activation occurred. Additional modification studies further probed substrate accessibility to the heme molecule by reacting HRP with smaller alkylhydrazines, namely ethylhydrazine and methylhydrazine (Ator *et al.*, 1987). These reactions also result in alkylation of the δ-*meso* heme position. Reconstitution of HRP apoenzyme with δ-*meso*-ethylheme renders HRP unable to oxidize guaiacol (2-methoxyphenol) (Ator *et al.*, 1987). This reconstituted protein, however, binds guaiacol 2.8 fold better than the unmodified enzyme (Harris *et al.*, 1993), suggesting that the ethyl group inhibits guaiacol activity by deterring electron transfer through the heme edge rather than by sterically hindering substrate binding.

NMR studies support the chemical modification studies by positioning HRP-bound aromatic molecules within 5 Å of the 8-methyl group of the heme in the resting state enzyme. The protons of the substrate aromatic ring are equally distanced from the heme iron, leading to the prediction that the plane of the aromatic ring faces the heme iron (Figure 3.2) (Sakurada *et al.*, 1986; Morishima and Ogawa, 1979). NMR and optical difference spectroscopy studies of substrate binding have also been performed on the cyanide-ligated HRP, a six coordinate species in which the iron ligation state resembles that of Compound

I and Compound II (Hosoya *et al.*, 1989; Morishima and Ogawa, 1979). These studies show aromatic molecules to bind cyanide-ligated HRP with similar affinities and positioning relative to that of the five coordinate resting state enzyme. These findings suggest that movement of the iron into the plane of the heme, which occurs with formation of six coordinate species, does not drastically alter substrate binding. In support of these NMR studies, the crystal structures of CCP, LIP, ARP, and PeP also show the δ-*meso* heme edge, specifically the 8-methyl group and the δ-*meso* heme position, to be the only region of the heme molecule that is accessible to substrates (Finzel *et al.*, 1984; Poulos *et al.*, 1993; Kunishima *et al.*, 1994; Patterson and Poulos, 1995).

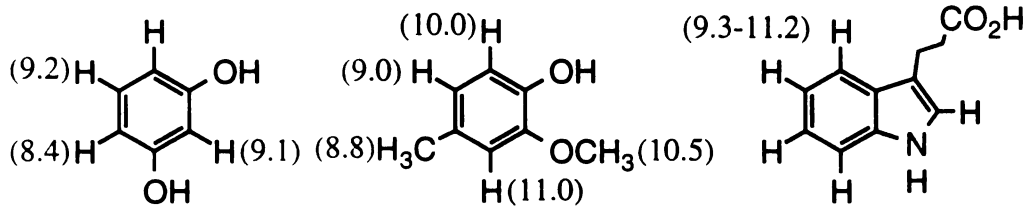

Resorcinol 2-Methyoxy-4-methylphenol Indole-3-propionic acid

Figure 3.2: NMR-estimated distances between the iron atom of resting state HRP and the hydrogen atoms of various bound substrates. The numbers in parenthesis correspond to the distance, measured in Å, that was determined from relaxation data.

There also exists a category of substrates that are oxidized by two electrons. These substrates include iodide (Roman and Dunford, 1972), thiocyanate (Modi *et al.*, 1991), thioanisole (Kobayashi *et al.*, 1986; and Kobayashi *et al.*, 1987), and sulfite (Roman and Dunford, 1973). Unlike the classic aromatic HRP substrates, Compound I is observed in the steady state turnover of these two electron-oxidized substrates. Mechanistically this suggests that either 1) during the two sequential single electron abstraction steps the reduction of Compound II is faster than that of Compound I (the reverse of classic substrate oxidation) or 2) a direct two electron transfer occurs (Figure 3.3).

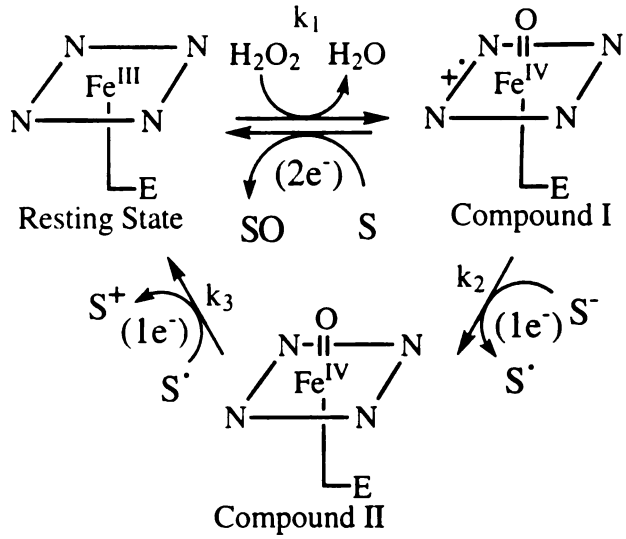

Figure 3.3: Catalytic cycle for the HRP-catalyzed oxidation of two electron-oxidized substrates. Oxidation is postulated to occur either through a direct two electron transfer ($2e^-$), reducing Compound I to the resting state, or through two single electron transfer steps with $k_2 < k_3$ ($1e^- + 1e^-$).

The first mechanism is supported by studies of iodide oxidation as catalyzed by LIP. Iodide oxidized by LIP has been postulated to mediate the one electron oxidation of EDTA (Shah and Aust, 1993). The resulting EDTA radical was detected by EPR and was only formed in the presence of iodide or known electron transfer mediators such as veratryl alcohol (Shah *et al.*, 1992; Shoemaker, 1990). These authors speculate that EDTA reduces the iodide radical generated by LIP. Consistent with this proposal, Compound II was observed in the steady state turnover of LIP-catalyzed oxidation of EDTA in the presence of iodide. The altered kinetics exhibited in the first mechanism may be influenced by the inability of the two electron oxidizable substrates to donate a proton to the distal histidine. As described in the introduction, a proton is taken up by the protein in the reduction of Compound I to Compound II, and concomitantly, the ferryl oxygen becomes hydrogen bonded to a distal residue. This residue is postulated to be the distal histidine. In the

oxidation of the two-electron-oxidized substrates, Compound I reduction may be delayed while the distal histidine draws a proton from solution.

In the second mechanism, the simultaneous transfer of two electrons would be most readily afforded through transfer of an oxygen atom, namely the ferryl oxygen. This oxygen transfer event is characteristic of P450s and is postulated to be mediated by substrate accessibility to the ferryl oxygen. Peroxidases do not typically catalyze peroxygenase reactions since the Compound I ferryl oxygen is largely inaccessible in these proteins; however, HRP is able to sulfoxygenate thioanisole. Labeling studies have shown that the oxygen in thioanisole sulfoxide is derived from H_2O_2, and therefore from the ferryl oxygen (Kobayashi *et al.*, 1986). In a manner that is typical of peroxidases, an electron is initially abstracted from thioanisole, leaving a sulfur radical cation which is postulated to combine with the ferryl oxygen with concomitant reduction of the iron atom (Figure 1.15). This mechanism is supported by the observed correlation between the oxidation potentials of a range of thioanisole derivatives and the rate of their sulfoxidation which is consistent with formation of positive charge in the transition state (Kobayashi *et al.*, 1986; and Kobayashi *et al.*, 1987). The transient formation of Compound II has also been detected in the reaction of HRP Compound I with 1-methoxy-4-methylthiobenzene (Pérez and Dunford, 1990). It has been postulated that thioanisole must bind near the ferryl oxygen in order for oxygen transfer to occur. Consistent with this theory, reconstitution of HRP with δ-*meso*-ethylheme does not inhibit thioanisole activity, suggesting that thioanisole and guaiacol interact with two distinct regions of the heme pocket.

Thioanisole is the only known two electron-oxidized substrate that retains the ferryl oxygen. Other substrates like iodide may similarly react with HRP to yield the oxygenated hypoiodous acid (IO^-), but detection of this product is difficult because the oxygen is rapidly displaced by iodide, sequentially generating I_2 and I_3^-. In the oxidation of [Cl^{35}] NaCl by MPO, [Cl^{35}] NaOCl was trapped as a product, supporting an oxygen transfer

mechanism for chloride oxidation (Harrison and Schultz, 1976). By analogy to MPO-catalyzed chloride oxidation, HRP-catalyzed iodide oxidation has been proposed to occur through oxygen transfer. Consistent with this proposal, iodide binding is distinct from that of resorcinol, a scenario that is reminiscent of the different binding sites proposed for guaiacol and thioanisole. NMR studies demonstrate that within HRP iodide binding does not displace resorcinol from the δ-*meso* heme edge (Sakurada *et al.*, 1987). The following studies characterize iodide oxidation relative to guaiacol and thioanisole oxidation. This comparison between HRP substrates is made to elucidate the mechanism of iodide oxidation and to provide insight into the determinants that control heme reactivity.

METHODS

Determination of Difference Spectra for Guaiacol, Iodide and Thioanisole Binding to HRP. Difference spectra were obtained with an SLM Aminco DW2000 UV/Vis spectrophotometer. To generate a difference spectrum, a pair of matched cuvettes were filled with 1 ml of 10 μM native HRP (Boehringer Mannheim) in 50 mM sodium acetate (pH 5.25). Acidic conditions were used because iodide binds with higher affinity as the pH is lowered. Difference spectra were generated for the three substrates by adding varying amounts of substrate to one cuvette and adding an equal volume of water (or methanol in the case of thioanisole/methanol stock solution) to the reference cuvette. The following substrate concentrations were used: a) 10, 20, 30, 40 μM potassium iodide; b) 0.5, 0.6, 0.75, 1.0, 1.25 mM thioanisole; c) 50, 100, 150, 200, 500 nM guaiacol and d) 1, 2, 5, 10, 20 mM guaiacol. The K_d values for substrate binding were determined by fitting the substrate concentrations and corresponding absorption changes to Equation 3.1.

$$\frac{1}{[S]} = \frac{[E]\,\Delta\varepsilon}{K_d\,\Delta A} - \frac{1}{K_d} \qquad \text{(Eqn 3.1)}$$

To determine whether iodide could displace enzyme-bound guaiacol, iodide (340, 680, 1020 μM final concentration) was added to both the cuvettes used to determine the

difference spectra for guaiacol (10 mM final concentration) binding. In a similar manner, the ability of iodide to displace enzyme-bound thioanisole was studied by adding iodide (340, 680 μM) to each of the cuvettes used to generate the thioanisole (1.5 mM) difference spectrum.

Preparation of δ-Meso-ethylheme and δ-Meso-methylheme. Selective alkylation of the δ-*meso* heme edge was achieved through reaction of HRP-bound heme with ethyl- and methylhydrazines (Ator *et al.*, 1987). The ethylation reaction mixture contained 160 nM HRP (Boehringer Mannheim) and 200 μM ethylhydrazine in 3 ml of 500 mM Na_2HPO_4, pH 7.0. Modification was initiated by the addition of 6.6 μmol H_2O_2. Over a period of a few minutes three additional 6.6 μmol aliquots of H_2O_2 were added, giving an 8.8 mM final concentration. The reaction proceeded for at least 1 h in the dark at room temperature with continual stirring. Excess reagents were removed with a G25 Sephadex column (20 ml hydrated gel, 20 x 1.3 cm^2). Heme was isolated by acidifying the eluted protein with acetic acid (25% v/v acetic acid/final solution) to bring the pH below 4. The acidified solution was extracted with three 1 ml volumes of ether. Alkylated heme was purified from unmodified heme by reverse phase HPLC using a Whatman partisil 10 ODS-3 column (68:32:1 0.1MeOH:H_2O:HOAc, 4 ml/min). The eluant containing δ-*meso*-ethylheme was collected and evaporated to dryness.

δ-*Meso*-methylheme was similarly generated by reaction of methylhydrazine with HRP. For optimal yields, the methylation reaction was stirred for 20 min, and the modified heme was isolated via HPLC using 64:36:1 0.1MeOH:H_2O:HOAc.

Preparation of HRP Apoprotein. In order to prepare functional apoenzyme, an HRP solution (10-15 mg in 1-2 ml H_2O) was acidified (pH<4) by dropwise addition of 0.1 N HCl. Heme was partitioned away from the protein with four 2 ml 2-butanone washes. Residual 2-butanone was removed from the aqueous apoenzyme preparation by dialyzing against 2 L H_2O for 2 h followed by overnight dialysis against 2 L 0.01 M borate buffer,

pH 9.0. The protein concentration of the dialyzed solution was determined with the Bradford assay (Bio-Rad).

Reconstitution of Alkylated Hemes with Apoprotein. The δ-*meso*-ethylheme obtained above was dissolved in a minimal amount of 0.01 N NaOH. This suspension was added dropwise to 1 mg apoprotein in borate buffer on ice, giving a final volume of 0.5-1.0 ml. Reconstitution proceeded on ice, with stirring, for 1 h. Unbound heme was removed with a G25 Sephadex gel filtration column (20 ml hydrated gel, 20 x 1.3 cm^2) equilibrated with Na_2HPO_4. A reconstitution control was similarly prepared using commercially available hemin in place of the alkylated heme. The hemin-reconstituted apoprotein was spectrophotometrically monitored for Compound I/II formation by the addition of 1-2 molar equivalents of H_2O_2, verifying that the apoprotein-generating procedure did not significantly alter the holoprotein.

For reconstitution of the methyl heme adduct, δ-*meso*-methylheme was dissolved in a minimal amount of DMSO (~500 μl) and added dropwise to 1 mg protein on ice. Prior to heme addition, the apoprotein volume was adjusted to 3 times the volume of the heme solution (the final DMSO concentration did not exceed 25% of the final reconstitution volume). The protein/heme solution was allowed to stir on ice for 1 h. To remove DMSO and unreconstituted heme, the protein was run through a Sepharose CL4B column (20 ml hydrated gel, 20 x 1.3 cm^2, equilibrated with 50 mM Na_2HPO_4, pH 7.0). Protein having native-like mobility and δ-*meso*-methyl-like spectroscopic properties (λ_{max} = 408 nm, native λ_{max} = 402 nm) was collected and used in the following assays.

Guaiacol Assay. Protein concentrations were based on the Soret absorbance (native ε_{402} = 95,000 $M^{-1}cm^{-1}$) and assumed that δ-*meso*-ethyl- and δ-*meso*-methylalkylations did not appreciably affect the native Soret absorbance. Given that δ-*meso*-methylheme-reconstituted HRP was susceptible to inactivation in the presence of H_2O_2, guaiacol oxidation was monitored with a stopped flow spectrophotometer (Applied Photophysics

Limited, Model SF.17MV, 10 mm path length). A 125 µl aliquot of 1.1 mM H_2O_2 in 50 mM NaH_2PO_4, pH 7.0, was mixed in the stopped flow chamber with an equal volume containing 10.2 mM guaiacol and 20 nM HRP in 50 mM Na_2HPO_4, pH 7.0 (250 µl final volume). Tetraguaiacol formation was monitored at 470 nm, and the corresponding rate was based on the initial 1-3 sec of reaction. The resulting rates were compared to native HRP-generated rates to obtain relative activities. Apoprotein was also assayed and shown to be essentially inactive, demonstrating the heme to be completely extracted.

Iodide Assay. Iodide oxidation was also monitored by stopped flow spectrophotometry, following I_3^- formation at 353 nm. An aqueous H_2O_2 solution (52.8 µM in 125 µl) was mixed with 3.4 mM KI and 20 nM protein in 100 mM sodium acetate, pH 5.25 (125 µl). Due to H_2O_2-dependent degradation of δ-*meso*-methylheme-reconstituted HRP, the rate determined for triiodide formation was based on the increase in absorption between 1 to 10 sec. Relative activities were generated by comparing the slopes of modified HRP to native HRP.

Inhibition of Guaiacol Activity by Iodide. HRP-catalyzed guaiacol oxidation was monitored in the presence of increasing amounts of iodide. Formation of oxidized guaiacol was monitored spectrophotometrically at 470 nm using an HP 8452A Diode Array spectrophotometer. In a typical assay, 5 pmoles HRP was added to 1 ml assay buffer containing 50 mM sodium acetate buffer (pH 5.25), guaiacol (2, 4, 8, 10, and 20 mM), potassium iodide (0, 100, 200, and 300 mM), and potassium nitrate (300, 200, 100, and 0 mM, added to maintain constant ionic strength). Guaiacol concentrations were generated from a 40 mM stock solution, made up in water and stirred for 20 minutes to ensure guaiacol resuspension. HRP was added immediately prior to assaying to prevent enzyme inactivation, which occurred upon incubation of the enzyme in assay buffer. H_2O_2 was added to initiate the reaction (440 nM final concentration). The reaction was monitored for 20 sec at 25°C. Enzyme- and H_2O_2-dependent triiodide formation also contributed to 470

nm absorption, and, consequently, were monitored independently and subtracted from the guaiacol-generated rate. Each concentration was assayed in triplicate and the values were fit to the Michaelis Menten equation (Equation 3.3) to obtain the corresponding V_{max} and K_m values (assisted by Kinet Asyst -James G. Robertson).

$$\frac{v}{V_{max}} = \frac{[S]}{(K_m + [S])} \qquad \text{(Eqn 3.2)}$$

Inhibition of Iodide Oxidation by Thioanisole. HRP-catalyzed iodide oxidation was monitored in the presence of varying amounts of thioanisole. Iodide oxidation was measured by spectrophotometric detection of triiodide formation. A typical assay mixture contained 1 pmole HRP in 1 ml assay buffer (50 mM sodium acetate, pH 5.25, potassium iodide (5, 10, 15, 20, 40, and 80 mM), potassium nitrate (75, 70, 65, 60, 40, and 0 mM to maintain constant ionic strength), and varying amounts of thioanisole (0, 0.5 , 1.0, and 1.5 mM). Vigorous stirring was needed to suspend thioanisole fully. H_2O_2 was added to initiate the reaction (110 nM final concentration). The reaction was monitored at 354 nm for 20 sec at 25°C. H_2O_2-dependent iodide oxidation was also measured and subsequently subtracted from the enzyme-catalyzed oxidation. Each concentration was performed in triplicate, and the obtained relative velocities (AU/s) were fit to the Michaelis Menten equation (Equation 3.2) to obtain V_{max} and K_m values (Kinet Asyst).

RESULTS

Substrate Binding as Characterized by Difference Spectra. The difference spectra for guaiacol, thioanisole, and iodide binding to HRP were determined at pH 5.25 because iodide binds poorly at neutral pH values. The difference spectra for guaiacol binding

varied from that obtained at pH 7, which demonstrates the binding of one guaiacol molecule (K_d = 11 mM) (Harris *et al.*, 1993). At pH 5.25, two molecules of guaiacol appear to bind (Figure 3.4). A high affinity guaiacol binding site (K_d = 0.42 μM) gives a maximum at 385 nm and a minimum at 422 nm. A low affinity guaiacol binding site (K_d = 2 mM) displays a maximum at 407 nm and is similar to that obtained at pH 7.

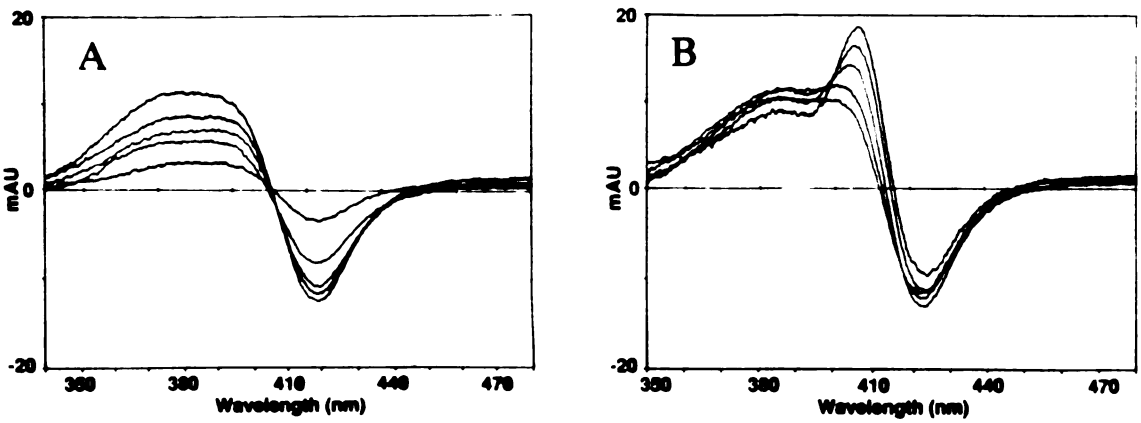

Figure 3.4: Difference spectra for high affinity (A) and low affinity (B) guaiacol binding to HRP. Guaiacol concentrations used to generate the spectra were 50, 100, 150, 200, and 500 nM for high affinity binding and 1, 2, 5, 10, and 20 mM for low affinity binding.

The difference spectrum measured for thioanisole binding to HRP at pH 5.25 is similar to that of the low affinity guaiacol site, displaying a maximum at 407 nm, but is of greater intensity (Figure 3.5). The K_d for thioanisole binding is estimated to be ~80 mM; however, this estimate is prone to error since the range of concentrations where thioanisole is soluble falls far below 80 mM. This thioanisole difference spectrum is markedly different from that determined at pH 7, which displays maxima at 382 and 423 nm and a minimum at 405 nm.

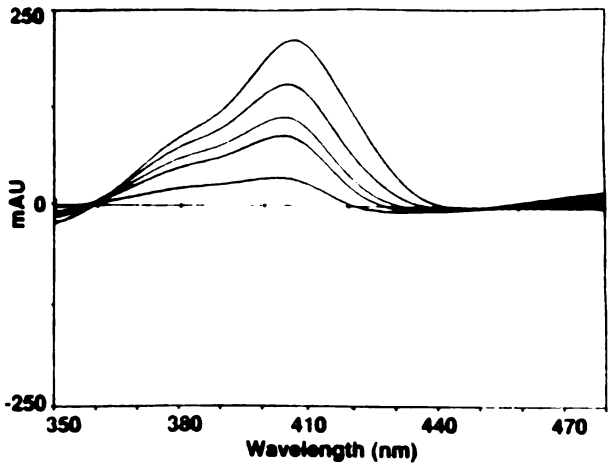

Figure 3.5: Difference spectra for HRP bound by 0.5, 0.6, 0.75, 1.0, and 1.25 mM thioanisole.

The difference spectra observed for iodide binding are similar to those of the high affinity guaiacol difference spectra and estimate the K_d value to be 68 μM for iodide binding at pH 5.25 (Figure 3.6).

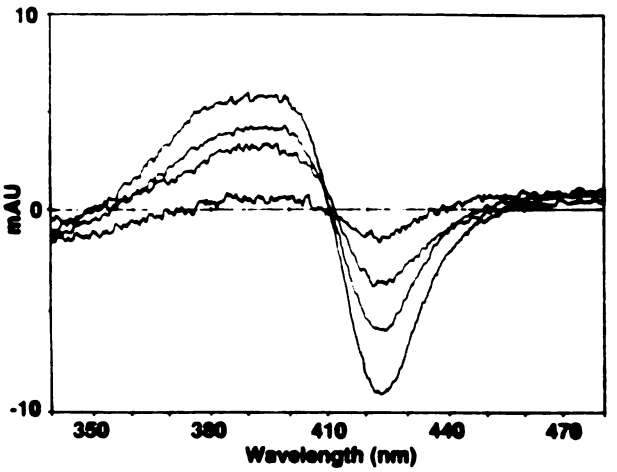

Figure 3.6: Difference spectra for 10, 20, 30, and 40 μM iodide binding to HRP.

The addition of a saturating amount of iodide to the pair of cuvettes used to generate the guaiacol difference spectra causes the high affinity guaiacol difference spectrum to disappear (Figure 3.7A). This suggests that either iodide displaces the avidly bound guaiacol molecule or perturbation of the Soret band in the reference cuvette caused by iodide binding is similar to, and thus balances out, that which is caused by the avidly bound guaiacol in the sample cuvette. The difference spectrum due to the low affinity binding of guaiacol remains when iodide is added to the pair of cuvettes used to generate the guaiacol difference spectrum. This suggests that iodide does not displace guaiacol from the low affinity binding site. Thus iodide and guaiacol (K_d = 2 mM) can bind HRP simultaneously. By similar reasoning, iodide also does not compete with the thioanisole binding site (Figure 3.7B). Addition of iodide to the pair of cuvettes used to generate the thioanisole difference spectrum does not displace thioanisole, but gives rise to a novel spectrum, indicating the ability of these two substrates to bind to HRP simultaneously.

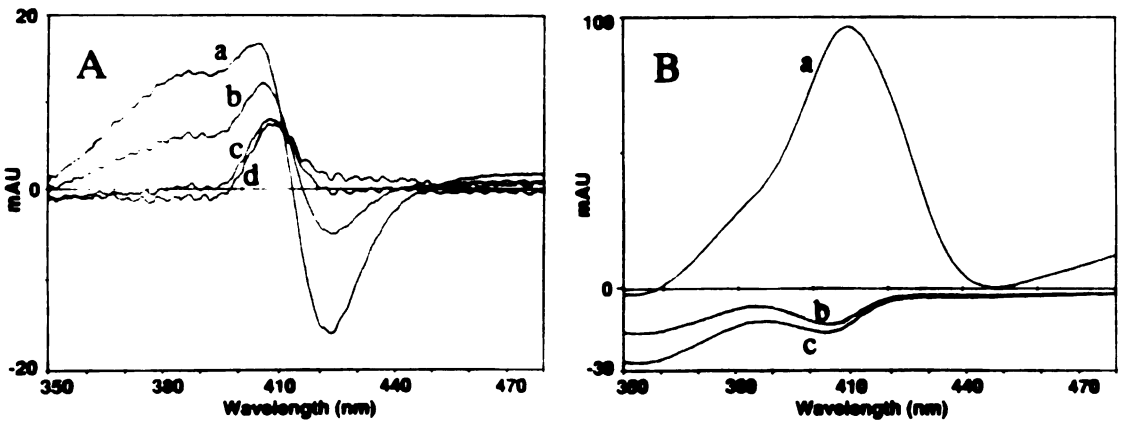

Figure 3.7: Influence of iodide on the difference spectrum obtained for HRP bound by guaiacol (A) and thioanisole (B). Iodide (a, 0; b, 340; c, 680; and d, 1020 μM) was added to both cuvettes used to generate the difference spectrum for the binding of 10 mM guaiacol by HRP (A). Iodide (a, 0; b, 340; and c, 680 μM) was added to both cuvettes used to generate the difference spectrum for the binding of 1.5 mM thioanisole by HRP (B).

Relative Activities for Guaiacol and Iodide Oxidation as Catalyzed by Modified HRP. To compare the HRP-catalyzed oxidation of iodide to that of guaiacol, their respective assays were performed on HRP modified by methyl-, ethyl-, and phenylhydrazines. In addition to assaying HRP reconstituted with δ-*meso*-methyl- and δ-*meso*-ethylhemes as described in the methods, phenylhydrazine-treated HRP was also prepared and tested for guaiacol and iodide activity. Treatment of HRP with phenylhydrazine was performed by Robert Z. Harris (Harris *et al.*, 1993) and generated, based on earlier characterization of this reaction, a modified protein containing two aryl groups per molecule of HRP (Ator and Ortiz de Montellano, 1987). As shown through labeling studies the protein is predominantly arylated, but modification of the heme at the δ-*meso*-heme edge also occurs. Table 3.1 lists the relative activities determined for guaiacol and iodide oxidation as catalyzed by native and modified HRP. The chemical modification

Table 3.1: Relative guaiacol and iodide activities measured for modified HRP. The reported values represent the average of experiments performed in duplicate for the δ-*meso*-ethylheme-reconstituted HRP and performed in triplicate for the δ-*meso*-methylheme-reconstituted HRP. The phenylhydrazine-treated HRP was assayed once.

HRP Modification	% Guaiacol Activity	% Iodide Activity
Native HRP	100.0	100.0
δ-*Meso*-ethyl-reconstituted HRP	2.4	9.2
δ-*Meso*-methyl-reconstituted HRP	165.3	34.9
phenylhydrazine-treated HRP[a]	2.4	3.8

[a]Phenylhydrazine-treated HRP was generated by Robert Z. Harris.

promoted by reaction of HRP with ethyl- and phenylhydrazines similarly inhibits guaiacol and iodide activities. This suggests that iodide oxidation, like guaiacol oxidation, occurs in the vicinity of the δ-*meso* heme edge. The guaiacol and iodide activities are inversely influenced by the presence of a δ-*meso*-methyl group. Relative to the native enzyme, the activity for HRP reconstituted with the methylated heme is 1.6 fold improved for guaiacol oxidation and 3 fold reduced for iodide oxidation.

Inhibition of Guaiacol Oxidation by Iodide. Inhibition studies were used to monitor the influence that iodide has on HRP-catalyzed guaiacol oxidation. Increasing the iodide concentration clearly decreases the V_{max} for guaiacol oxidation (Figure 3.8). This trend rules out the possibility that iodide is a competitive inhibitor of guaiacol oxidation and suggests that iodide and guaiacol bind HRP at different sites. The influence that iodide has

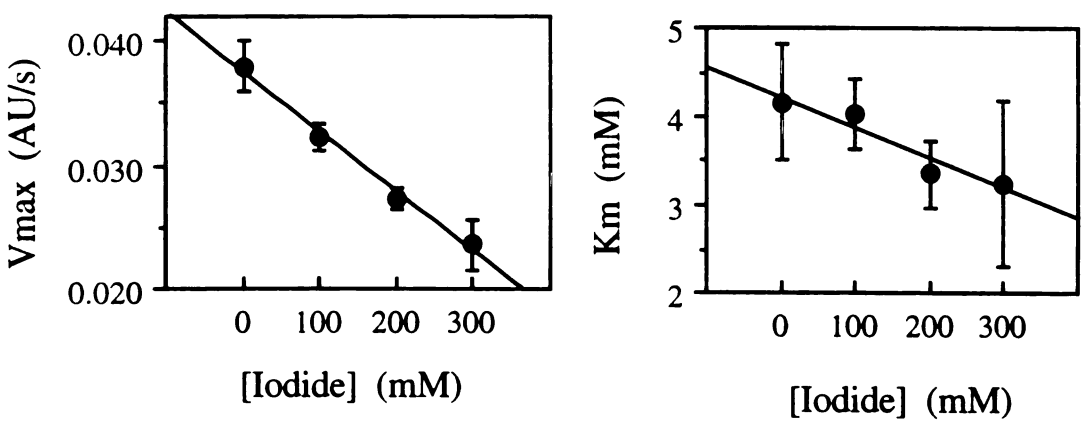

Figure 3.8: Inhibition studies demonstrate the influence that increasing iodide has on the V_{max} and K_m values for guaiacol oxidation. The data points represent the average values for three experiments, and the error bars show the calculated standard deviation.

on the K_m value for guaiacol oxidation is less definitive, given the high error obtained in fitting the data to the Michaelis Menten equation. Increasing iodide appears to either enhance or have no influence over the binding of guaiacol by HRP, suggesting that iodide

is either a mixed-type or classic noncompetitive inhibitor of guaiacol oxidation (Segel, 1976). Fitting the data to the equation describing mixed-type noncompetitive inhibition leads to an estimate for the value of K_i to be ~1.3 M. This value is greater than the iodide concentrations used in this study (100-300 mM), and is consistent with the small influence that iodide was observed to have on the kinetics of guaiacol oxidation. Assaying guaiacol activity in the presence of molar quantities of iodide was not performed because the high level of iodide activity displayed at these concentrations would mask the monitoring of tetraguaiacol formation.

Inhibition of Iodide Oxidation by Thioanisole. In order to compare iodide binding to that of thioanisole, inhibition studies were pursued monitoring iodide oxidation in the presence of increasing thioanisole concentrations. Thioanisole was found to clearly decrease the V_{max} and essentially have no influence over the K_m for iodide oxidation (Figure 3.9). These kinetic results suggest that thioanisole is a noncompetitive inhibitor of

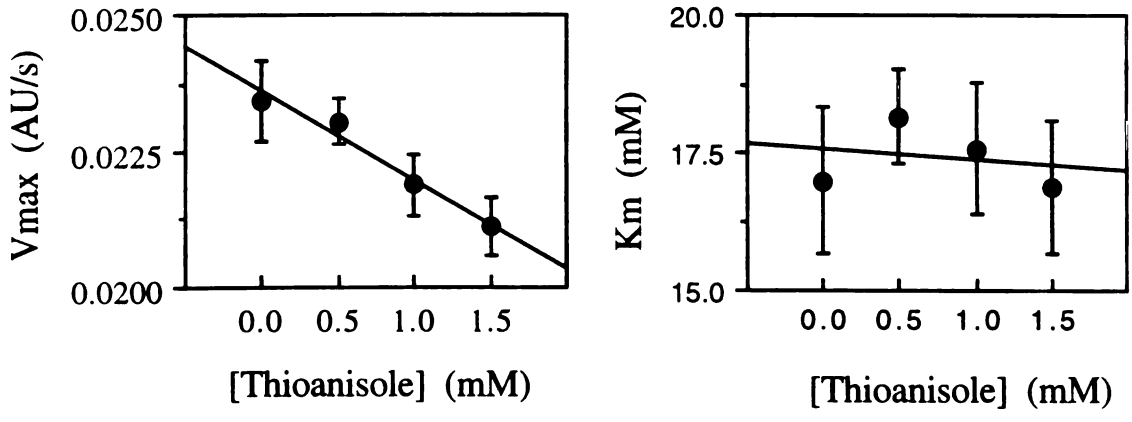

Figure 3.9: Inhibition studies on iodide oxidation by thioanisole. The influence that increasing thioanisole has on the V_{max} and K_m values is illustrated. The data points represent the average values obtained for three experiments, and the error bars show the calculated standard deviations.

iodide oxidation. The K_i value describing thioanisole inhibition is estimated to be 13.0 mM by fitting the data to the classic equation describing noncompetitive kinetics. However, this value is prone to error since the concentrations used to generate this value were limited by the solubility of thioanisole and were at least 10 fold lower than 13 mM.

DISCUSSION

Substrate binding to hemoproteins can be advantageously investigated by optical difference spectroscopy. The binding of substrate in the vicinity of the heme alters the environment of the heme molecule through hydrogen bonding and hydrophobic interactions and causes minor changes in the Soret absorbance. Three types of difference spectra have been reported for HRP (Hosoya *et al.*, 1989). Unfortunately, the differences among these spectra seem to reflect the nature of the substrate/ligand rather than the manner in which the substrate is bound by HRP. This is demonstrated by hydroquinone and resorcinol, which have been shown to compete for the same site within HRP yet exhibit distinct difference spectra (Hosoya *et al.*, 1989). Thus the distinct nature of the difference spectra displayed by iodide, guaiacol, and thioanisole is probably due to the differing chemical properties of these three substrates. The difference spectrum for substrate binding can also fluctuate with pH, as is demonstrated by the spectra obtained in this study which differ from those measured at pH 7.0 (Harris *et al.*, 1993) The binding of a second high affinity guaiacol molecule as the pH is decreased from 7.0 to 5.25 presumably reflects changes in the ionization state of the active site of HRP because guaiacol ionization is not significantly altered between pH 7 and 5.25. The low affinity site at pH 5.25 (K_d = 2 mM) is likely to be the single guaiacol binding site observed at pH 7 (K_d = 11 mM) since their respective Kd values are similar and they display similar difference spectra (λ_{max} = 407 nm).

The difference spectra obtained for thioanisole at pH 5.25 also differ from those obtained at pH 7.0 (Harris et al., 1993). At pH 7, the difference spectrum for thioanisole

binding displays maxima at 382 and 424 nm and a minimum at 405 nm. At pH 5.25, the difference spectrum for thioanisole is characterized by a single peak at 407 nm, and the intensity corresponding to the difference between the minimum and maximum points of absorption increases by 25 fold relative to the pH 7 spectrum obtained with similar levels of thioanisole. The difference spectrum for thioanisole binding thus appears to be sensitive to ionization of the active site of HRP.

The difference spectrum obtained for HRP bound by iodide resembles that of the avidly bound guaiacol molecule (K_d = 0.42 μM). Thus the loss of the high affinity guaiacol difference spectrum with the addition of iodide to the pair of cuvettes used to generate the 10 mM guaiacol difference spectrum is probably due to iodide in the reference cuvette balancing out perturbation of the Soret caused by the avidly bound guaiacol in the sample cuvette. The addition of saturating amounts of iodide has no detectable influence on the weakly bound guaiacol molecule. Thus the 2 mM K_d guaiacol binding site and the iodide binding site appear to be distinct. This finding is consistent with NMR studies which revealed the inability of iodide to displace resorcinol from its binding site (Sakurada *et al.*, 1987). Difference spectroscopy also demonstrated that iodide was unable to displace thioanisole, suggesting that HRP is bound by iodide and thioanisole at differing sites. Robert Z. Harris in our research group has also shown that the addition of thioanisole to a pair of cuvettes used to generate a guaiacol difference spectrum produces insignificant changes in the spectrum, suggesting that thioanisole and guaiacol bind HRP at differing sites (Harris *et al.*, 1993). Collectively, these studies suggest that three distinct binding sites exist for guaiacol, iodide, and thioanisole in the *resting state enzyme*.

Given that the resting state enzyme is chemically distinct from Compound I inhibition studies were performed to determine the influence that iodide would have on guaiacol activity and the influence that thioanisole would have on iodide activity. Thioanisole inhibits iodide oxidation in a noncompetitive manner. The classification of

iodide as an inhibitor of guaiacol oxidation is more ambiguous given the error in the calculated K_m values. However, increasing iodide concentrations clearly decrease the V_{max} values of guaiacol oxidation, excluding iodide from being a competitive inhibitor. These findings suggest that iodide cannot displace guaiacol and that thioanisole cannot displace iodide in their respective interactions with Compound I. Thioanisole was also shown by Robert Z. Harris to be a noncompetitive inhibitor of guaiacol oxidation (Harris *et al.*, 1993). Collectively these inhibition studies suggest that three distinct sites for the binding of iodide, guaiacol, and thioanisole also exist for the catalytically active Compound I species.

The modifications induced by reaction of HRP with methyl- and ethylhydrazines have been shown to alkylate the δ-*meso*-heme edge, and reconstitution of HRP apoenzyme with δ-*meso*-ethylheme suppresses guaiacol activity. These studies led to the conclusion that guaiacol oxidation occurs at the δ-*meso*-heme edge. Alternatively, thioanisole sulfoxidation is postulated to occur in the vicinity of the ferryl oxygen because it requires oxygen transfer. Consistent with this theory, reconstitution with δ-*meso*-ethylheme or treatment with phenyldiazene does not inhibit thioanisole sulfoxidation. In a similar manner to guaiacol oxidation, iodide oxidation is inhibited by substitution of an ethyl group at the δ-*meso* position and by modifications promoted by phenylhydrazine treatment. These results suggest that iodide is oxidized near the heme edge. In NMR studies performed on iodide binding by HRP, iodide is bound equidistantly from the 1- and 8-methyl heme groups and within 10 Å of the heme iron. The binding of aromatic substrates has also been investigated by NMR and appears to occur within 5 Å of the 8-methyl heme group and 8-12 Å away from the heme iron. Collectively these studies and the activities of modified HRP suggest that iodide binding occurs near the heme edge and lies adjacent to the guaiacol binding site (Figure 3.10).

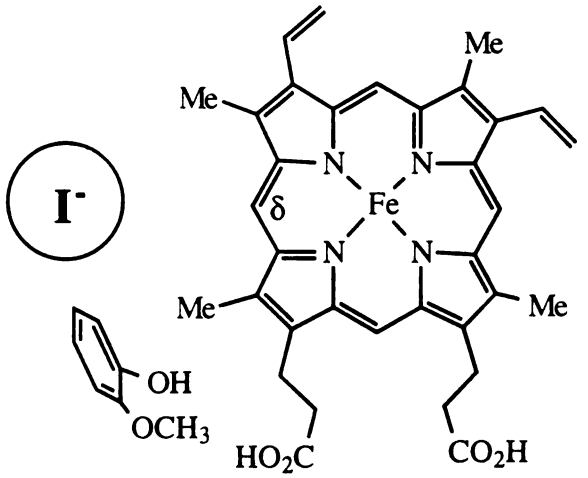

Figure 3.10: Proposed binding of iodide and guaiacol to HRP. Guaiacol binding is drawn so that the plane of the aromatic ring faces the heme iron, allowing the protons of the aromatic ring to be equally distanced from the iron atom. Both substrates are oxidized near the heme edge, so their binding is predicted to occur slightly above or slightly below the plane of the heme. This positioning allows for optimal orbital overlap for electron abstraction by the heme edge.

Interestingly, iodide and guaiacol activities are inversely influenced by reconstitution of HRP with δ-*meso*-methylheme. The corresponding guaiacol activity is enhanced and iodide activity is slightly reduced relative to their respective native activities. Heme and protein modification could feasibly perturb the heme pocket, potentially influencing both the reactivity of the Compound I species and the binding of substrates near the heme edge. Alkylation at the δ-*meso* heme position, in particular, is expected to compromise the planarity of the heme molecule in order to accommodate the methyl and ethyl groups which are sterically constrained by the neighboring 1- and 8-methyl heme groups. The resulting perturbed heme structure probably influences the stabilities of the Compound I and Compound II species, which may explain the accelerated guaiacol and

thioanisole (shown by Robert Z. Harris) activities exhibited by HRP reconstituted with δ-*meso*-methylheme. This reasoning, however, is not consistent with the influence that the methyl group has in reducing iodide activity. The methyl group may alter orbital overlap between the perturbed heme molecule and the substrate, improving electron transfer from guaiacol and deterring electron transfer from iodide. Alternatively, methylation of the δ-*meso* position could influence the binding of substrates near the heme edge. The δ-*meso*-methyl group is not likely to hinder guaiacol binding since ethylation at the δ-*meso* position improves the binding of guaiacol relative to that exhibited by the native enzyme, decreasing the K_d from 11 to 4 mM (Harris *et al.*, 1993). However, iodide binding which occurs at an equal distance from the 1- and 8-methyl groups and is likely to require closer positioning to the heme edge, since it is less easily oxidized than guaiacol, could be hindered by the δ-*meso*-methyl group.

These studies support the δ-*meso* heme edge as the site within HRP where iodide is oxidized. This finding implies that iodide is oxidized through electron abstraction at the δ-*meso* heme edge rather than by oxygen transfer at a site that is proximal to the ferryl oxygen. Further insight as to the mechanism of iodide oxidation may be given by mutagenesis studies. Treatment of HRP with diethylpyrocarbonate is speculated to modify the distal histidine and inactivates the protein with respect to both guaiacol and iodide peroxidase activities (Bhattacharyya *et al.*, 1993; Bhattacharyya *et al.*, 1992). Diethylpyrocarbonate modification does not influence Compound I formation or guaiacol binding, suggesting that the distal histidine may assist in regulating electron abstraction by Compound I or Compound II. Accordingly, removal of the distal imidazole group through mutation may deter iodide oxidation by decreasing the rate of electron abstraction. The distal histidine also appears to provide a barrier between substrates and the ferryl oxygen of Compound I. Thus mutagenesis studies aimed at removing the distal imidazole group may

also alter the mechanism of iodide oxidation, either by enhancing the rate of iodide oxidation or by allowing HRP to oxidize Cl^-.

CONCLUSIONS

In the characterization of iodide oxidation as catalyzed by HRP, iodide has been compared to the substrates guaiacol and thioanisole. The similarities between guaiacol and iodide oxidation, in particular their sensitivity to ethylation of the δ-*meso* position, suggest that iodide, like guaiacol, is oxidized through the δ-*meso* heme edge, presumably through two sequential electron abstraction steps. The details of the mechanism of iodide oxidation warrant further investigation in order to understand why reduction of Compound I is rate limiting in iodide oxidation. These studies also show that iodide and thioanisole are bound by HRP at differing sites. The existence of three differing binding sites for guaiacol, iodide, and thioanisole offers an explanation for the differing oxidative reactions undergone by these substrates. Substrate binding by the protein may modulate heme reactivity by controlling how the substrate is positioned relative to the ferryl oxygen and the heme edge components of Compound I. Thus, in addition to the postulated role that the protein plays in restricting access of substrates to the heme, these studies suggest that substrate binding that is controlled by the protein can also serve to restrict where substrates interact with the heme molecule.

Chapter 4: Mutagenesis of Distal Residues to Examine the Roles that the Catalytic Histidine and Accessibility to the Heme Iron Play in Peroxidase and Peroxygenase Activities

INTRODUCTION

Peroxidase catalysis is predominantly promoted by the highly conserved peroxidase residues found at the distal side of the heme molecule. The distal histidine is postulated to activate peroxide in the formation of Compound I, and the distal residues are proposed to form a protein barrier that restricts the transfer of the ferryl oxygen to substrates (Chapter 1). The distal histidine is an invariant residue throughout the bacterial, fungal, and plant peroxidase superfamily. The peroxidase crystal structures of CCP (Finzel *et al.*, 1984), ARP (Kunishima *et al.*, 1994), LIP (Poulos *et al.*, 1993), AXP (Patterson and Poulos, 1995), and PeP (Poulos, unpublished structure) collectively show the distal histidine to be situated directly above the heme iron. The $N_{\varepsilon 2}$ nitrogen atom of the imidazole ring is directed towards the heme iron, a position that is postulated to allow for the activation of peroxide in the formation of Compound I (Poulos and Kraut, 1980) (Figure 4.1). The recruitment of the distal histidine by the peroxidases allows for the deprotonation of weakly acidic H_2O_2 (pKa 11.6) (Everett and Minkoff, 1953), generating the nucleophilic peroxide anion that attacks the iron in the generation of a ferric peroxide complex. Subsequently, the protonated imidazole is postulated to donate the abstracted proton to the distal oxygen of the Fe-peroxide complex, affording the heterolytic cleavage of the O-O bond with the formation of a water molecule. The Compound I species retains two oxidative equivalents. One electron is typically taken from the porphyrin, leaving a porphyrin radical cation, and the other is obtained by oxidizing Fe(III) to Fe(IV). CCP deviates from prototypic peroxidases by displaying a protein radical in lieu of a porphyrin radical cation. The critical role that the invariant distal histidine plays in Compound I formation is suggested by

mutagenesis studies performed on CCP. Mutagenesis of this residue to a leucine in CCP causes a 10^5 fold reduction in the rate constant for Compound I formation (Erman and Vitello, 1992).

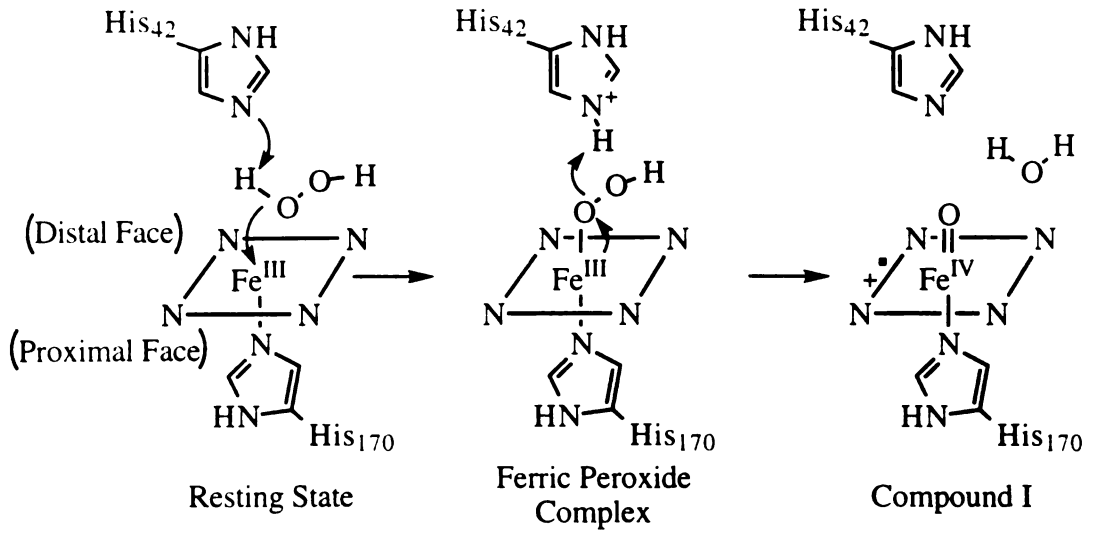

Figure 4.1: The postulated general acid/base catalytic role played by the distal histidine in Compound I formation.

The distal histidine is also postulated to play a significant role in the reduction of Compound I and Compound II (Figure 4.2). The reduction of Compound I involves the abstraction of an electron from a substrate molecule, neutralizing the porphyrin radical cation. This step is activated by the deprotonation of an ionizable group of pKa 5.1 (Dunford, 1982). During the reduction of Compound I to Compound II, a proton is taken up by the protein and a hydrogen bond forms between the Compound II ferryl oxygen atom and a distal residue (Yamada and Yamazaki, 1974; Oertling and Babcock, 1988). Given the proximity of the distal histidine to the ferryl oxygen, it is speculated that the distal imidazole is the ionizable group that hydrogen bonds to the ferryl oxygen. The reduction of Compound II to the resting state involves the abstraction of an electron from a second substrate molecule (Figure 4.2). This step of the peroxidase cycle is promoted by

the protonation of a heme-linked group of pKa 8.6. This ionizable group is postulated to be the distal histidine because the hydrogen bond to the ferryl oxygen is lost upon deprotonation of this group (Sitter *et al.*, 1985). The increased basicity of the distal histidine exhibited by the Compound II species relative to the Compound I species is presumably caused by the assistance provided by the ferryl oxygen in retaining the imidazole proton. Hydrogen bonding between the ferryl oxygen and the distal histidine is probably promoted in Compound II, relative to Compound I, because its Fe-O bond is 0.3 Å longer than that of Compound I. The proton that is hydrogen bonded to the ferryl oxygen in Compound II is proposed to assist in the formation of the water molecule from the ferryl oxygen.

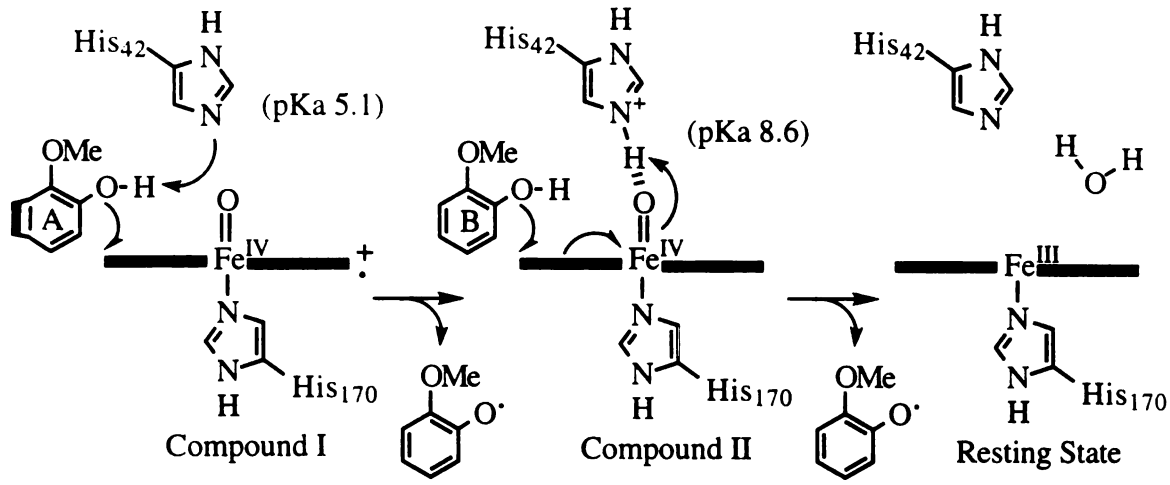

Figure 4.2: Proposed mechanisms for the oxidation of classic peroxidase substrates by Compound I and Compound II. The guaiacol molecules are labeled A and B to emphasize that two molecules are oxidized in the reduction of Compound I to the resting state species. The pKa values that regulate the reduction of Compound I and Compound II are thought to reflect the ionization of the distal histidine and are indicated in parentheses.

An invariant arginine is positioned adjacent to the distal histidine in the peroxidase crystal structures (Figure 1.6). This residue is postulated to assist in Compound I formation by stabilizing the negative charge that forms on the distal oxygen during O-O bond scission. Mutation of this residue to a leucine in CCP causes a 100-fold reduction in the rate constant for Compound I formation (Erman and Vitello, 1992). Mutating this residue to a lysine, which preserves the positive charge, does not appreciably influence the rate of Compound I formation.

A highly conserved phenylalanine, Phe 41 in HRP, also neighbors the distal histidine and is situated such that the plane of the phenyl group lies parallel to the plane of the heme (Figure 1.6). Unlike the distal histidine and arginine residues which are invariant among the bacterial, fungal and plant peroxidase superfamily, the distal phenylalanine is conserved only among the class II and class III peroxidases (Welinder, 1992a). The class I peroxidases, which includes CCP, contain a tryptophan at this position. Within the peroxidase crystal structures, these three distal residues--His 42, Arg 38, and Phe(Trp) 41 (numbering based on HRP sequence)--form the majority of the protein contacts to the distal heme face. Thus these residues are likely to represent the major barrier between substrates and the ferryl oxygen of Compound I.

As highlighted in Chapter 3, accessibility to the ferryl oxygen is postulated to be a major feature that determines whether oxygen transfer or electron abstraction occurs. Substrate accessibility to the peroxidase heme molecule is restricted to the δ-*meso* heme edge as revealed by peroxidase crystal structures. This restricted accessibility is further supported by NMR and chemical modification studies which demonstrate that both substrate binding and modification occur at this heme edge. NMR nuclear Overhauser effects and relaxation data show that peroxidase substrates, like resorcinol and 2-methoxy-4-methylphenol, bind within 5 Å of the 8-methyl heme group (Sakurada *et al.*, 1986). Consistent with these findings, the reaction of methyl-, ethyl-, and phenylhydrazines with

HRP yields modifications that are limited to the δ-*meso* heme edge (Ator and Ortiz de Montellano, 1987; Ator *et al.*, 1987). In contrast, the reaction of phenylhydrazine with P450s yields formation of an iron-phenyl complex (Jonen *et al.*, 1982), which is postulated to be afforded by the accessibility of the heme iron to the enzyme-produced phenyl radical. The accessibility of the heme iron within P450s is thought to permit transfer of the ferryl oxygen to substrates in P450-catalyzed hydroxylation and epoxidation reactions (Figure 4.3). The differing accessibility of the heme iron that distinguishes the peroxidases from

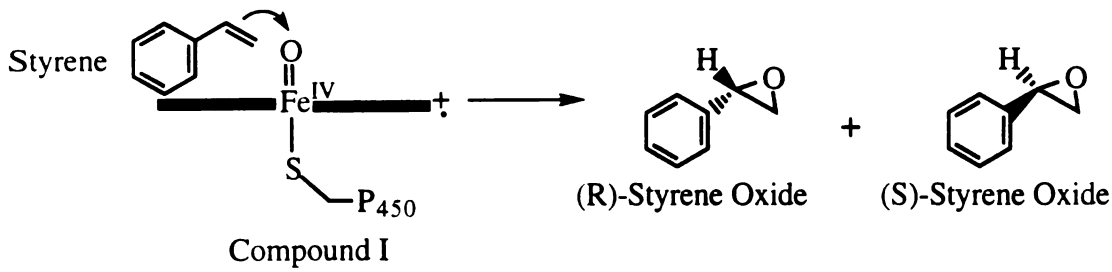

Figure 4.3: P450-catalyzed styrene epoxidation. The accessibility of the ferryl oxygen of the P450 Compound I-like species is proposed to allow the transfer of this oxygen atom to substrates.

the P450s is proposed to limit the catalytic function of peroxidases to electron abstraction by the heme edge. Thus peroxidases typically reduce substrates, like guaiacol, by one electron (Figure 4.2). Thioanisole is a unique molecule that is a peroxygenase substrate for both P450s and peroxidases. In HRP-catalyzed thioanisole sulfoxidation the peroxide-derived ferryl oxygen is incorporated into the sulfoxide product (Kobayashi et al., 1986). It is surmised that HRP binds this molecule proximal to the ferryl oxygen in order that oxygen transfer to this substrate can occur (Chapter 3).

In order to test the postulated multifaceted roles of the distal residues, His 42 and Phe 41 were mutated to smaller inert residues to address the role that these residues play in

activating peroxide and in providing a protein barrier which maintains an inaccessible Compound I ferryl oxygen. Peroxygenase assays, namely thioanisole sulfoxidation and styrene epoxidation, were employed to test oxygen transfer activity promoted by these mutations. Modification by phenyldiazene was also utilized to probe changes, promoted by mutation of the distal residues, to substrate accessibility to the heme molecule.

MATERIALS & METHODS

UV/Vis Spectrophotometric Detection of Compound I/Compound II. Compound I spectra were generated for the plant and recombinant proteins by adding one equivalent of peroxide to the resting state species (~7 nmol of protein). The addition of one equivalent of $K_4Fe(CN)_6$ to the resulting Compound I species generated Compound II, and the addition of a second equivalent of $K_4Fe(CN)_6$ to this Compound II species regenerated the resting state enzyme. Excess peroxide (> 500 equivalents) or mCPBA were required in promoting Compound I formation for H42A- and H42V-HRP.

Rate of Compound I Formation as Determined Through Stopped Flow Spectrophotometry. The rate of Compound I formation was determined by following the exponential decay of absorption at 411 nm (an isosbestic point between Compound II and resting state HRP, determined from the spectra in Figure 4.4) using stopped flow spectrophotometry, slit width 0.25 mm, at 25°C (Applied Photophysics Limited, Model SF.17MV). To observe Compound I formation under pseudo-first order conditions, 0.25 μM HRP was mixed with an excess amount of hydrogen peroxide (2.5, 5.0, 8.0, 11.0, 15.0, and 25.0 μM) in 20 mM Na_2HPO_4, pH 7.0. The equations outlined below describe the reaction of HRP with H_2O_2 and were used to generate the rate constant for Compound I formation, k_1. The first order decay in absorption was fit to the equation $A_t=A_0e^{-k(obsd)t} + C$. The second order rate constant was determined by taking the slope of the plot, k(obsd)

versus the H_2O_2 concentration. H42A HRP required increased H_2O_2 concentrations (0.025-1.5 mM) to see 411 nm decay.

$$HRP + H_2O_2 \xrightarrow{k_1} \text{Compound I} + H_2O$$

$$-d[HRP]/dt = k_1[HRP][H_2O_2]$$

$$-d[HRP]/dt = k_{(obsd)}[HRP]$$

$$k_{(obsd)}=k_1[H_2O_2]$$

Steady State Kinetics of the H42A- and H42V-HRP Reaction. Steady state kinetics were studied by measuring the initial rates of ABTS oxidation while varying both the concentration of ABTS (1.25, 1.67, 2.5, 5.0, and 10.0 mM) and the concentration of H_2O_2 (65, 85, 125, and 250 mM). At these H_2O_2 levels nonenzymatic ABTS oxidation did not occur in a detectable manner. The final assay volume was 1 ml and contained 500 nM H42A- or H42V-HRP and 100 mM KH_2PO_4, pH 6.0. ABTS oxidation was conducted at 20°C and was followed at 414 nm (ε_{414}= $3.6x10^4$ $M^{-1}cm^{-1}$) (Childs and Bardsley, 1975). Peroxidase cycling can be described by a modified version of ping pong kinetics (Equation 4.1, with v = -d[ABTS]/dt). Typically the rate of conversion of Compound II to resting state (k_3) is slower than the rate of conversion of Compound I to Compound II (k_2), reducing equation (4.1) to equation (4.2).

$$2[HRP]_o/v =((k_2+k_3)/(k_2k_3))(1/[ABTS]) + (1/k_1)(1/[H_2O_2]) \quad (4.1)$$

$$2[HRP]_o/v = (1/k_3)(1/[ABTS]) + (1/k_1)(1/[H_2O_2]) \quad (4.2)$$

Determination of k_2, the Rate Constant for Reduction of Compound I. The rate constant for the reduction of Compound I was determined by monitoring the pseudo-first order reaction of Compound I with excess $K_4Fe(CN)_6$ by stopped flow spectrophotometry. Native-, rWT-, and F41A-HRP (0.2 μM), dialyzed extensively against water to remove contaminating reductants, were mixed with 0.15 μM H_2O_2 in 2 ml

of water and were immediately placed in the first syringe of the stopped flow spectrophotometer. $K_4Fe(CN)_6$ (0.8, 2.6, 4.4, 6.2, and 8.0 μM) in 20 mM Na_2HPO_4, pH 7, was placed in the second syringe. Stopped flow mixing diluted the reported concentrations to half their original value. Compound II formation was monitored at 411 nm, an isosbestic point between the resting state enzyme and the Compound II species. The Compound I species of 0.6 μM H42A- and H42V-HRP were formed with 3.4 μM mCPBA in 2 ml of water. In this manner complete Compound I formation was spectrophotometrically observed to occur within a 2 min incubation period. The stopped flow Compound I solution was therefore allowed to stand for 2 min prior to 1:1 mixing with $K_4Fe(CN)_6$ (3, 6, 10, 15, 22, 30 μM post mixing) in the stopped-flow apparatus.

The following equations that describe the reaction of Compound I with $K_4Fe(CN)_6$ were used to generate the rate constant for Compound II formation, k_2. The first order

$$\text{Compound I} + Fe(CN)_6^{4+} \xrightarrow{k_2} \text{Compound II} + Fe(CN)_6^{3+}$$

$$-d[\text{Compound I}]/dt = k_2[\text{Compound I}][Fe(CN)_6^{4+}]$$

$$-d[\text{Compound I}]/dt = k_{(obsd)}[\text{Compound I}]$$

$$k_{(obsd)}=k_2[Fe(CN)_6^{4+}]$$

decay in absorption was fit to the equation $A_t=A_oe^{-k(obsd)t} + C$. The second order rate constant was determined by taking the slope of the plot, k(obsd) versus $Fe(CN)_6^{4+}$ concentration.

Guaiacol Assay. Guaiacol activity was measured to monitor the rWT activity during purification and to compare peroxidase activity among the plant and recombinant proteins. Sample activity was determined spectrophotometrically at 20°C. The value $\varepsilon_{470} = 2.75\ cm^{-1}mM^{-1}$ was used to convert the units of the spectrophotometrically measured rates into rates of guaiacol consumption. This extinction coefficient was determined by plotting the 470 nm absorption versus the corresponding concentration of peroxide. Two guaiacol molecules are consumed per molecule of peroxide. Enzyme (~10 pmol) was

mixed with 5.1 mM guaiacol in 20 mM Na_2HPO_4, pH 7.0 (1 ml final volume). H_2O_2 (0.5 mM, final) was added to initiate the reaction.

Determination of the Rate and Stereochemistry of Thioanisole Sulfoxidation. In assaying thioanisole activity of the wild-type and mutant proteins, 25 µM enzyme in 20 mM sodium phosphate buffer, pH 7.0, was combined with 5 mM thioanisole on ice. The reaction was initiated by the addition of H_2O_2 (683 µM, added every 2 min). Supplementing the reaction with peroxide throughout the course of the assay promotes linear product formation by maintaining high peroxide levels. Aliquots (500 µl) were taken at various time points, combined with 50 nmol acetophenone internal standard, and extracted with 500 µl CH_2Cl_2. The organic layer was isolated and partially dried under a stream of argon leaving a volume of ~10 µl. The concentrated sample was diluted with 50 µl 80% hexanes, 20% isopropyl alcohol and loaded onto a chiracel OD HPLC column (Daicel Chemical Industries, LTD.). The (R)- and (S)-thioanisole sulfoxides were isocratically eluted with 80% hexanes, 20% isopropyl alcohol at a flow rate of 0.5 ml/min using a Hewlett Packard model 1040A instrument equipped with a diode array detector. The eluant was monitored at 254 nm with a bandwidth of 6 nm. The retention times of (S)- and (R)-thioanisole sulfoxides were 20.9, 27.0 and 46.2 min, respectively.

Determination of the Rate and Stereochemistry of Styrene Epoxidation. Enzyme (25 µM) in 20 mM sodium phosphate buffer, pH 7.0, was mixed with styrene (10 mM final concentration) at 4 °C. The reaction was initiated by the addition of H_2O_2 (683 µM added every two minutes, as described above for thioanisole oxidation). Aliquots (500 µl) were taken at various time points and mixed with 4.6 nmol of the internal standard *trans*-ß-methyl styrene. This mixture was extracted with 500 µl CH_2Cl_2, and the organic layer was isolated and carefully evaporated to a volume of ~10 µl under a stream of Ar. The concentrated extract was analyzed by gas chromatography on a DB-1 column (0.25 mm x 30 m, J & W Scientific) programmed to run at 80 °C for 3 min and then rise at 4 °C/min to

150 °C (Hewlett Packard, Model 5890). The retention times for *trans*-ß-methylstyrene and styrene oxide were 9.0 and 10.0 min, respectively. The stereochemistry of styrene epoxidation was also analyzed by gas chromatography, using a 0.25 mm x 30-m Chiraldex G-TA capillary column (Advanced Separation Technologies, Inc., Whippany, NJ) programmed at 90 °C for 50 min. The retention times for (S)- and (R)-styrene oxides were 26.8 and 28.1 min, respectively.

Reaction of HRP Mutants with Phenyldiazene. The wild-type and mutant HRP proteins in 100 mM K_2HPO_4, pH 7.4, were treated with phenyldiazene prepared by diluting 2 µl 5.67 M methyl phenyldiazene carboxylate azo ester ($PhN{=}NCO_2Me$) in 200 µl 0.1 KOH. Phenyldiazene (0.11 µmol) was added every 5 min until no changes were observed spectrophotometrically. For 10 µM enzyme (in 2 ml buffer), 0.57 µmol of phenyldiazene was added in total. The reaction was incubated for 10 additional minutes. These reactions were carried out at room temperature (~25 °C). Ascorbate, 50 µl of a 50 mM solution or a few grains of the solid ascorbate salt, were added to the reaction, and the resulting solutions were gel filtered (Sephadex G-25, 1.5 cm x 10 cm). The eluted protein was treated to one of two workups, allowing for the analysis of either modified hemes or N-phenylprotoporphyrin IX products. Workup A served to extract all the phenyldiazene-modified hemes. In workup A the protein eluted from the gel filtration column was acidified with glacial acetic acid (final 25% v/v) and extracted with three 1 ml volumes of ether. The extract was concentrated to dryness on a rotary evaporator and was resuspended in 100 µl 6:4:1 MeOH:H_2O:AcOH (solution A) for HPLC analysis on a Partisil ODS-3.5 µm Alltech column. The column was eluted with 80% buffer A, 20% solution B (10:1 MeOH:AcOH), at a flow rate of 1 ml/min. The eluant was monitored at 416 nm.

Workup B promoted the conversion of iron-phenyl complexes to N-phenyl protoporphyrin IX products. The protein eluted from the gel filtration column was added to 10 ml freshly mixed 95:5 CH_3CN:H_2SO_4 and incubated overnight at 4°C in the dark.

The resulting solution was concentrated to 2 ml on a rotary evaporator and was extracted with three 1 ml volumes of CH_2Cl_2. The CH_2Cl_2 extracts were combined and were washed once with 1 ml H_2O to remove residual acid. The isolated organic layer was dried on a rotary evaporator and resuspended in 100 µl solution A for HPLC analysis on the reverse phase column used above. The column was eluted isocratically with 55:45:10 MeOH:H_2O:HOAc at a flow rate of 1 ml/min. The eluant was monitored at 416 nm. Myoglobin was similarly reacted with phenyldiazene to generate N-phenylprotoporphyrin IX standards.

RESULTS

UV/Vis Spectrophotometric Characterization of Resting State, Compound I, and Compound II Species of Recombinant Proteins. The resting state, Compound I, and Compound II spectra displayed by rWT HRP (Figure 4.4) were equivalent to those of the native enzyme (λ_{max} = 402 nm) (Figure 1.9). F41A HRP deviated slightly from the native spectrum, displaying a 4 nm red shifted, shoulderless Soret absorption (λ_{max} = 406 nm). Compound I and Compound II spectra obtained for F41A HRP appeared to be native-like; however, the Compound I spectrum decayed more rapidly to the Compound II spectrum in the absence of reductants. The resting state spectra of H42A- and H42V-HRP were essentially superimposable on that of the native enzyme (Figure 4.4D), but Compound I and Compound II spectra could not be obtained in the manner employed to generate these species for the native enzyme. For the distal histidine mutants, the decay of the Soret band that is characteristic of Compound I formation was only observed with the addition of > 500 equivalents of H_2O_2. This excessive level of peroxide eventually caused the Soret intensity to decrease to an extent that is indicative of heme degradation. The addition of excess $K_4Fe(CN)_6$ (100 equivalents) to this spectrum deterred heme degradation and caused the Soret absorption to increase in a manner that is indicative of regeneration of the resting state spectrum (Figure 4.4D). A Compound II species was not observed in the

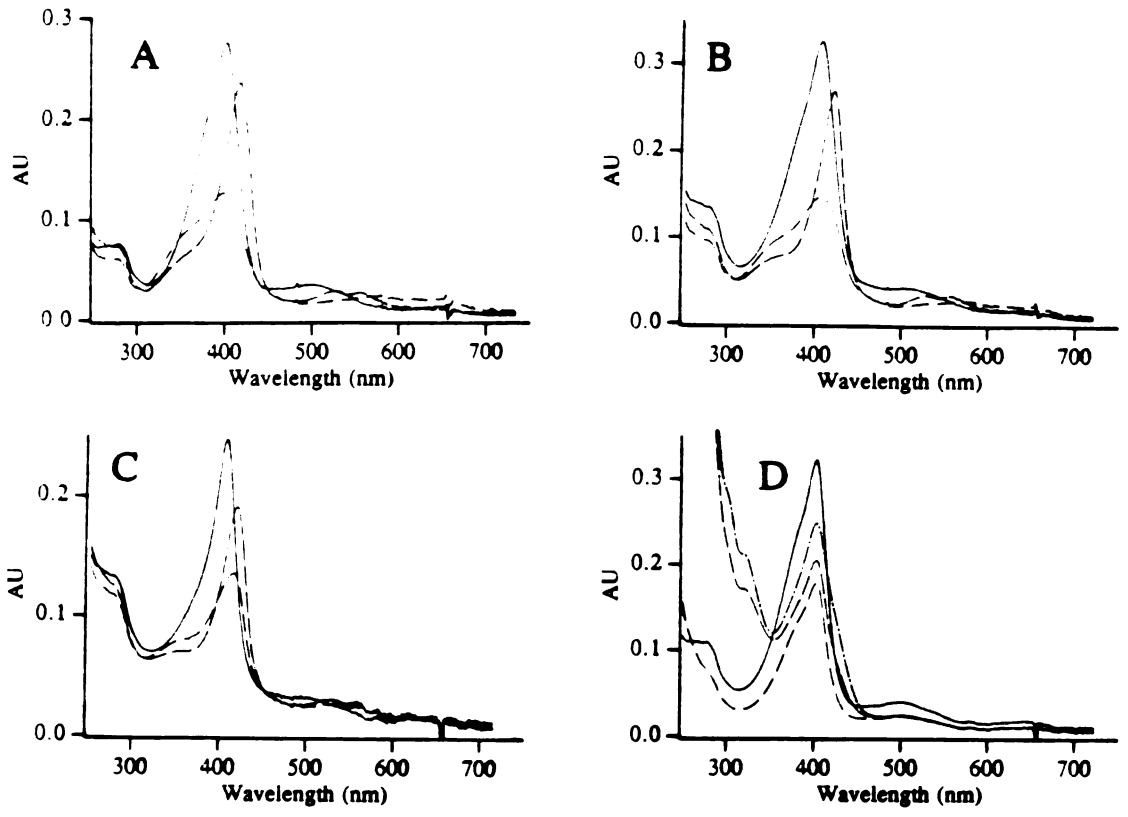

Figure 4.4: Spectral characterization of the resting state, Compound I, and Compound II species of native- (A), rWT- (B), F41A (C), and H42A-HRP (D). For the wild-type and F41A proteins, 1 equivalent of H_2O_2 was added to the resting state species (solid line) to generate Compound I (dashed line). One equivalent of ferrocyanide was subsequently added to generate Compound II (dashed and dotted line). The addition of excess peroxide (1000 equivalents) to H42A HRP (D) caused a time-dependent loss in Soret absorption (dashed line). The addition of 100 equivalents of ferrocyanide partially regenerated the resting state spectrum in a time-dependent manner (dashed and dotted line).

regeneration of the resting state spectrum. A Compound I-like spectrum could also be obtained for the distal histidine mutants by the addition of five equivalents of mCPBA

(Figure 4.5). Unlike the peroxide-generated Compound I spectrum, the mCPBA-generated Compound I spectrum decayed slowly (~15 min), in the absence of reducing agents, to a resting state-type spectrum. Alternatively, immediate regeneration of the resting state spectrum occurred upon addition of one equivalent of $K_4Fe(CN)_6$ (Figure 4.5). A Compound II spectrum was not detected as an intermediate prior to return of the resting state spectrum.

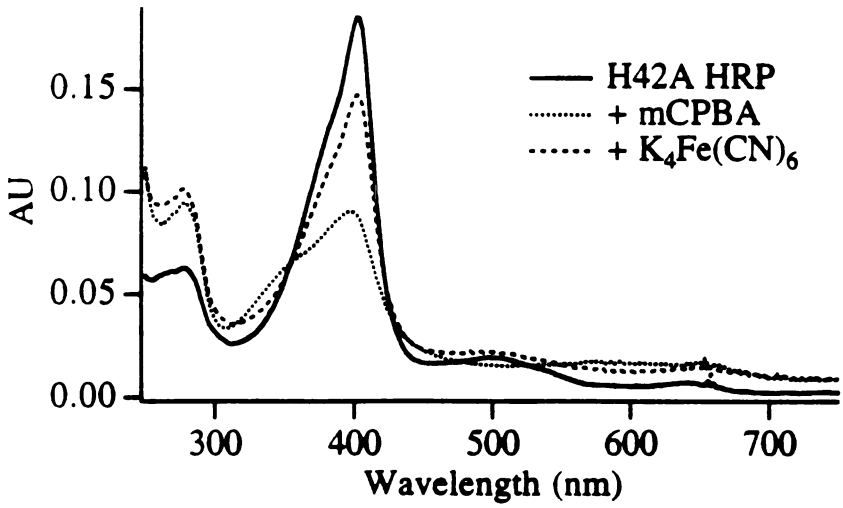

Figure 4.5: Absorption spectra of H42A HRP sequentially reacted with 5 equivalents mCPBA and 1 equivalent ferrocyanide.

Rate of Compound I Formation. A typical stopped flow spectrophotometric trace of Compound I formation showed an exponential decay at 411 nm that leveled off within 20 msec. The plots of k(obsd) versus peroxide concentration were similar for native-, rWT-, and F41A-HRP (Figure 4.6). The second order rate constants, derived from these plots, are listed in Table 4.1. The values obtained for rWT- and F41A-HRP were markedly similar to that obtained for the native enzyme, suggesting that Compound I formation is not appreciably influenced by either the polyhistidine tag that is present in the recombinant protein or removal of the distal phenylalanine.

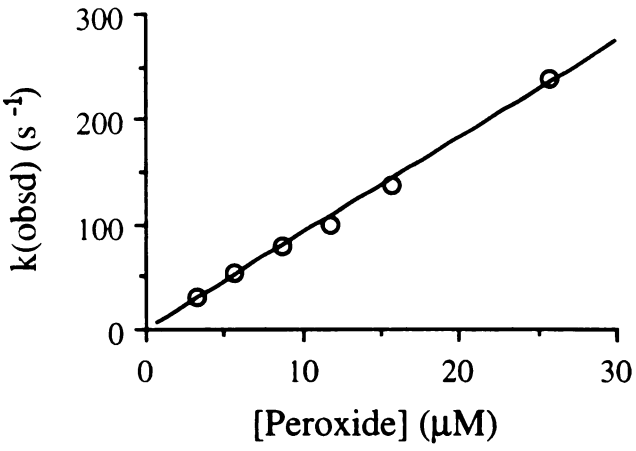

Figure 4.6: Dependence of the pseudo-first order rate constant of Compound I formation, $k_{(obsd)}$, on peroxide concentration. The data shown were determined for rWT HRP as described in the methods.

Table 4.1: The second order rate constants determined for Compound I formation. The values listed for native-, rWT-, and F41A-HRP were determined by monitoring 411 nm decay as described in this section. The values listed for H42A- and H42V-HRP were determined by the steady state kinetic analysis of ABTS oxidation that is described in the text. Each experiment was performed in duplicate and the average, including the deviation between values, is listed.

Enzyme	k_1 ($M^{-1}s^{-1}$)
Native	0.85 (±0.03) $x10^7$
rWT	0.89 (±0.04) $x10^7$
F41A	1.34 (±0.18) $x10^7$
H42A	1.94 (±1.16) $x10^1$
H42V	1.00 (±1.98) $x10^1$

H42A- and H42V-HRP required greater than 500 equivalents of H_2O_2 to produce the exponential decay at 411 nm that is characteristic of Compound I formation in the native enzyme. The corresponding pseudo-first order rate constants were found to depend on peroxide concentration in a nonlinear manner (Figure 4.7).

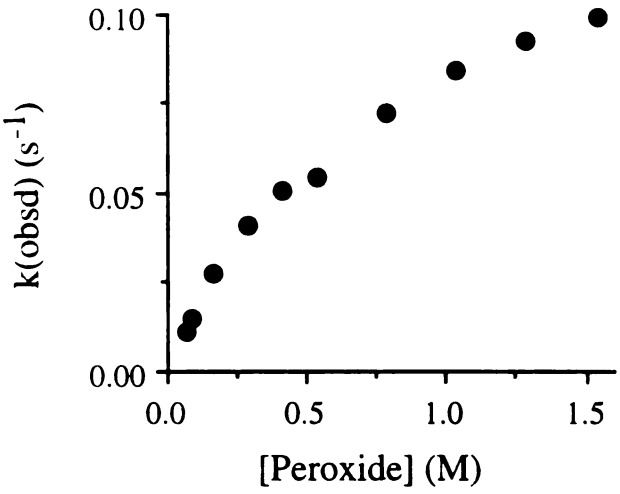

Figure 4.7: Nonlinear dependence of the pseudo-first order rate constant of Compound I formation, $k_{(obsd)}$, on peroxide concentration.

The addition of 0.5 M H_2O_2 to H42A HRP was found by UV/Vis spectrophotometry to cause the resting state Soret to decay sequentially to a Compound III-type spectra (within 30 sec) followed by further decay to a species containing ~680 nm absorption (possibly verdoheme). These species were previously observed when native enzyme was treated with excess peroxide and/or with hydroperoxides or peroxybenzoic acids (Nakajima and Yamazaki, 1980, Marklund, 1973, Bagger and Williams, 1971). The native enzyme forms a Compound III in the presence of excess H_2O_2 that arises through a Compound I species. Formation of the 680 nm species has also been observed for the native enzyme and in one instance was speculated to arise through an alternative oxidative pathway which was independent of Compound I formation (Marklund, 1973). Consequently, the above procedure used to obtain the second order rate constants for

H42A HRP Compound I formation may be obscured at higher peroxide concentrations (> 0.5 M) by the formation of alternative oxidized species in addition to Compound I. The formation of these species would interfere with measurements of Compound I formation at 411 nm. Thus this protocol does not appear to be suitable for determining the rate constants for H42A- and H42V-HRP Compound I formation. Interestingly, the behavior of H42A- and H42V-HRP differs greatly from native enzyme in the rate of Compound I formation, but is similar to native enzyme in supporting the formation of species characteristic of higher oxidized states when exposed to excessive peroxide concentrations.

Steady State Kinetics of H42A HRP. In lieu of directly following Compound I formation for H42A- and H42V-HRP, assays were performed under steady state conditions to obtain rate constants for Compound I formation and for substrate oxidation. This approach required moderate levels of peroxide, relative to those used above, circumventing the formation of Compound III and the 680 nm species obtained with high peroxide levels. Assaying the reaction in the presence of substrate also favored rescue of the reactive Compound I species to give normal enzyme cycling rather than the formation of inactive oxidized heme species.

H42A and H42V-HRP-catalyzed ABTS oxidation trailed off in a time-dependent manner under the assay conditions used. This is probably due to the inactivation by peroxide that is seen when native HRP is exposed to peroxide concentrations greater than 1 mM (Baynton *et al.*, 1994). Initial rates were measured to exclude the effects of enzyme inactivation. The resulting data were plotted as $2[HRP]_o/v$ versus 1/[ABTS]. This primary plot gave a series of approximately parallel lines as observed for the native enzyme (Figure 4.8). A secondary plot was generated by plotting the y-intercept of the primary plot versus $1/[H_2O_2]$ (Figure 4.9). The rate of Compound I formation (k_1) was determined from the inverse slope taken from this secondary plot and was calculated to be 19 $M^{-1}s^{-1}$ for H42A

HRP and 10 $M^{-1}s^{-1}$ for H42V HRP. These values are ~10^6 fold lower than the rate constant obtained for native HRP.

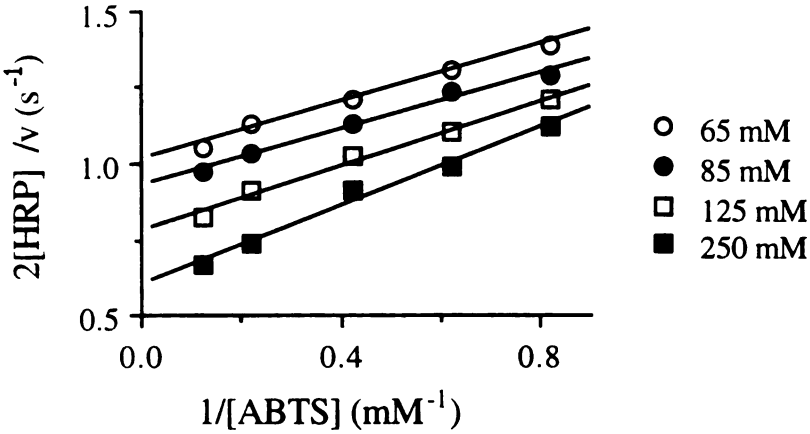

Figure 4.8: Primary plot displaying steady state ABTS activities as catalyzed by H42A HRP. The measured activities are plotted in a double reciprocal fashion to determine the rate constants for Compound I formation and substrate oxidation. The peroxide concentrations used to obtain the series of parallel lines are indicated in the legend.

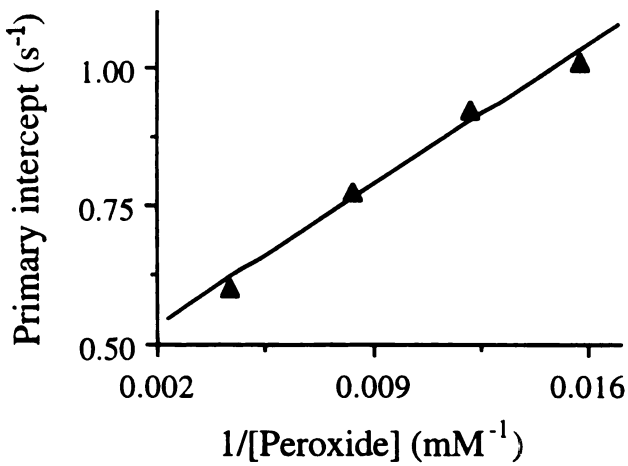

Figure 4.9: Secondary plot generated for the ABTS steady state kinetic analysis of H42A HRP. According to equation 4.2, the y-intercept from the primary plot in Figure 4.8 was in turn plotted versus the reciprocal of the peroxide concentration to obtain the rate constant for Compound I formation, k_1.

The primary plot was also used to determine the rate constant for ABTS oxidation. In native HRP, Compound II turnover is normally rate limiting and steady state kinetics yield a value for k_3. However, we have been unable to detect Compound II formation for the distal histidine mutants, suggesting that reduction of this species is rapid. Consequently, k_2 may be smaller than k_3 for H42A HRP. In this situation the steady state analysis should afford a value for k_2 using equation 4.3. The reciprocal values of the

$$2[HRP]_o/v = (1/k_2)(1/[ABTS]) + (1/k_1)(1/[H_2O_2]) \qquad (4.3)$$

slopes calculated for the parallel lines in Figure 4.8 were averaged to obtain k_2. The resulting values correspond to $1.9 \pm 0.3 \times 10^3$ $M^{-1}s^{-1}$ for H42A HRP and $1.6 \pm 0.3 \times 10^3$ $M^{-1}s^{-1}$ for H42V HRP. For native HRP, k_3 was determined to be 7.2×10^5 $M^{-1}s^{-1}$ at pH 5 (Chapter 6) and k_2 is expected to be ~40 fold higher, by analogy to the oxidation of other peroxidase substrates (Marnett *et al.*, 1986). Reduction of Compound I by the distal histidine mutants appears to be at least 100 fold slower. This suggests that the distal histidine plays a role in the reduction of Compound I as well as the formation of Compound I, although clearly the latter is most prominently influenced by removal of the distal histidine.

Rate Constant for Compound II Formation. A plot of the pseudo-first order rate constant versus ferrocyanide concentration is shown in Figure 4.10. Native-, rWT-, and F41A-HRP give similar second order rate constants (Table 4.2). This further establishes that removal of the distal phenylalanine has little influence on peroxidase cycling. The measured values of k_2 for H42A- and H42V-HRP were ~5 times lower than for native HRP. This suggested that the distal histidine only plays a small role in the reduction of Compound I by ferrocyanide.

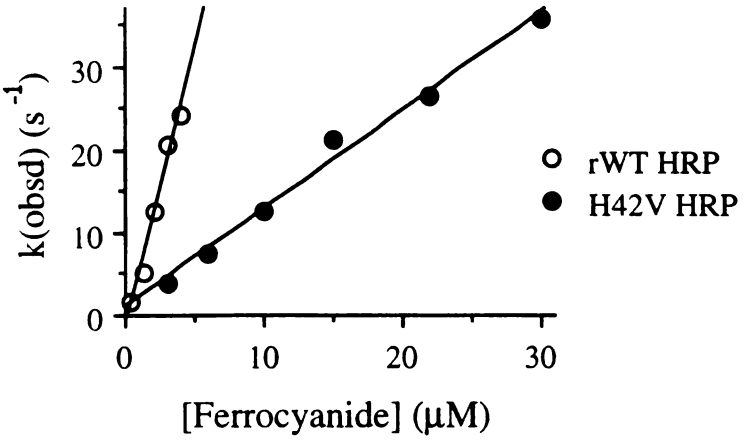

Figure 4.10: The linear dependence of the pseudo-first order rate constant on the concentration of ferrocyanide. The value of the slope was used to determine k_2, the rate constant for the reduction of Compound I.

Table 4.2: The second order rate constants determined for the reduction of Compound I by ferrocyanide.

Enzyme	k_2 ($M^{-1}s^{-1}$)
Native	7.6×10^6
rWT	6.6×10^6
F41A	6.7×10^6
H42A	1.2×10^6
H42V	1.2×10^6

Guaiacol Activity. rWT- and F41A-HRP exhibited native-like guaiacol peroxidase activity, and the distal histidine mutants displayed significantly reduced rates of guaiacol activity which corresponded to ~10^5 fold decrease from native activity (Table 4.3). This

dramatic drop in peroxidase activity mirrors the decreased rate of Compound I formation observed for these distal histidine mutants (Table 4.1).

Table 4.3: Rates of guaiacol, thioanisole, and styrene oxidation as catalyzed by the native and recombinant proteins. For thioanisole sulfoxidation and styrene epoxidation, the enantiomeric excess is reported within the parentheses.

Enzyme	Guaiacol Oxidized[a] (nmol sec^{-1} μmol^{-1})	Sulfoxide Produced[b] (%S) (nmol sec^{-1} μmol^{-1})	Styrene Oxide Produced[b] (%S) (nmol sec-1 μmol-1)
Native	$1.6 \pm 0.6 \times 10^6$	6.0 ± 1.1 (82.9)	trace
rWT	$1.5 \pm 0.4 \times 10^6$	1.2 ± 0.2 (65.6)	trace
F41A	$2.0 \pm 2.0 \times 10^6$	131 ± 23 (64.6)	0.11 ±.0.00 (38.0)
H42A	$2.1 \pm 0.0 \times 10^1$	15.1 ± 1.6 (91.8)	0.35 ±0.04 (82.2)
H42V	$2.2 \pm 0.5 \times 10^1$	11.2 ± 0.2 (92.6)	0.35 ± 0.06 (80.8)
P450 cam	ND	58.3 (28)	18.3 (74)

[a]Guaiacol oxidation was performed at 25 °C. [b]Thioanisole sulfoxidation and styrene epoxidation were performed at 4 °C. [c]The rates of $P450_{cam}$-catalyzed thioanisole sulfoxidation and styrene epoxidation were determined at 25 °C by Julie Fruetel (Fruetel *et al.*, 1994; Fruetel *et al.*, 1992).

Thioanisole Sulfoxidation. Thioanisole sulfoxidation was assayed at 4°C because rates measured at 25°C for the mutant proteins leveled off quickly, presumably due to enzyme inactivation. Similar inactivation was observed in the oxidation of guaiacol by F41A HRP and is probably due to turnover-dependent inactivation since F41A HRP is as thermally stable as the native enzyme (Chapter 2). Consequently, thioanisole sulfoxidation

was monitored over the course of 5 min and the distal histidine mutants were monitored for 15 min. At 4°C, thioanisole was oxidized non-enzymatically at a rate of 2.5 pmol s^{-1}. This value was subtracted from the measured data to obtain the reported enzymatic rates and enantiomeric excess values (Table 4.3).

The wild-type proteins displayed similar sulfoxidation rates, with the native enzyme displaying 5 fold higher activity relative to the recombinant protein (Table 4.3). The enantioselectivity of the reaction between the native- (83% ee) and rWT-HRP (66% ee) proteins also differed slightly. This might result from the differences in glycosylation or from the polyhistidine tag found at the N terminus of rWT HRP. Three of eight glycosylated asparagine residues within native HRP -Asn 186, 198, and 214- are found within a sequence unique to this peroxidase. In the sequence alignment of lignin peroxidase with HRP, a gap is inserted into this region in lignin peroxidase (Welinder, 1992a). The residues that flank this gap, Val 184 and Asp 185, lie within the substrate channel of lignin peroxidase (Poulos *et al.*, 1993). We might expect that this unique HRP sequence would also constitute a portion of the solvent accessible channel and that differences in glycosylation resulting from expression in insect cells could affect how substrate is presented to the ferryl oxygen. This altered presentation of substrates could possibly alter the enantiospecificity of the sulfoxidation reaction.

F41A displayed a 20 fold higher rate of thioanisole sulfoxidation than the native enzyme. The enantiospecificity of the reaction was similar to rWT, suggesting that thioanisole binding was not significantly altered in the recombinant protein by removal of the distal phenyl group.

A two to ten fold improvement in the rate of sulfoxidation was observed for the distal histidine mutants relative to the wild-type proteins. This activity exhibited by the distal histidine mutants was sensitive to the peroxide concentration present in the assay. A five fold decrease in the peroxide concentration caused a 2-3 fold decrease in the rates of

sulfoxidation. This suggested that Compound I formation in H42A- and H42V-HRP was partially rate limiting since the same decrease in peroxide concentration did not influence the thioanisole sulfoxidation rates of the wild-type and F41A proteins. H42A- and H42V-HRP displayed similar enantioselectivities, 92% ee and 93% ee, respectively. These values are significantly higher than those measured for native-, rWT- and F41A-HRP, suggesting that thioanisole binding is altered by removal of the distal histidine.

Styrene Epoxidation. Styrene epoxidation rates were assayed at 4°C to reduce the enzyme inactivation observed at 25°C. Non-enzymatic styrene epoxidation did not occur under these conditions. The styrene epoxidation reaction was monitored over the course of 20 min for F41A HRP and for 10 min for the distal histidine mutants. Only trace amounts of styrene oxide were detected with the wild-type proteins (Table 4.3). F41A-, H42A- and H42V-HRP, however, gave improved activities that were easily quantitated. The distal histidine mutants displayed styrene epoxidation activity that was slightly higher than that of F41A HRP despite the much lower rates of Compound I formation (Table 4.1). This is reversed from the rates determined for thioanisole sulfoxidation for these mutants. F41A HRP preferentially formed (R)-styrene oxide (62% ee), displaying similar enantioselectivity to that displayed for thioanisole sulfoxidation. (R)-Thioanisole sulfoxide is structurally similar to (S)-styrene oxide. In contrast, H42A- and H42V-HRP show enantioselectivity that is opposite to that of F41A HRP.

Reaction of HRP Wild-type and Mutant Proteins with Phenyldiazene. Phenyldiazene was allowed to react with the recombinant proteins to probe the altered solvent accessibility to the heme group. The addition of phenyldiazene caused similar Soret band decay for native-, rWT- and F41A-HRP, although the F41A reaction occurred more rapidly (within 5 min versus ~20 min) and Soret band decay occurred to a greater extent (Figure 4.11). H42A- and H42V-HRP also displayed a decreased Soret absorption but were unique in exhibiting spectra that contained numerous maxima, including one at 434

nm. Gel filtration cleaned up the near UV region of the spectra but did not alter the Soret region, suggesting that absorption in this region was due to heme bound by the enzyme and not due to phenyldiazene oxidation products.

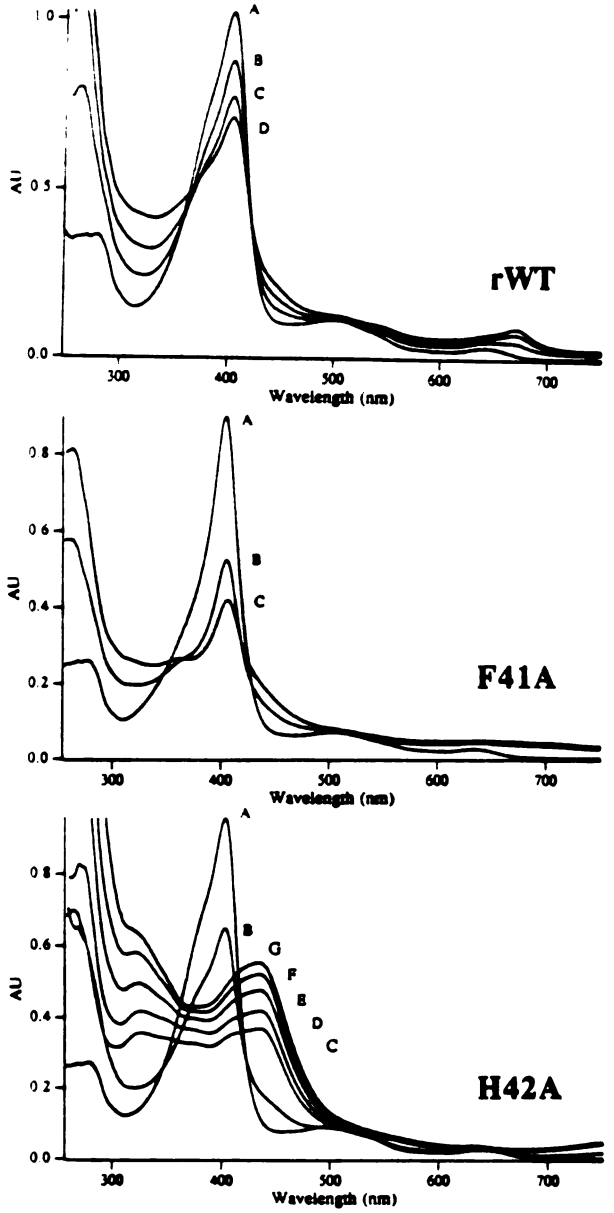

Figure 4.11: Time-dependent decay in Soret absorption observed for the reaction of phenyldiazene with rWT-, F41A-, and H42A-HRP. Plot a: spectra of rWT-HRP (10 nmol) observed with the addition of 0 (A), 57 (B), 113 (C), and 170 (D) nmol phenyldiazene. Plot b: spectra of F41A-HRP (10 nmol) observed with the addition of 0

(A), 57 (B), and 113 (C) nmol phenyldiazene. Plot c: spectra of H42A-HRP (10 nmol) observed with the addition of 0 (A), 57 (B), 113 (C), 170 (D), 227 (E), 284 (F), and 340 (G) nmol phenyldiazene.

In the analysis of modified hemes (workup A), the resulting HPLC chromatogram for rWT HRP was native-like, displaying three heme derived products as observed previously for the reaction of phenylhydrazine with native HRP (Ator and Ortiz de Montellano, 1987) (Figure 4.12). As determined by standards, the peaks eluting at retention times of 5.5 and 7 min corresponded to 8-hydroxymethylheme and unmodified heme. Presumably, the peak eluting at 12 min corresponded to δ-*meso*-phenylheme. These peaks were not obtained to an appreciable extent in the F41A HRP chromatogram, suggesting that the heme within F41A HRP is extremely susceptible to modification and/or degradation. A novel peak, representing the major product, eluted at 9 min with λ_{max} = 400 nm. The structure of the modified heme corresponding to this peak has not been identified. Phenyldiazene-treated H42A- and H42V-HRP also gave novel chromatograms that were equivalent to one another. The major peak in these chromatograms corresponded to unmodified heme.

In the analysis of N-phenylprotoporphyrin IX products (workup B), native-, rWT-, and F41A-HRP failed to produce the N-phenyl adducts generated in the reaction of phenyldiazene with myoglobin, catalase, and P450s. This was demonstrated by the lack of such products in the corresponding HPLC chromatograms. However, the distal histidine mutants displayed products that coeluted with the N-phenylprotoporphyrin IX standards generated within myoglobin. Interestingly, the N-phenyl adducts were formed in enantioselective fashion (B:A:C:D 7:23:0:70) (Figure 4.13). This differs from myoglobin, where nearly equal formation of the four isomers occurs (21:24:26:29).

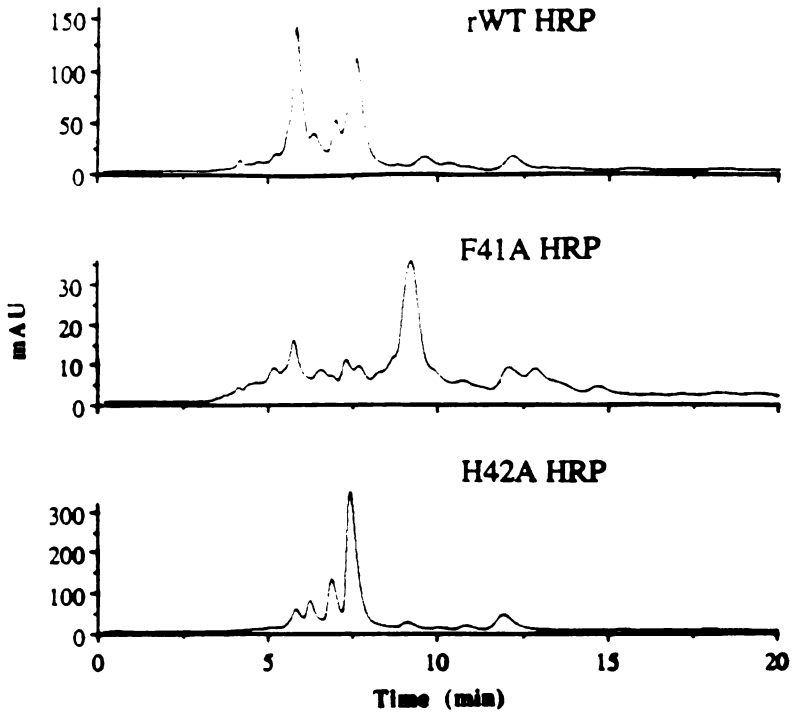

Figure 4.12: HPLC chromatograms of the modified hemes obtained from the reaction of phenyldiazene with rWT-, F41A-, and H42A-HRP. The peaks exhibiting the retention times 5.5, 7, and 12 min correspond to 8-hydroxymethylheme, unmodified heme, and δ-*meso*-phenylheme, respectively.

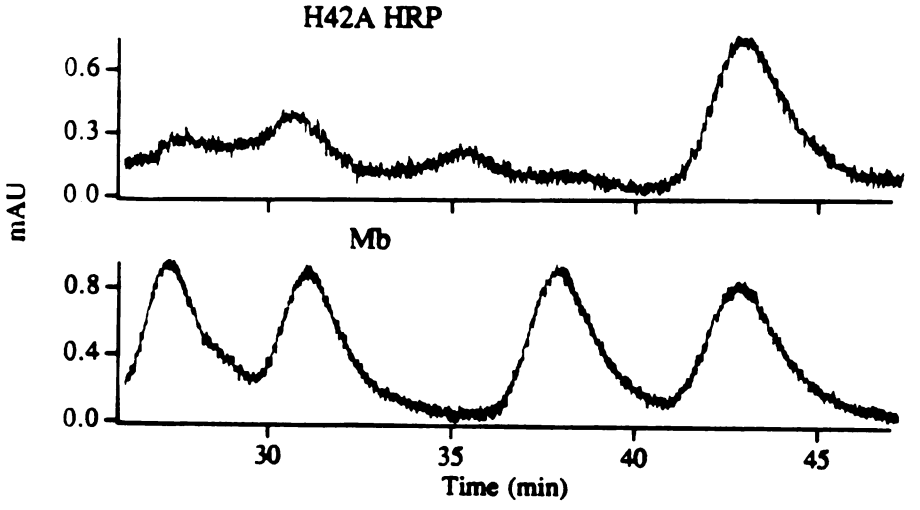

Figure 4.13: HPLC chromatograms of N-phenylprotoporphyrin IX products obtained from the reaction of phenyldiazene with myoglobin and H42A HRP. The N-

phenylprotoporphyrin IX isomers B, A, C, and D elute with retention times 27.3, 31.0, 37.8 and 42.7 min, respectively.

DISCUSSION

As discussed in Chapter 2, peroxidase function displayed by rWT HRP is equivalent to that observed for the plant enzyme. The studies presented in this chapter demonstrate rWT HRP to exhibit native-like Compound I formation and Compound II formation. Furthermore, the accessibility of the rWT HRP-bound heme molecule, as probed by modification with phenyldiazene, is similar to that of the native enzyme. Thus, the polyhistidine tag and the differing glycosylation patterns that distinguish rWT HRP from native HRP do not appreciably influence peroxidase function. Peroxygenase activity, namely thioanisole sulfoxidation, is slightly altered between the two wild-type enzymes. Thioanisole sulfoxidation is five fold slower for rWT HRP relative to native HRP. This may be explained by differences in the binding of thioanisole by native- and rWT-HRP, since the enantiomeric excess of the (S)-thioanisole sulfoxide varies between the two proteins. Differences in glycosylation between the two wild-type proteins may account for the altered activity displayed by rWT HRP.

Removal of the distal phenyl group through mutation also does not significantly alter peroxidase activity, but does sensitize the F41A mutant to turnover-dependent inactivation. As illustrated by the relatively rapid decay of Compound I to Compound II for F41A- versus rWT-HRP, Phe 41 is likely to play a role in stabilizing Compound I. This postulated stabilizing role does not appear to influence the reactivity of Compound I, since the rate of reduction of the F41A Compound I species by $K_4Fe(CN)_6$ is comparable to that measured for the reduction of the wild-type Compound I species (Table 4.2). The distal phenylalanine, being resistant to oxidation, may serve to isolate the highly oxidized heme associated with Compound I, preventing the oxidation of distal residues that could

potentially inactivate the enzyme. Thus the distal phenylalanine may serve to promote tight regulation of electron transfer between substrate and the heme molecule.

Compound I formation is severely deterred in the distal histidine mutants. The increased H_2O_2 concentrations required to facilitate Compound I formation are probably needed to increase peroxide anion levels to promote formation of the iron-peroxide complex in the absence of the distal histidine. In the steady state analysis of ABTS oxidation performed at pH 6, the anionic peroxide species is found at a concentration that is reduced 4.5×10^6 fold relative to the neutral peroxide. Substantial ABTS activities for 500 nM H42A- and H42V-HRP require 65 mM H_2O_2, the smallest peroxide concentration used in this experiment. This level of peroxide corresponds to 160 nM of the peroxide anion. Thus a 1:3 ratio of the peroxide anion to the enzyme is required to see significant peroxidase activity. The decreased rate of Compound I formation exhibited by the distal histidine mutants parallels the decreased rate of guaiacol peroxidation, which is reduced by five orders of magnitude (Table 4.3). Thus rapid peroxidase cycling is shown to be supported by rapid peroxide activation.

ABTS and $K_4Fe(CN)_6$ oxidation characterized independently of Compound I formation also shows that removal of the distal imidazole influences the oxidation of peroxidase substrates. In particular the rates of reduction of Compound I and Compound II appear to be reversed from those found for the native enzyme. This conclusion may be drawn from the reaction of H42A Compound I with $K_4Fe(CN)_6$ which shows the Compound I spectrum to decay directly to the resting state spectrum (Figures 4.4 & 4.5). In the native enzyme the slower rate of Compound II reduction relative to Compound I reduction, allows detection of the Compound II intermediate. The rate that H42A- and H42V Compound I is reduced by $K_4Fe(CN)_6$ is only five fold slower than that of the native enzyme (Table 4.2). This suggests that (a) the distal histidine plays a minor role in the reduction of Compound I and (b) the rate of reduction of Compound II, which is

speculated to be greater than 1.2 x 10^6 $M^{-1}s^{-1}$ when reduced by ferrocyanide, is faster than that displayed by the native enzyme. This latter conclusion suggests that the distal histidine also plays an insignificant role in promoting the reduction of Compound II. In regenerating the resting state species from Compound II in the native enzyme, the hydrogen bond donated by the distal histidine is speculated to provide a proton to the ferryl oxygen for the formation of a water molecule. This reasoning may explain the dramatic decrease in native HRP peroxidase activity observed when this hydrogen bond is lost under alkaline conditions (Dunford and Stillman, 1976). Thus we might expect H42A- and H42V-HRP, which do not have a distal imidazole to donate a hydrogen bond to the ferryl oxygen, to display an inactive Compound II species. However, turnover studies performed on H42A HRP demonstrated two guaiacol molecules to be oxidized per molecule of H_2O_2 (data not shown), suggesting that both oxidative equivalents of Compound I are used by H42A HRP to oxidize substrates. The surprising activity of the H42A- and H42V-Compound II species may be allowed by the cavity created by the H42A mutation which could permit solvent molecules to protonate the ferryl oxygen in the formation of a water molecule in the reduction of Compound II (Figure 4.14). Alternatively, the activity of the Compound II

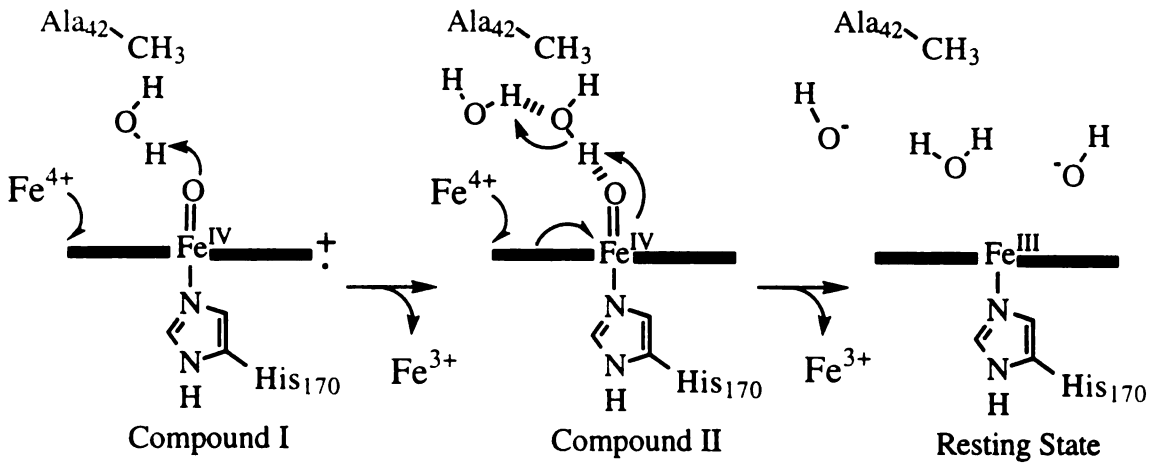

Figure 4.14: Postulated mechanism of the oxidation of ferrocyanide by Compound I and Compound II as catalyzed by H42A HRP. $K_4Fe(CN)_6$ is represented by Fe^{4+}.

species of the distal histidine mutants may be due to the substrate being able to oxidize the heme iron directly. As demonstrated by the peroxygenase studies described below, the distal mutants display improved accessibility to the ferryl oxygen of Compound I. Interestingly, only one equivalent of ferrocyanide is required to regenerate the H42A HRP resting state spectrum from the Compound I spectrum. Thus we expect one oxidizing equivalent to be retained by the ferrocyanide-reduced species shown in Figure 4.5. The regenerated resting state spectrum demonstrates that this oxidizing equivalent is not detected by electronic absorption spectroscopy suggesting that it is not associated with the heme molecule. The spectrally-invisible oxidative equivalent may be associated with the protein in the form of a protein radical. EPR studies, aimed at elucidating the nature of this oxidizing equivalent, should determine the electronic structure of the H42A HRP Compound I species. If the Compound II species of H42A HRP is characterized by a protein radical, it would suggest that the hydrogen bond between the distal histidine and the Compound II ferryl oxygen stabilizes the oxidative equivalent associated with this species.

The role that the distal histidine plays in the reduction of Compound I is substrate-dependent, as suggested by the significant influence that removing the distal imidazole has on the oxidation of ABTS versus ferrocyanide. The disparity between the rates of oxidation of ABTS and $K_4Fe(CN)_6$ as measured for the distal histidine mutants may be based on the manner in which these substrates were assayed. ABTS steady state turnover was assayed in the presence of relatively high peroxide concentrations (65-250 mM) while the single turnover oxidation of $K_4Fe(CN)_6$ by Compound I was performed with five equivalents (3.4 μmol) of mCPBA. The presence of excess peroxide in the ABTS assay and the accessibility of the ferryl oxygen of H42A and H42V Compound I may cause the distal histidine mutants to display catalase activity where two peroxide molecules disproportionate into one water molecule and one dioxygen molecule. Alternatively, the

structural differences between ABTS and $K_4Fe(CN)_6$ may deter the former from directly reducing Fe(IV) to Fe(III) and cause ABTS oxidation by Compound II to be rate-limiting. Ferrocyanide is smaller than ABTS and, consequently, may be able to directly reduce Fe(IV).

As is characteristic of the native enzyme, rWT HRP displayed weak peroxygenase activity relative to the P450s (Table 4.3). Thioanisole sulfoxidation catalyzed by HRP is 10-50 fold less active than that observed for $P450_{cam}$, and styrene epoxidation catalyzed by HRP is at least three orders of magnitude slower than that observed for $P450_{cam}$. In contrast, F41A HRP-catalyzed peroxygenase activity occurs at a rate that is more similar to the P450s. This mutant sulfoxidizes thioanisole ten fold faster than rWT HRP and oxidizes styrene at least ten fold faster than rWT HRP. Thus, shrinking the bulky phenylalanine side chain into that of an alanine appears to improve substrate accessibility to the ferryl oxygen. Inspection of the distal residues in the CCP and PeP crystal structures reveals that Phe 41 is likely to play only a minor role in restricting substrate accessibility to the ferryl oxygen. The distal histidine, which sits directly over the iron, is likely to be the predominant barrier restricting access to the iron atom. Improved ferryl accessibility in the F41A mutant is therefore likely to occur through partial migration of the distal histidine into the cavity created by removal of the phenyl group. Interestingly, the predicted increase in distal histidine mobility does not deter peroxide activation in the formation of Compound I. Improved iron accessibility in the F41A mutant was not improved to the extent that it allows an iron-phenyl complex to form. Reaction of F41A HRP with phenyldiazene yields heme modification that is more characteristic of the native enzyme than of the P450s (Figure 4.12). The enantioselectivities displayed by F41A HRP in oxidizing thioanisole and styrene are conserved, suggesting that these two substrates may bind in a similar manner. Regarding thioanisole sulfoxidation, the enantioselectivity is preserved relative to

rWT HRP. This suggests that substrate binding is similar between the two proteins and that the cavity created by the F41A mutation does not appreciably perturb substrate binding.

The distal histidine mutants display improved peroxygenase activities relative to rWT HRP. The rate of thioanisole sulfoxidation was 10 fold slower than that measured for the F41A mutant. This decreased ability to sulfoxidize thioanisole can be attributed to Compound I formation being partially rate limiting for the distal histidine mutants. Thus these mutants have conflicting features. The cavity created by removing the imidazole group allows substrate access to the ferryl oxygen, but removal of this catalytic group also greatly retards Compound I formation and slows reaction cycling. H42A- and H42V-HRP oxidize styrene three fold faster than F41A HRP, and, collectively, these rates are ~50 fold slower than those observed for thioanisole sulfoxidation. Thus the slower overall rate of styrene epoxidation is less limited by the weakened ability to form Compound I in the absence of the distal histidine, and the extent by which the ferryl oxygen is accessible appears to limit the rate of styrene epoxidation. The improved enantioselectivity exhibited by H42A- and H42V-HRP in the oxidation of thioanisole signifies a change in substrate binding within these mutants. This further supports the view that removal of the distal histidine influences the immediate environment surrounding the ferryl oxygen since this region is speculated to interact with peroxygenase substrates to promote oxygen transfer. In styrene epoxidation, the distal histidine mutants preferentially produce (S)-styrene oxide. This enantiomer is opposite in conformation to the (S)-thioanisole sulfoxide which is predominantly formed by H42A- and H42V-HRP. This may suggest the existence of two distinct binding sites for styrene and thioanisole. However, removal of the distal histidine may also loosen the binding of styrene, allowing movement of the vinyl group relative to the ferryl oxygen (Figure 4.15).

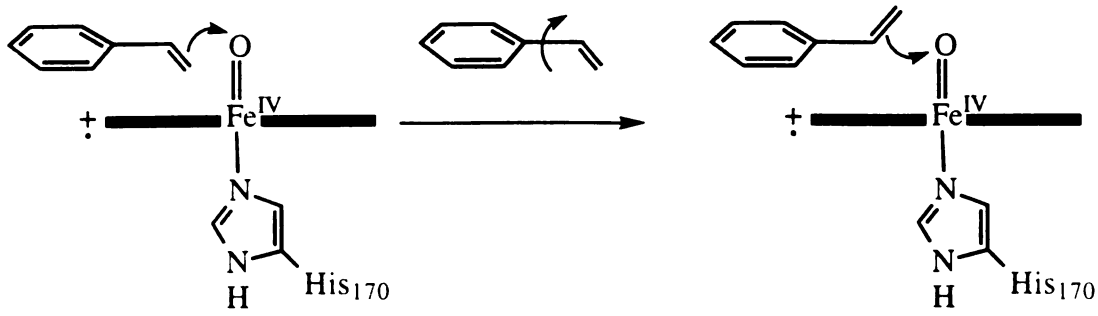

Figure 4.15: Possible mechanism for differing enantioselectivity of H42A- and H42V-HRP-catalyzed styrene epoxidation. The rotation of the vinyl group, allowed by freer movement of the styrene molecule within the cavity created by the H42A mutation, may allow differing attack of the vinyl group π electrons on the ferryl oxygen of Compound I.

Improved ferryl accessibility within both H42A- and H42V-HRP is most dramatically shown by the formation of iron-phenyl complexes (λ_{max} = 434 nm) when these mutants are treated with phenyldiazene (Figure 4.11). Treating these complexes with strong acid promotes the migration of the phenyl group to the pyrrole nitrogen, generating the N-phenyl complexes observed by HPLC analysis (Figure 4.13). The phenyl group of the iron-phenyl complex generated within P450s can be shifted to the pyrrole nitrogen in one of two ways. Equal shifting to all four pyrrole nitrogens is achieved with the addition of strong acid. These conditions also cause the protein to denature. The iron-phenyl complex generated within myoglobin can be similarly treated and yields equal formation of the four N-phenylprotoporphyrin IX isomers (Figure 4.13) (Swanson and Ortiz de Montellano, 1991). Alternatively, the addition of ferricyanide to the iron-phenyl complex generated within P450s promotes the migration of the phenyl group within the intact protein and typically yields the four isomers in varying proportions (Ortiz de Montellano, 1995). This has been used extensively to learn the topology of P450 active sites. Ferricyanide does not shift the phenyl group of the iron-phenyl complex within myoglobin.

The differing reactivities exhibited by myoglobin and P450s have been attributed to the differing fifth heme ligands found in these two proteins. The phenyl group of the iron-phenyl complex generated within H42A- and H42V-HRP, as is observed with myoglobin, does not shift with the addition of ferricyanide. However, the migration of the phenyl group, promoted by strongly acidic conditions, yields unequal proportions of the four N-phenyl isomers (B:A:C:D 7:23:0:70). This may suggest that under the acidic conditions used to promote the iron to nitrogen shift, the protein is still intact and promotes shifting of the phenyl group to the D pyrrole ring. Interestingly, the D pyrrole is the most accessible nitrogen found in the peroxidase crystal structures.

CONCLUSIONS

The most significant role played by the distal residues in HRP cycling is the peroxide-activating role played by His 42 in the formation of Compound I. The removal of this imidazole group through mutagenesis decreases the rate of peroxidase activity to a level that is comparable to the rates of peroxygenase activities. This finding suggests that the distal histidine alone promotes the rapid rate of peroxidase activity and that P450s are not hindered by the absence of a distal histidine because oxygen transfer rates are slow. Within HRP, increasing access to the ferryl oxygen was afforded through replacing bulky distal heme residues by residues of smaller size. The increased peroxygenase activity exhibited by F41A-, H42A-, and H42V-HRP supports the theory that increasing access to the heme iron improves the feasibility of oxygen transfer.

Chapter 5: Rescue of Compound I Formation for the Distal Histidine (H42A) HRP Mutant by Exogenous Imidazoles

INTRODUCTION

The distal histidine, His 42 in HRP, is a crucial residue to peroxidase catalysis and is postulated to act as a general acid/base catalyst in the three steps that make up the peroxidase cycle. This distal residue predominantly supports the rapid formation of Compound I formation, as is clearly seen from the H42A HRP, H42V HRP, and H52L CCP mutants, for which the rate of Compound I formation is decreased by 5-6 orders of magnitude (Chapter 4; Newmyer and Ortiz de Montellano, 1995; Erman *et al.*, 1993). The distal histidine is postulated to initiate Compound I formation by deprotonating a molecule of peroxide in the vicinity of the heme iron (Figure 5.1). This action generates the nucleophilic peroxide anion that can readily attack the ferryl oxygen, facilitating formation

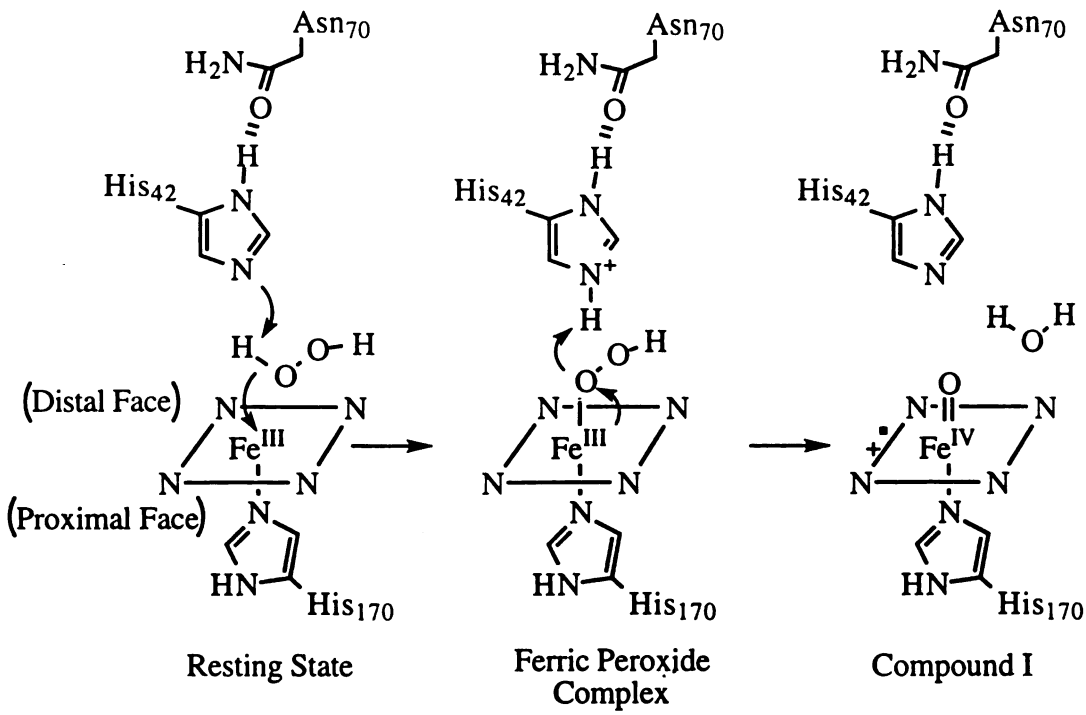

Figure 5.1: Proposed role for the distal histidine in the mechanism of Compound I formation. Residue numbering is based on the HRP sequence.

of the ferric peroxide complex (Fe-OOH). Two electrons are subsequently donated from the heme iron to the iron-oxygen bond, and the proton initially abstracted by the distal histidine is thought to be donated to the distal oxygen of the ferric peroxide complex. These events promote the heterolytic cleavage of the dioxygen bond, resulting in release of the distal oxygen as a molecule of water. The heme of the remaining Compound I species retains the proximal oxygen atom of the peroxide (Adediran and Dunford, 1983) and two oxidation equivalents in the form of a porphyrin radical cation and an oxidized iron atom, Fe(IV) (Dolphin *et al.*, 1974; Moss *et al.*, 1969).

Other heme pocket residues assist the distal histidine in promoting Compound I formation. An invariant distal asparagine forms a hydrogen bond with the distal histidine. This interaction is featured in the crystal structures that have been solved for CCP (Finzel *et al.*, 1984), LIP (Poulos *et al.*, 1993), ARP (Kunishima *et al.*, 1994), AXP (Patterson and Poulos, 1995), and PeP (Poulos, unpublished structure). The catalytic function of this hydrogen bond has only recently been explored. The analogous residue in HRP, Asn 70 (Welinder, 1992a), was mutated to a valine (Nagano *et al.*, 1995), and the resulting mutant is ~25 fold less reactive in the formation of Compound I. The distal asparagine residue probably promotes Compound I formation by structurally and functionally influencing the distal histidine. This hydrogen bond acceptor may act to orient the imidazole by hydrogen bonding the $N_{\delta 1}$ nitrogen atom so that the $N_{\varepsilon 2}$ nitrogen atom sits directly over the heme iron and is free to accept a proton in the formation of Compound I. Hydrogen bonding to Asn 70 is also likely to modulate the basicity of the distal histidine, although this role has not been examined.

The essential role that the distal histidine plays in Compound I formation largely influences the rate of peroxidase catalysis. This theory stems from the decrease in peroxidase activity that parallels the 10^5 decrease in the rate of Compound I formation when His 42 is mutated to an alanine or valine in HRP (Chapter 4). Removal of an

essential residue in other enzymes--*e.g.*, lysine in aspartate aminotransferase (Toney and Kirsch, 1989), lysine in ribulose bisphospate carboxylase (Harpel and Hartman, 1994), and aspartate in trypsin (Perona *et al.*, 1994)--has similarly generated mutant proteins which exhibited either weak or no activity. For these enzymes, partial rescue of mutant activity was promoted by the addition of exogenous compounds that mimicked the functional group lost through mutation (amines and acetates). The rescue of activity by exogenous compounds has helped in assigning the role that the functional group plays in catalysis. The following experiments explore the possibility of binding exogenous imidazole to the H42A HRP mutant and examine the ability of imidazole to rescue Compound I formation and peroxidase activity.

MATERIALS & METHODS

Imidazole Rescue of H42A HRP Guaiacol and ABTS Activities. Guaiacol and ABTS activities were assayed in the presence of several imidazole derivatives which included imidazole, 1-methylimidazole, 2-methylimidazole, and 1,2-dimethylimidazole. Both assays were carried out at 25°C. In assaying guaiacol activity, 500 nM H42A HRP was added to 5.1 mM guaiacol in 100 mM K_2HPO_4, pH 6.0. H_2O_2 was added to initiate the reaction (0.5 mM final concentration). Guaiacol oxidation, defined as the absorption gained at 470 nm with the loss of one guaiacol molecule, was monitored spectrophotometrically (ε_{470} = 2.75 $mM^{-1}cm^{-1}$). In assaying ABTS activity, 50 nM H42A HRP was added to 5 mM ABTS in 100 mM Na_2HPO_4, pH 7.0. H_2O_2 was added to initiate the reaction (0.5 mM final concentration), and ABTS radical cation formation was monitored at 414 nm (ε_{414} = 36 $mM^{-1}cm^{-1}$) (Childs and Bardsley, 1975). A high concentration (~5 M) imidazole solution (pH adjusted to 7.0) was prepared and aliquotted into each assay in increasing amounts (5-50 mM final concentration, based on the concentration of the neutral imidazole form at pH 7 as calculated by the Henderson-

Hasselbalch equation). Aliquots of a 5 M NaCl solution were added to maintain constant ionic strength (0.5 M).

Determination of the pH Profile for H42A HRP Guaiacol Activity, Determined in the Presence and Absence of Imidazole. Guaiacol activity was monitored spectrophotometrically as stated above. H42A HRP (10 μM) and guaiacol (5 mM) were added to assay buffer of varying pH: 25 mM solutions of acetate (pH 4-5.5), phosphate (pH 6-8) and borate (pH 8.5-10) were used to assay a wide pH range. The ionic strength was adjusted to 0.1 M with NaCl. H_2O_2 was added to initiate the reaction (0.5 mM final concentration). H42A HRP was assayed alone and in the presence of either 1 mM 1,2-dimethylimidazole or 2-methylimidazole.

K_d of 2-Methylimidazole and 1,2-Dimethylimidazole Binding to H42A HRP. Difference spectroscopy was used to estimate the K_d for 2-methylimidazole and 1,2-dimethylimidazole binding by H42A HRP. Enzyme/imidazole solutions were prepared and scanned spectrophotometrically (300-550 nm). The sample solution contained H42A HRP (10 μM final concentration) and varying amounts of either 2-methylimidazole or 1,2-dimethylimidazole (0.24 -2.3 M) in 100 mM Na_2HPO_4, pH 7.0. These amounts were prepared by adding varying volumes of a concentrated, aqueous imidazole solution that had been adjusted to pH 7.0. These high imidazole concentrations gave residual absorption in the visible region, so the reference cuvette solution contained a similar level of imidazole in 100 mM Na_2HPO_4 buffer. A spectrum of 10 μM H42A HRP in Na_2HPO_4 was subtracted, using Cary 1E Spectrophotometer software, from the experimental spectra to give the final difference spectra used in the K_d calculation. The above solutions were allowed to equilibrate 1 h with periodic mixing prior to scanning.

Rescue of H42A HRP Compound I Formation With a Series of 1,2-Disubstituted Imidazoles. A series of 1-methyl-2-substituted imidazoles were synthesized, using literature protocols. 1,2-Dimethylimidazole, available through Aldrich, was further

purified by distillation under reduced pressure. 2-Ethyl- and 2-propylimidazoles were N-methylated with iodomethane as was reported for the N-methylation of ethyl imidazole-4-carboxylate (Takeuchi *et al.*, 1978). 1-Methyl-2-bromoimidazole was synthesized by generating the imidazolium ion with n-butyllithium and treating this intermediate with 1,2-dibromoethane (Miller *et al.*, 1994). 1-Methyl-2-butylimidazole was similarly generated by treating the imidazolium ion with 1-bromobutane. Reaction of 1-methylimidazole with paraformaldehyde yielded 1-methyl-2-(hydroxymethyl)imidazole (Reese *et al.*, 1993). The structures and purities of all the materials synthesized were verified by H^1 NMR and mass spectrometry. The molecular volume of the 1,2-disubstituted imidazoles was determined using a program written by Dan Gschwend (UCSF).

Compound I formation was assayed by following the decrease in absorption at 402 nm at 25°C. The assay solution included 2 μM H42A HRP in 100 mM sodium phosphate, pH 7.0. Varying levels of 1,2-disubstituted imidazoles were mixed into the enzyme solution, giving a 1 ml final volume. The resulting solutions were incubated for 1 h prior to initiating the formation of Compound I by the addition of H_2O_2, which was also added in varying concentrations. The extinction coefficient, $\varepsilon_{402} = 5.24 \times 10^4\ M^{-1}cm^{-1}$, was used to convert the raw data into rates of Compound I formation. This constant was determined by monitoring the decrease in absorption at 402 nm upon addition of partial equivalents of H_2O_2 to rWT HRP.

RESULTS

Imidazole Rescue of Guaiacol and ABTS Activities. The dependence of guaiacol and ABTS activities on the concentration of the free base form of imidazole is shown in Figure 5.2. The concentration of the neutral imidazole form is plotted because the pH profile discussed below shows that the rescue of activity is due to the free base form.

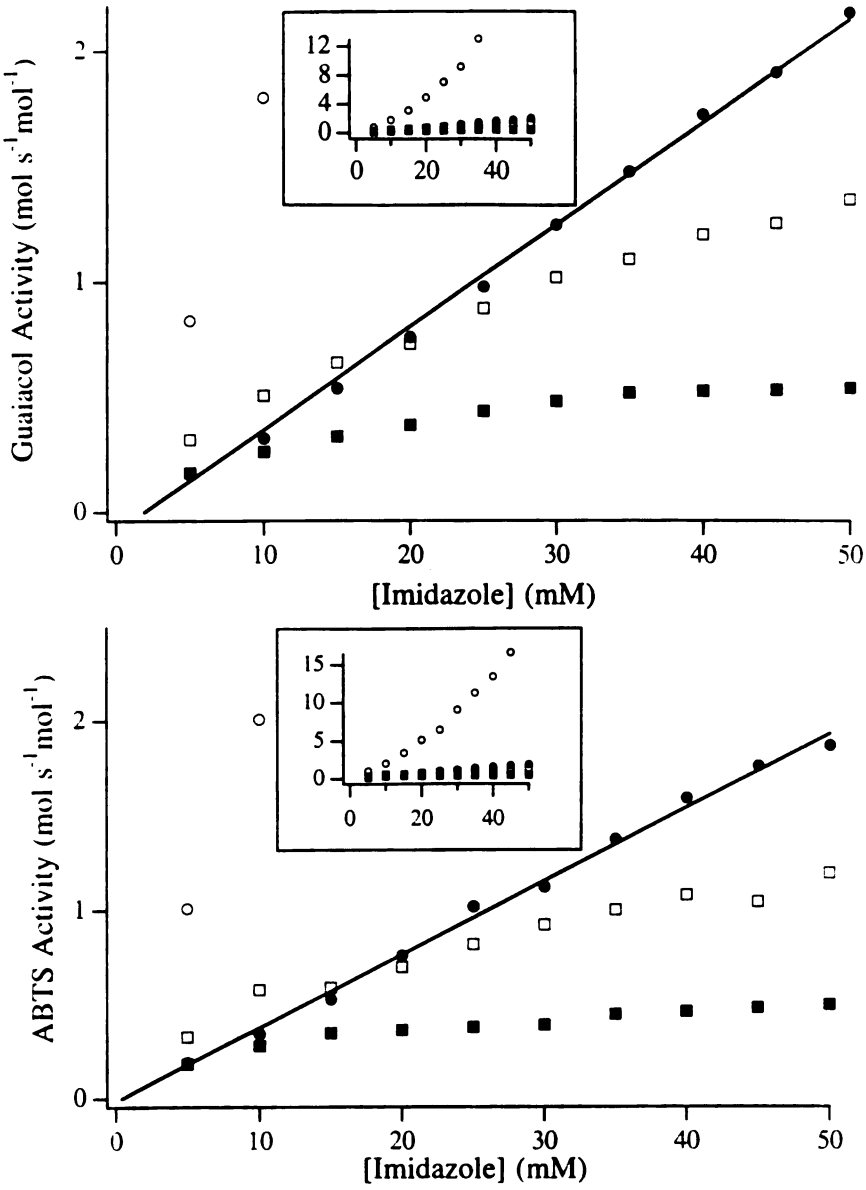

Figure 5.2: Rescue of H42A HRP-catalyzed oxidation of guaiacol and ABTS by exogenous imidazole (imidazole, open squares; 1-methylimidazole solid squares; 2-methylimidazole, open circles; and 1,2-dimethylimidazole, solid circles). The plotted imidazole concentrations refer to the amount of the unprotonated form present at pH 7. The inset found within each plot shows an expanded version of the corresponding plot.

To varying extents imidazole and 1-methyl-, 2-methyl-, and 1,2-dimethylimidazoles effectively enhanced peroxidase activity. Presumably each imidazole was able to substitute

for the missing distal histidine that was removed through mutagenesis. For imidazole and 1-methylimidazole this improvement in activity diminished with increasing imidazole concentration. This leveling off effect is consistent with the ability of imidazole (K_d ~150 mM) and 1-methylimidazole (K_d ~200 mM) to coordinate to the heme iron as demonstrated spectrophotometrically by a shift of the Soret band (λ_{max} = 402 nm for the resting state) to λ_{max} = 412 nm (Figure 5.3). Coordination of imidazole to the sixth heme position would hinder Compound I formation, effectively inhibiting peroxidase activity. The enhancement

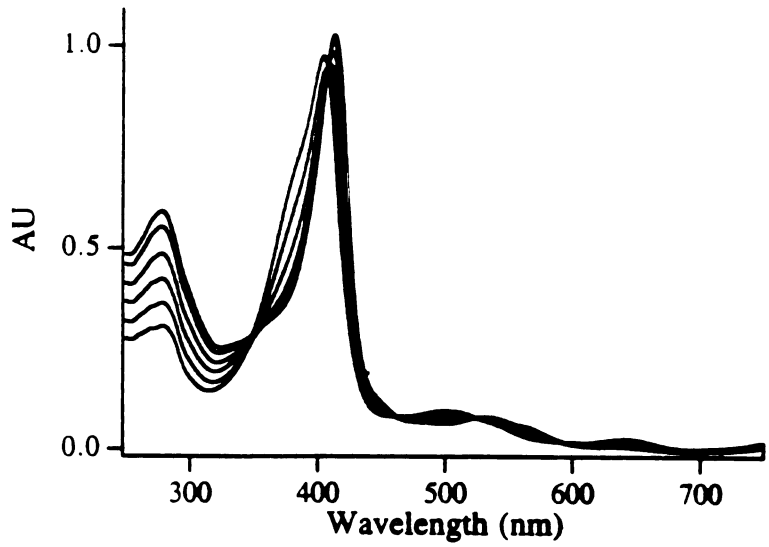

Figure 5.3: Coordination of imidazole to H42A HRP as demonstrated by the shift of the Soret band (λ_{max} = 402 nm to λ_{max} = 412 nm). Imidazole (0, 19, 43, 68, 93, and 118 mM final concentrations) was added to 10 μM H42A HRP, 100 mM K_2HPO_4 buffer, pH 6.0. These imidazole concentrations refer to the total amount of imidazole (free base + protonated forms).

of activity by the 2-substituted imidazoles did not level off at higher imidazole concentrations (Figure 5.2). Increasing the concentration of 1,2-dimethylimidazole rescued H42A HRP peroxidase activity in a linear manner. Over a similar range, 2-methylimidazole more effectively rescued activity, and the extent of the rescue improved

with increasing concentration in a nonlinear manner. Consistent with these findings, 2-methylimidazole and 1,2-dimethylimidazole did not cause the red shift of the heme Soret that is characteristic of coordination at the sixth position by imidazole. As observed with the proximal histidine mutant of heme oxygenase (Wilks *et al.*, 1995), 2-substituted imidazoles were unable to coordinate to the heme iron, presumably due to steric hindrance by the 2-methyl group.

The imidazole-dependent rates of guaiacol and ABTS oxidation, as catalyzed by 1,2-dimethylimidazole-rescued H42A HRP, were calculated from the slopes obtained in Figure 5.2 (Table 5.1). H42A HRP-catalyzed oxidations of guaiacol and ABTS are

Table 5.1: Guaiacol and ABTS activities determined for native-, rWT- and H42A-HRP and for 1,2-dimethylimidazole-rescued H42A-HRP. Guaiacol and ABTS activities were assayed with similar conditions to those described in the text for monitoring 1,2-dimethylimidazole-rescued H42A HRP activity. Enzyme concentrations of 5 nM, 5 nM, and 5 μM were used in assaying the guaiacol activity of native-, rWT-, and H42A-HRP, respectively. Enzyme concentrations of 5 nM, 5 nM, and 0.5 μM were used in assaying the ABTS activity of native-, rWT-, and H42A-HRP, respectively.

Enzyme	Imidazole	Guaiacol Activity $M\ s^{-1}\ M^{-1}$	ABTS Activity $M\ s^{-1}\ M^{-1}$
Native	none	$1.36\ (\pm 0.04) \times 10^{3}$	$1.24\ (\pm 0.02) \times 10^{2}$
rWT	none	$1.37\ (\pm 0.10) \times 10^{3}$	$1.24\ (\pm 0.09) \times 10^{2}$
H42A HRP	none	$5.36\ (\pm 0.10) \times 10^{-3}$	$6.90\ (\pm 2.30) \times 10^{-2}$
H42A HRP	1,2-diMeIm[a]	$4.56\ (\pm 0.70) \times 10^{1}$	$3.91\ (\pm 0.93) \times 10^{1}$

[a]Actual units are $M^{-1}s^{-1}$, with the error based on the mean of the slope (Figure 5.2).

rescued to an equal extent by 1,2-dimethylimidazole. This in an interesting result considering that at pH 7 the guaiacol activity exhibited by rWT HRP is 10 fold higher than its ABTS activity. An effective concentration of 3 M 1,2-dimethylimidazole (the free base form) is able to restore native ABTS activity at pH 7.0. Native guaiacol activity is restored by an effective 30 M concentration of 1,2-dimethylimidazole at pH 7.0.

pH Profile of 2-Methyl- and 1,2-Dimethylimidazole-Rescued H42A HRP Guaiacol Peroxidase Activity. To further study these imidazole derivatives, rescued guaiacol activity was measured at varying pH values. Low imidazole concentrations (1 mM) were used to limit changes in the pH caused by the addition of imidazole and were found to alter the pH in a minimal manner ($\leq$ 0.2 pH units). The measured pH values are plotted versus activity as shown in Figure 5.4. H42A HRP activity increases linearly with increasing pH. This profile significantly differs from that of native HRP, both in guaiacol oxidation and in Compound I formation (H42A HRP is rate-limited by Compound I formation). With the addition of 1,2-dimethylimidazole, the pH profile for H42A HRP shows that deprotonation of a group with a pKa value of 8.0 $\pm$ 0.2 improves activity. This pKa value corresponds to that of 1,2-dimethylimidazole itself (pKa 7.9) (Grimmett, 1980), suggesting that the unprotonated imidazole is the rescuing species. This form could accept a proton from peroxide in proximity to the heme iron, promoting formation of the ferric peroxide complex with ensuing formation of Compound I. 2-Methylimidazole (pKa 7.6) (Grimmett, 1980) gave a pH profile with a similar point of inflection at pH 7.8 $\pm$ 0.4. The overall increase in activity between the base and conjugate base forms was ~3 times more for 2-methylimidazole than 1,2-dimethylimidazole.

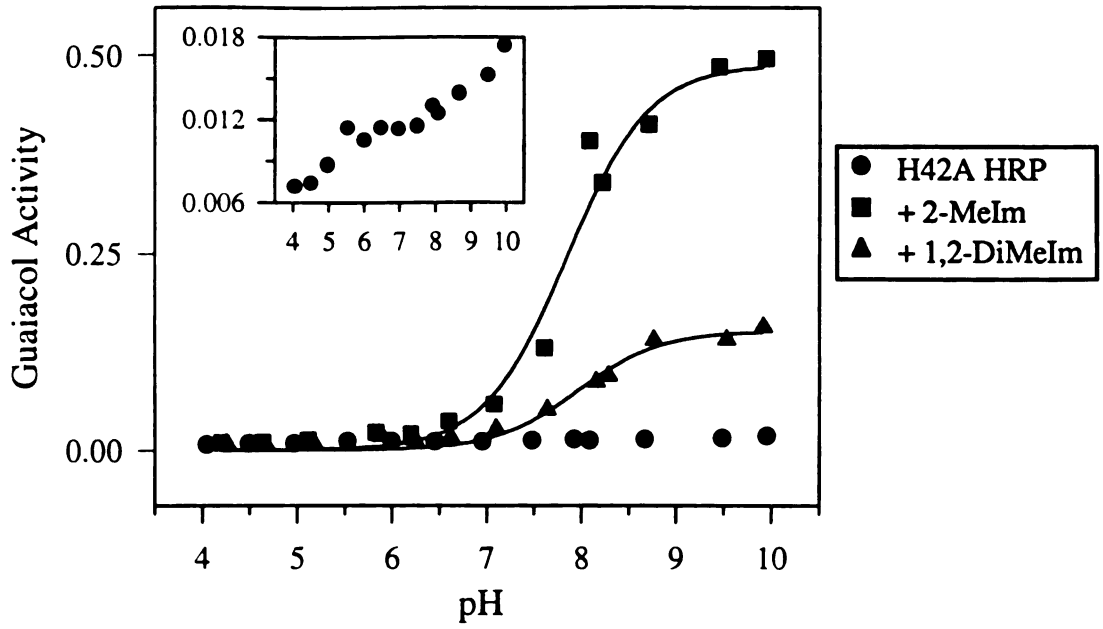

Figure 5.4: pH profile for H42A HRP assayed in the absence and presence of 1 mM 2-methyl- or 1,2-dimethylimidazole. Guaiacol activity (mol s^{-1} mol^{-1}) catalyzed by H42A HRP in the absence of imidazole is shown in an expanded form in the inset.

Determination of K_d Values for 2-Methyl- and 1,2-Dimethylimidazoles Binding to H42A HRP. The difference spectra produced by addition of 2-methylimidazole and 1,2-dimethylimidazole to H42A HRP displayed minima at 383 and 402 nm and maxima at 416 and 419 nm, respectively (Figure 5.5). The differences between the minima and maxima and the corresponding imidazole concentrations were fit to the following equation. The resulting K_d values for 2-methylimidazole and 1,2-dimethylimidazole were 2.5 (± 0.2) M and 2.9 (± 1.3) M, respectively.

$$\frac{\Delta A}{\Delta A_{max}} = \frac{[S]}{(K_d + [S])} \qquad \text{(Eqn 5.1)}$$

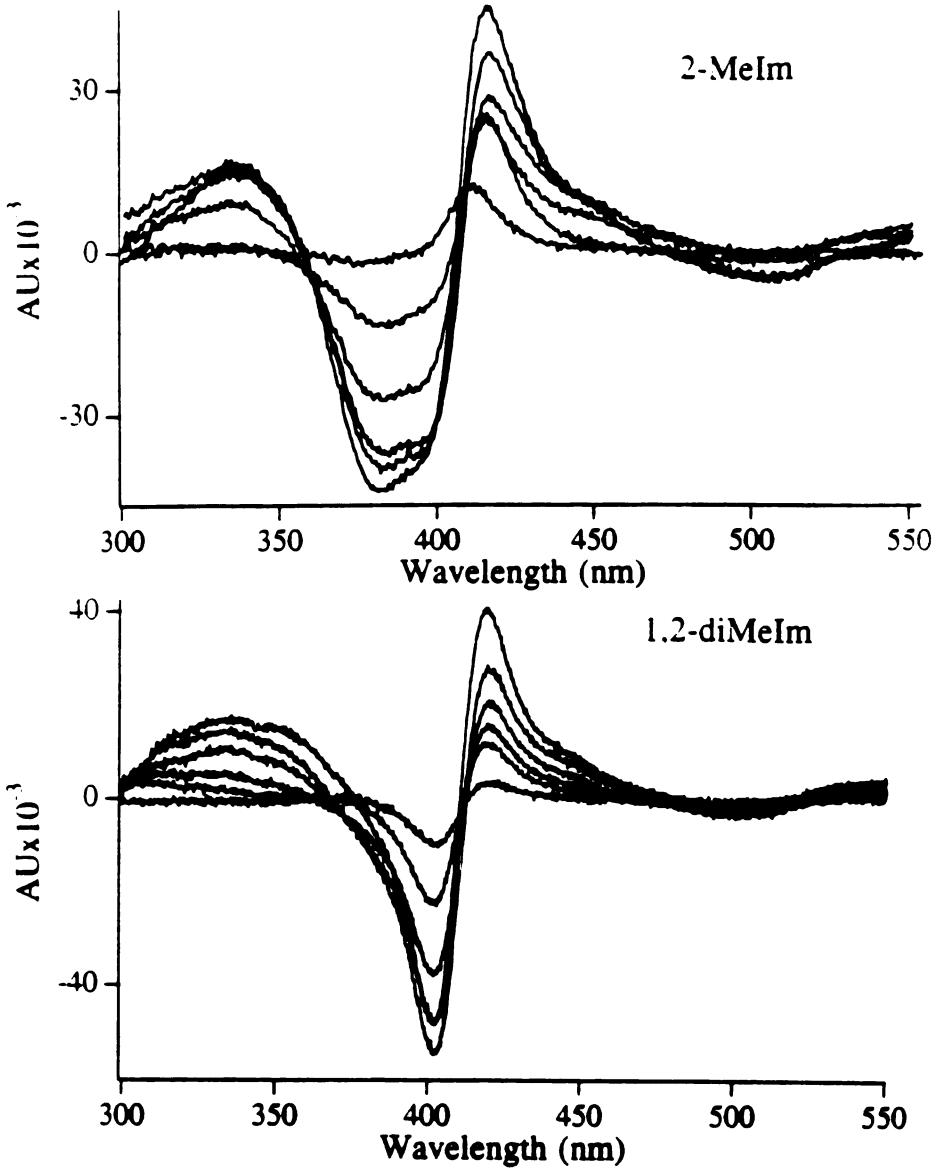

Figure 5.5: Difference spectra obtained for H42A HRP bound by 2-methyl- and 1,2-dimethylimidazoles.

The K_d was also determined for the binding of 1,2-dimethylimidazole to cyanide-bound HRP. Cyanide coordination to the sixth heme position of H42A HRP was indicated by a red shift of the Soret λ_{max} and by the appearance of α/ß bands in the visible region. In the presence of cyanide, a similar difference spectrum to that reported above was obtained

at lower 1,2-dimethylimidazole concentrations (Figure 5.6). This difference spectrum displayed maximum absorption at 426 nm and minimum absorption at 399 nm. The K_d value, determined as described above, was found to be 174 mM. 1,2-Dimethylimidazole binding was significantly improved for cyanide-ligated HRP in comparison to that determined for the protein in the absence of cyanide.

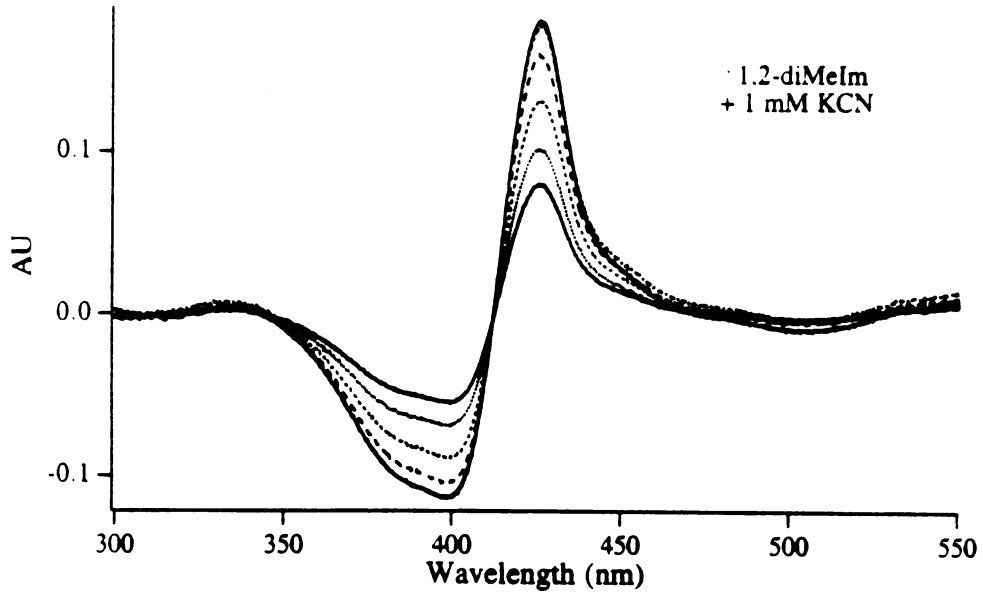

Figure 5.6: Difference spectra observed with the binding of 2-methylimidazole to cyanide-ligated H42A HRP.

Rescuing Compound I Formation with a Series of 1,2-Disubstituted Imidazoles. The rescue by imidazole is likely to involve the activation of peroxide since Compound I formation is rate limiting for H42A HRP. In the presence of 100 mM 2-methylimidazole or 1,2-dimethylimidazole, one equivalent of H_2O_2 gave partial Compound I formation. The addition of ten equivalents of H_2O_2 gave nearly complete and immediate formation of Compound I (Figure 5.7). In the absence of imidazole, 500 equivalents of H_2O_2 are needed to see slow Compound I formation (in ~10 min). In the absence or presence of

imidazole, the Compound I species decays back to the resting state within minutes without the detectable formation of a characteristic Compound II species. In the absence of imidazole, the Soret absorption is not fully regained, indicating that heme degradation occurs (Figure 4.5). However, in the presence of imidazole, the resting state Soret absorption is fully regained (Figure 5.7). This suggests that imidazole protects the H42A Compound I species from heme degradation pathways.

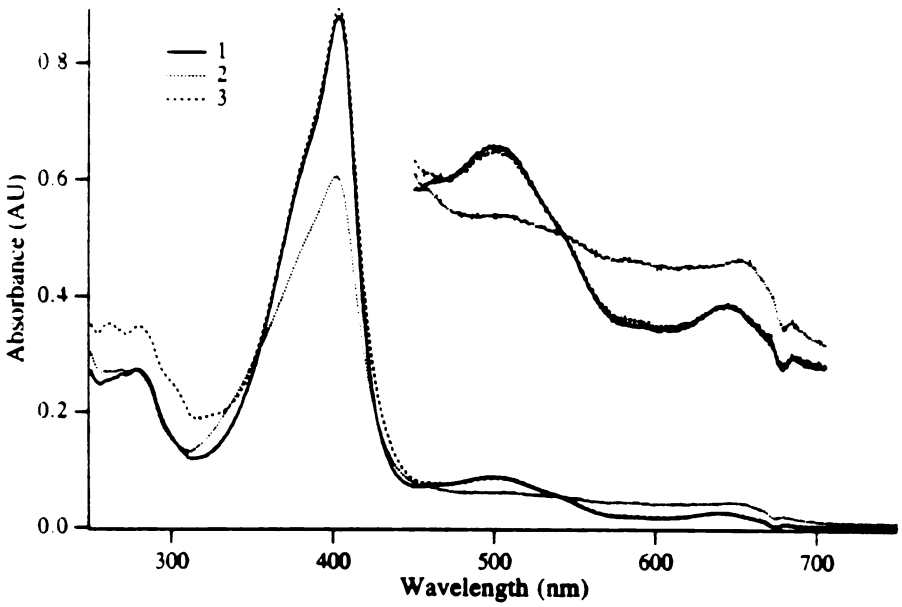

Figure 5.7: Rescue of H42A HRP Compound I formation and enzyme turnover by 1,2-dimethylimidazole. In the presence of 100 mM 1,2-dimethylimidazole, the resting state H42A mutant (2 μM) (1, solid line) was treated with ten equivalents H_2O_2, leading to immediate formation of Compound I (2, dotted line). The subsequent addition of one equivalent $K_4Fe(CN)_6$ caused the immediate regeneration of the resting state spectrum (3, dashed line).

To further characterize the mechanism of imidazole rescue, a series of 1,2-disubstituted-imidazoles was synthesized and the compounds were assayed for their ability

to rescue Compound I formation. Substituents at the 2 position were varied with respect to size and electron withdrawing ability. N-methylated imidazoles were used to prevent the hydrogen bonding that might occur between imidazole molecules. They were also easier to work with synthetically. The 2 position was substituted to give a series of imidazole derivatives that could not coordinate to the iron and that would encompass a wide pKa range. The pKa of the imidazoles was determined by adding partial equivalents of acid to a 10 mM solution of the imidazole derivative. The pH was determined and plotted versus log ($[A^-]/[HA]$) (using the Henderson-Hasselbalch equation). In monitoring 1,2-disubstituted imidazole-rescued Compound I formation, the imidazole concentration was kept in the lower mM range (1-25 mM), and a high buffer concentration was used to minimize the effects of fluctuating imidazole levels on the ionic strength or pH. The high K_d value for 1,2-dimethylimidazole indicates that the levels of imidazole used in this experiment yield only a fraction of imidazole-bound H42A HRP. Hydrogen peroxide levels were also kept relatively low (13.7-109 μM final concentration) to avoid formation of Compound III, which would shift the Soret band and decrease the absorption at 402 nm. Compound I formation followed an exponential decay over a 3-5 min period. Only partial conversion of resting state to Compound I was observed as indicated by the total drop in absorption. Complete conversion would drop the absorbance to half the intensity of the original Soret band. The total absorption change observed in the 402 nm decay increased with increasing imidazole and with increasing peroxide. Using equation 5.2 the rate of Compound I formation was plotted versus peroxide concentration, and the resulting plot gave a series of lines that intercepted at the origin (Figure 5.8A). To obtain a peroxide-independent rate, the slopes of these lines were plotted versus imidazole concentration according to Equation 5.3 (Figure 5.8B). The slope of this secondary plot was taken as the imidazole-dependent rate constant for imidazole-rescued Compound I formation (Table 5.2). The y-intercept for this plot demonstrated that imidazole-independent Compound I formation also contributed

to the measured velocities. The corresponding rate constant, 16 $M^{-1}s^{-1}$, is similar to that determined via steady state kinetics (19 $M^{-1}s^{-1}$) (Table 4.1).

$$d[\text{Cmpd-I}]/dt = k_1^{imid}[\text{H42A HRP}][\text{Imid}][H_2O_2] + k_1[\text{H42A HRP}][H_2O_2] \quad \text{(Eqn 5.2)}$$

$$\text{slope}/[\text{H42A HRP}] = k_1^{imid}[\text{Imid}] + k_1 \quad \text{(Eqn 5.3)}$$

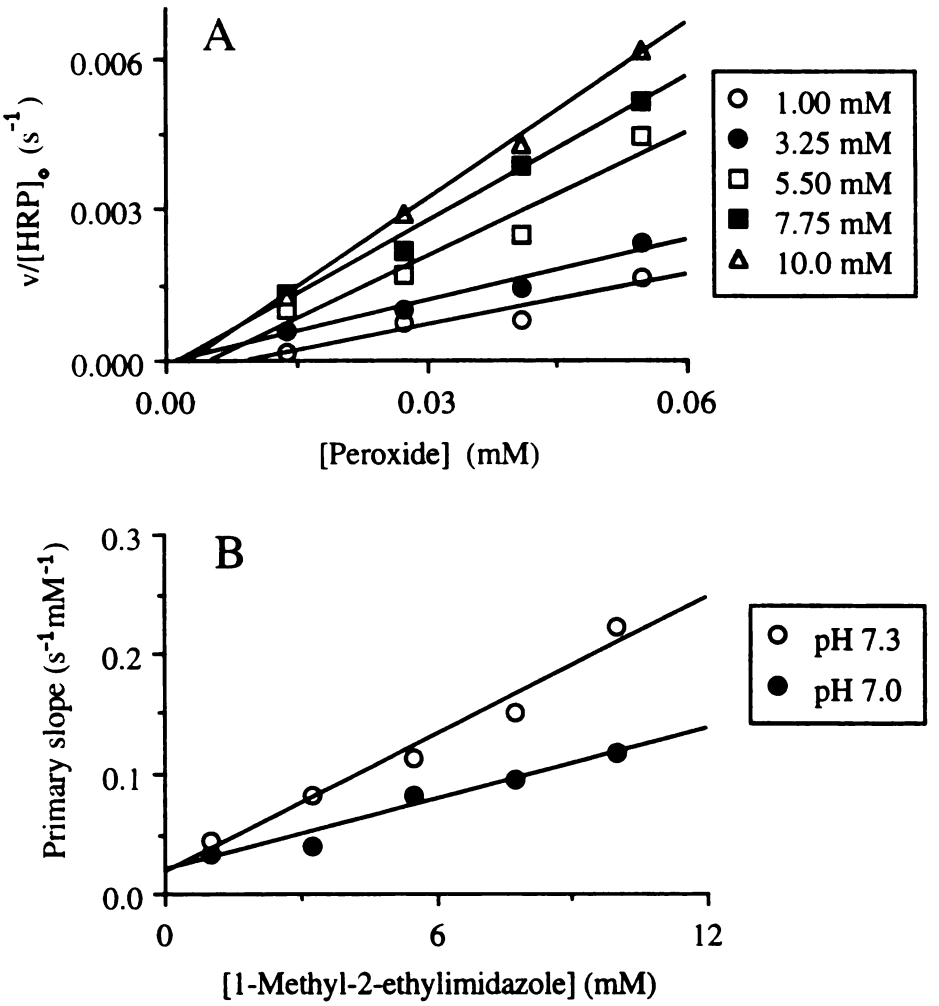

Figure 5.8: Dependence of H42A Compound I formation on H_2O_2 and 1-methyl-2-ethylimidazole concentration. Using equation 5.2, the rates of Compound I formation are plotted versus peroxide concentration (A). The concentration of 1-methyl-2-ethylimidazole used to generate each line is indicated in the legend. Using equation 5.3, the slopes of plot A were in turn plotted versus the corresponding concentration of 1-methyl-2-ethylimidazole

(B). The slope of this line yields the value for k_1^{imid}, the rate constant for imidazole-dependent Compound I formation. Plot B also shows the rescue of Compound I formation by 1-methyl-2-ethylimidazole at pH 7.3.

Table 5.2: Acidities, molecular volumes, and the imidazole-dependent rate constants of Compound I formation determined for 1,2-disubstituted imidazoles. The imidazole-dependent rate constants for Compound I formation are listed both with respect to the total imidazole concentration (Im + ImH) and the concentration of the free base species (Im).

2-Imidazole Substituent	pKa	Volume (Å^3)	k_1^{imid} ($M^{-2}s^{-1}$) (Im + ImH^+)	k_1^{imid} ($M^{-2}s^{-1}$) (Im)
methyl	8.2	109.4	9.9×10^{-3}	1.6×10^{-1}
ethyl	8.1	126.8	1.0×10^{-2}	1.4×10^{-1}
propyl	8.1	145.8	3.9×10^{-3}	5.7×10^{-2}
butyl	8.1	164.7	3.1×10^{-3}	4.2×10^{-2}
hydroxymethyl	6.9	116.5	4.6×10^{-3}	7.9×10^{-3}
bromo	4.1	113.9	7.5×10^{-4}	7.5×10^{-4}

Other 1,2-disubstituted imidazoles were synthesized and assayed for their ability to promote Compound I formation. These imidazoles contained the following groups at the 2 position: CN, CH_2CN, OCH_3, CH_2Cl, CHO, and $CHCH_2$. Unfortunately these compounds only gave small amounts of Compound I that corresponded to a rate that was less than the imidazole-independent rate. It is likely that these imidazoles either serve as substrates or are not stable to aqueous conditions. Some of these imidazoles are electron rich, making them potential peroxidase substrates. Evidence that these molecules could act

as substrates is provided by the formation of a UV active product when 1-methyl-2-acetonitrylimidazole was treated with H42A HRP and peroxide. 1-Methyl-2-(chloromethyl)imidazole and 1-methyl-2-methoxyimidazole were unstable in aqueous solution. In both cases TLC analysis revealed that exposing these imidazoles to water caused decomposition to more polar products.

Based on the pH profile of rescued H42A HRP, we expect that the neutral imidazole species is the active form. To test this, Compound I formation was also assayed with 1-methyl-2-ethylimidazole at pH 7.3 (Figure 5.8B). At this pH value twice as much of the free base form is present, and the resulting imidazole-dependent rate constant (18.9×10^{-3} $M^{-2}s^{-1}$) is 1.89 fold greater than the rate constant determined at pH 7.0 (9.92×10^{-3} $M^{-2}s^{-1}$). This provides further support that the deprotonated imidazole is the active form. The imidazole-dependent rate constants were therefore calculated with respect to the level of the unprotonated form present (Table 5.2).

The influence that the size of the rescuing imidazole has on its ability to promote Compound I formation was analyzed by comparing the N-methyl-2-alkylimidazoles, which display similar pKa values. The logarithms of the rate constants for the methyl-, ethyl-, propyl-, and butyl-substituted imidazoles were plotted versus molecular volume (Figure 5.9). The resulting plot showed a linear dependence between the size of the imidazole and its ability to rescue activity ($\log k_1^{imid} = 0.537 + (-0.117 \times \text{Molecular Volume})$, $r^2 = 0.92$). The value of the slope of this line was used to adjust $\log k_1^{imid}$ to correct for the variation in volume. The resulting size-corrected value, $\log k_1^{imid} - (-0.117 \times \text{Molecular Volume})$, was plotted versus pKa. This yielded the Brønsted plot shown in Figure 5.10 ($\log k_1^{imid}(corr) = -4.333 + (0.589 \times pKa)$, $r^2 = 0.945$). The slope of this plot ($\beta = 0.589$) indicates that ~60% of the rescued imidazole is protonated in the transition state leading to Compound I formation in H42A HRP.

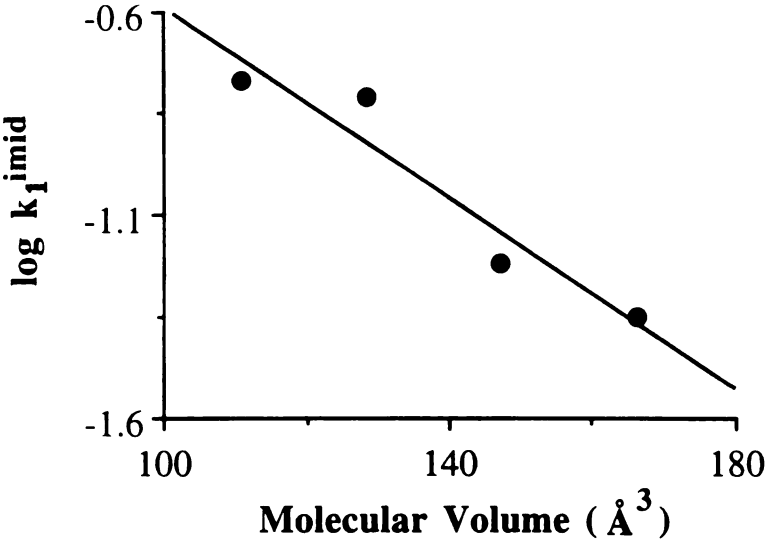

Figure 5.9: Dependence of the molecular volume for the series of 1-methyl-2-alkyl-imidazoles on their ability to rescue Compound I formation. The data for the methyl-, ethyl-, propyl- and butyl-substituted imidazoles are plotted.

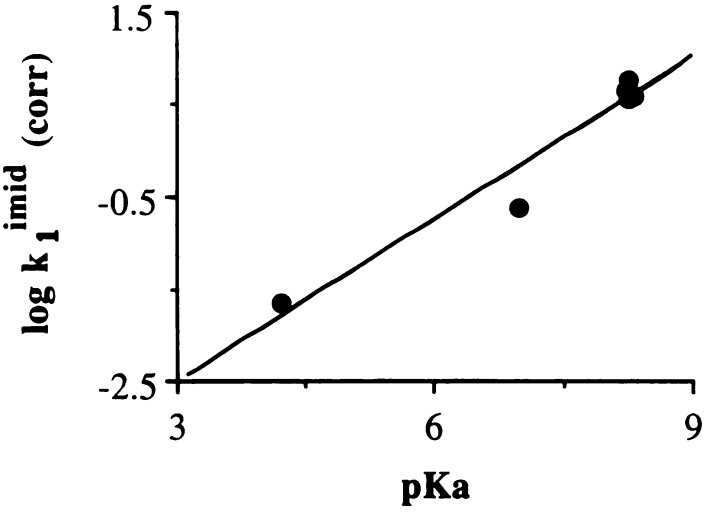

Figure 5.10: Influence of the 1,2-disubstituted imidazole pKa on the size-corrected rate of rescued Compound I formation. The data for the methyl-, ethyl-, propyl-, butyl-, hydroxymethyl-, and butyl-substituted imidazoles are plotted.

In the rescue of H42A HRP, the recovery of guaiacol and ABTS activities is greater for 2-methylimidazole than for 1,2-dimethylimidazole, and greater for imidazole than for 1-methylimidazole. The weaker ability of the N-methylated-imidazoles to rescue activity may result from the inability of the substituted nitrogen atom to hydrogen bond. In the native enzyme Asn 70 hydrogen bonds to His 42, and this interaction is thought to enhance the ability of the distal histidine to abstract a proton from peroxide. Mutation of Asn 70 to a valine in HRP causes an ~25 fold reduction in the rate of Compound I formation (Nagano *et al.*, 1995). Imidazole derivatives which contain two unsubstituted nitrogens can potentially bind in a similar orientation to that of the native distal histidine, with one protonated nitrogen atom hydrogen bonding to Asn 70 and the other nitrogen atom being free to abstract a proton from peroxide (Figure 5.11). The hydrogen bond to Asn 70 could influence the rescuing imidazole in the same manner as Asn 70 influences the distal histidine, and, consequently, non-N-methylated-imidazoles could activate peroxide more readily.

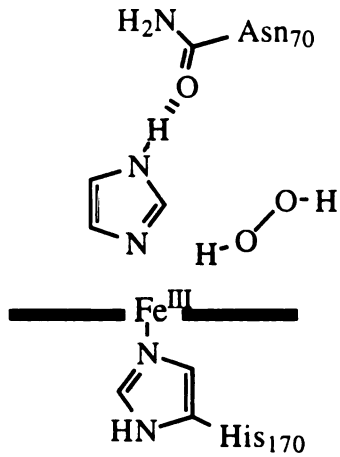

Figure 5.11: Proposed binding of imidazole by H42A HRP Asn 70. Similar binding could occur for 2-methylimidazole which also contains two free nitrogen atoms, relative to the N-methylated 1-methyl- and 1,2-dimethylimidazoles.

Alternatively, the higher activity of the 2-substituted imidazoles in rescuing H42A HRP activity could be mediated by a mechanism analogous to that proposed for the enhancement of native HRP peroxidase activity by nitrogenous compounds, including imidazole (Kuo and Fridovich, 1988). This enhancement is thought to involve hydrogen bonding of the distal histidine to the nitrogenous compound. As is the case for Asn 70, hydrogen bonding to the nitrogenous compound would help to increase the basicity of His 42. A similar effect would be expected with imidazole-rescued H42A HRP if one imidazole nitrogen atom functions in peroxide activation and the other is hydrogen bonded to a second exogenous imidazole (Figure 5.12). This latter explanation for the differing

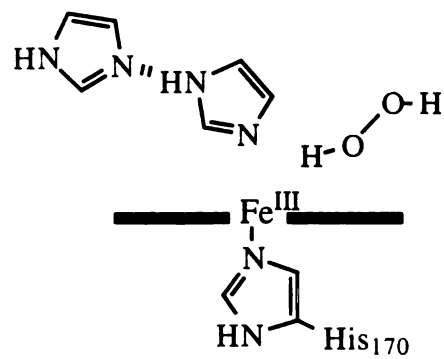

Figure 5.12: Proposed mechanism for the involvement of more than one molecule of 2-methylimidazole in the initial peroxide-deprotonating step of Compound I formation.

abilities of the imidazole derivatives to rescue activity seems most plausible, since the rescue of guaiacol and ABTS activities occurs in a nonlinear manner with regard to 2-methylimidazole concentration (Figure 5.2). This nonlinear dependence suggests that more than one molecule of 2-methylimidazole participates in the rescue of catalytic activity. If the greater activity of 2-methylimidazole versus 1,2-dimethylimidazole is based on the ability of the former to hydrogen bond to Asn 70, then the rescue of activity should follow a first order dependence with respect to imidazole.

The pH profile for H42A HRP is markedly different from that for the native enzyme. We might expect H42A HRP, which is largely limited by Compound I formation, to exhibit a similar pH profile to that of Compound I formation determined for the native enzyme. Native Compound I formation is promoted by the protonation of an ionizable group of pKa ~2.5 (Araiso and Dunford, 1980 and 1981; Dunford and Araiso, 1979). Although this value is markedly reduced from the typical pKa value exhibited by histidine residues, the differing profile obtained for H42A HRP suggests that the ionizable group in the native enzyme might be the distal histidine. For H42A HRP, the linear increase in guaiacol activity that is observed with increasing pH could reflect an increase in the peroxide anion as the pH is raised. In the absence of the distal histidine, the peroxide anion would yield the ferric peroxide species that then gives Compound I. However, the fact that the rate does not increase in a logarithmic manner suggests that the deprotonation of peroxide is not solely rate limiting.

The pH profile for the rescue of guaiacol oxidation demonstrates that the free base form of the imidazole is the species responsible for stimulating H42A HRP activity. This suggests that the major role of the rescuing imidazole is to deprotonate the peroxide since this is the only proposed step in Compound I formation that involves the neutral imidazole. In comparing the activities at alkaline (pH 10) and acidic (pH 4) conditions, the unprotonated imidazole improves activity 20-fold for 1,2-dimethylimidazole and 50-fold for 2-methylimidazole. When the pH is increased from 4 to 10 the protonated imidazole is essentially fully deprotonated to the free base form, increasing the active form of the imidazole by 100-fold. Since a corresponding 100-fold gain in activity is not observed when increasing the pH from 4 to 10, the role that the imidazole plays in deprotonating peroxide is only partially rate-limiting. The greater stimulation of peroxidase activity afforded by 2-methylimidazole versus 1, 2-dimethylimidazole is not likely to be due to differences in the affinity of the enzyme for each molecule, since their respective K_d values

are similar. Enhanced activity could arise through the participation of more than one 2-methylimidazole molecule in Compound I formation, as described earlier. It is also interesting to note that the native pH profile is not restored to H42A HRP upon the addition of imidazole; instead, the rescuing imidazole behaves as it would in aqueous solution. This suggests that hydrogen bonding and other interactions between the native enzyme and the distal histidine that influence the pKa of this residue, like that found between Asn 70 and His 42, are not occurring with the rescuing imidazole.

The difference spectra for 1,2-dimethylimidazole and 2-methylimidazole required high imidazole concentrations, demonstrating that these two molecules bind weakly to H42A HRP. To determine whether the difference spectra observed under high imidazole concentrations were due to imidazole coordination to the heme iron, a similar experiment was conducted in which 1 mM cyanide was incubated with the enzyme in the presence of 1,2-dimethylimidazole. Cyanide binds with high affinity to the sixth heme position in native HRP (K_d = 2 μM at pH 7) (Dunford and Stillman, 1976) and, at saturating concentrations, would prevent the coordination of imidazole to the sixth heme position. However, instead of observing a decrease in the affinity of H42A HRP for 1,2-dimethylimidazole, cyanide-coordinated HRP displayed an increased binding affinity. This enhanced affinity suggests the imidazole binding site lies in the vicinity of the sixth coordinate position. As revealed through NMR, the distal histidine in the native enzyme is proximal to, and forms a hydrogen bond with, the nitrogen of the coordinated cyanide (Thanabal *et al.*, 1988). The 14 fold improvement in 1,2-dimethylimidazole binding when cyanide is ligated to the mutant corresponds to ~1.6 kcal/mol of energy, which can be easily provided by a hydrogen bond to the nitrogen atom of the coordinated cyanide. Iron movement into the plane of the heme also occurs upon formation of a 6-coordinate species. This movement may cause protein movement, which could in turn improve imidazole binding. However, ligation of cyanide to native HRP does not normally influence

substrate binding as elucidated by NMR and optical difference spectroscopy studies, suggesting that only slight changes of the heme pocket are manifested by the coordination of the distal axial position. The existence of a cavity that could bind imidazole in the immediate vicinity of the heme iron in the H42A mutant is suggested by the ability of the mutant to catalyze peroxygenase reactions and to form an iron-phenyl complex when treated with phenyldiazene (Chapter 4). The weak binding of 2-methylimidazole and 1, 2-dimethylimidazole by resting state H42A HRP suggests that this cavity provides few good interactions with the bound exogenous imidazole. It suggests, furthermore, that the cavity is somewhat restricted with respect to the size of the binding imidazole. Thus, binding larger imidazole derivatives may be more difficult, which is consistent with the debilitating influence that increased size has on the rescuing effect of 1,2-disubstituted imidazoles.

Like the pH profile of imidazole-rescued H42A HRP, an increase in pH also stimulates the ability of 1-methyl-2-ethyl imidazole to rescue Compound I formation. These studies confirm that the free base form of the imidazole is the rescuing species. Given that the only feasible reaction that the neutral imidazole could contribute to Compound I formation is to deprotonate the peroxide, this is likely to be the major step rescued by the imidazole. A Brønsted analysis was performed to gain insight into the nature of the transition state of the peroxide deprotonating step. This linear free energy relationship has been used widely in mechanistic investigations of chemical reactions to probe the structure of the transition state. The Brønsted plot relates the logarithm of the rate constant to the pKa of a general acid or general base catalyst and predicts the degree of proton transfer or the amount of positive charge that develops on the catalyst in the transition state. The Brønsted analysis performed on H42A HRP with a series of 1,2-disubstituted imidazoles demonstrates that ~60% positive charge accumulates on the rescuing imidazole in the transition state of Compound I formation. The development of partial positive charge on the imidazole in the transition state suggests that negative charge

develops on the proximal peroxide oxygen atom; however, given that this deprotonation reaction is likely to occur near the heme iron, it seems likely that partial formation of the ferryl oxygen bond may occur concomitantly with proton transfer. This mechanism is illustrated in Figure 5.13.

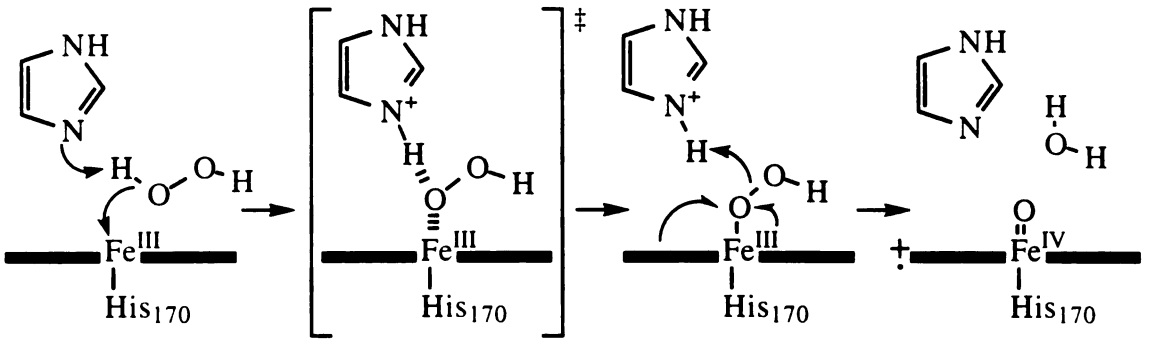

Figure 5.13: Proposed mechanism for Compound I formation by imidazole-rescued H42A HRP.

CONCLUSIONS

Compound I formation and peroxidase activity are parially restored to the distal histidine mutant H42A HRP by the addition of exogenous imidazoles. Imidazoles substituted at the 2 position are unable to coordinate to the distal axial heme position and consequently are the most effective in rescuing peroxidase function. Weak binding of 2-methylimidazole and 1,2-dimethylimidazole by H42A HRP appears to occur at the distal cavity created by the H42A mutation. The bound imidazole does not appear to be secluded from the solvent since the pH dependence of imidazole-rescued peroxidase activity is fully influenced by the protonation of the imidazole as it occurs in aqueous solution. Finding that the free base form of the imidazole is most effective at rescuing peroxidase activity suggests that imidazole predominantly functions in deprotonating peroxide in the formation of Compound I. This deprotonation step is the only step in Compound I formation that would utilize the neutral imidazole. Relative to the distal histidine in the native protein, the

rescuing imidazole is highly mobile at the distal heme face. In the native protein, movement of the distal histidine is restricted by (a) the tether to the C_α backbone and (b) the hydrogen bond to Asn 70 which restricts rotation of the C_β-C_γ bond. The imidazole that binds weakly to H42A HRP obviously lacks the heme tether and also does not form a hydrogen bond with Asn 70, as indicated by the similar K_d values exhibited by 2-methylimidazole and 1,2-dimethylimidazole. If a hydrogen bond were formed between the rescuing imidazole and a distal reside, imidazole-rescued Compound I formation for H42A HRP may be improved in a manner that is analogous to Asn 70-promoted Compound I formation in the native enzyme. This might be achieved by mutating Asn 70 to aspartate, glutamate, or glutamine residues. The resulting double mutants, H42A/N70D-, H42A/N70E-, and H42A/N70Q-HRP, would either provide a stronger hydrogen bond accepting group in the cavity created by the H42A mutation or improve the accessibility of the hydrogen bond accepting group by further extending the group into the distal cavity. Characterizing these mutants may elucidate the role that the distal hydrogen bond accepting group plays in the binding of imidazole, including the restriction of rotation around the C_β-C_γ bond. These mutants could also be studied to learn the role that hydrogen bonding plays in influencing the basicity of the distal histidine.

Chapter 6: Rescue of the Activity of the Proximal Histidine (H170A) HRP Mutant by Exogenous Imidazole

INTRODUCTION

The fifth heme ligand distinguishes classes of hemoproteins and thus is speculated to play a role in regulating heme chemistry. For this reason the enigmatic role that the proximal ligand plays in hemoprotein function has been studied widely, using model heme systems and mutagenesis approaches. Amino acid ligands that are common to hemoproteins include histidine (globins and peroxidases), tyrosine (catalases), and cysteine (P450s). The electron density donated by these ligands to the heme iron is postulated to influence its reactivity. Thus, mutating the proximal histidine in myoglobin to a tyrosine or cysteine reduces the Fe^{3+}/Fe^{2+} reduction potential from 50 mV to -190 mV and -230 mV, respectively (Adachi *et al.*, 1993). Donation of electron density to the iron atom is proposed both to promote the heterolytic cleavage of the dioxygen bond of the ferric peroxide complex (Traylor and Popovitz-Biro, 1988) and to stabilize highly oxidized heme states such as Compound I (Walker *et al.*, 1976; Doeff *et al.*, 1982; Tondreau and Sweigert, 1984; Du and Loew, 1995). Additionally, the tethering nature of the protein ligand may help to maintain an open sixth coordination site by pulling the heme iron away from the plane of the heme.

The proximal histidine heme ligand of the bacterial, fungal, and plant peroxidases is hydrogen bonded to an aspartate residue, as suggested by sequence alignments and the crystal structures for CCP (Finzel *et al.*, 1984), AXP (Patterson and Poulos, 1995), LIP (Poulos *et al.*, 1993), ARP (Kunishima *et al.*, 1994), and PeP (unpublished result). The strong hydrogen bond provided by the aspartate residue distinguishes the peroxidases from the globins, which contain a histidine ligand that is only weakly hydrogen bonded to a backbone carbonyl (Bolton and Perutz, 1970; Ladner *et al.*, 1977). The strong hydrogen

bond displayed by the peroxidase proximal histidine is postulated to partially or completely deprotonate the imidazole group, increasing its imidazolate character and its ability to donate electron density to the heme iron (Figure 6.1). Resonance Raman studies suggest

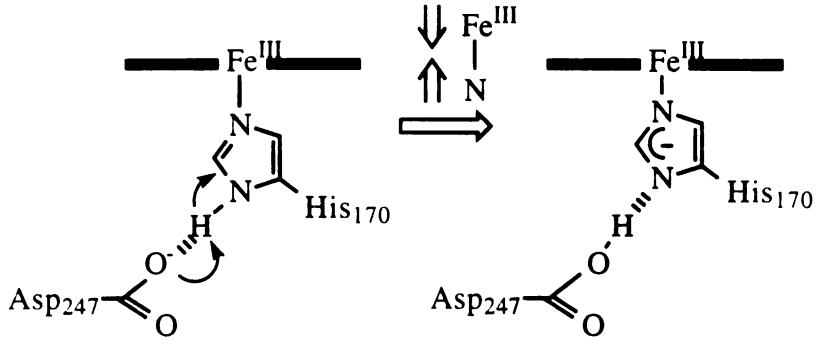

Figure 6.1: The proximal peroxidase aspartate residue is proposed to deprotonate the proximal imidazole. The resulting imidazolate character of the peroxidase proximal ligand is postulated to donate additional electron density to the heme iron relative to the neutral imidazole ligand found in myoglobin. Thus, the imidazolate ligand displays a stronger iron-nitrogen bond, as illustrated above by the shortening of the iron-nitrogen bond. The residue numbering is based on the HRP sequence.

that the imidazolate ligand in model heme complexes strengthens the iron-nitrogen bond relative to that in imidazole-heme complexes (Stein *et al.*, 1980). NMR studies of peroxidases and myoglobin also establish a correlation between the increasing strength of the imidazole hydrogen bond and an increase in the Fe^{3+}/Fe^{2+} reduction potential (Banci *et al.*, 1991; Banci *et al.*, 1993). Improved electron donation by the imidazolate ligand is thought to be partially responsible for the contrasting reactivity with peroxide that is observed for peroxidases versus globins. Compound I is formed 10^6 times faster, and is of a more stable nature, in the peroxidases versus the globins (McCarthy and White, 1983; George and Irvine, 1955).

Mutagenesis of the histidine fifth heme ligand in CCP to a glutamine or glutamate produces functional mutants that form Compound I in a native-like manner. Under saturating substrate conditions, these mutants oxidize both cytochrome c and ferrocyanide as well or faster than the native enzyme (Choudhury *et al.*, 1994). The crystal structures of these mutants show that the carbonyl oxygens of the glutamate and glutamine side chains hydrogen bond to Asp 235, the residue that corresponds to Asp 247 in HRP. The native-like activity exhibited by these mutants suggests that altering the chemical nature of the fifth heme ligand has little influence over the formation and stabilization of Compound I and argues that the primary role of the proximal ligand is to tether the iron. These conclusions, however, are clouded by the weak cytochrome c activity that is exhibited by CCP H175C, which displays 7% of native CCP activity. The crystal structure of this mutant reveals that the cysteine sulfur atom is oxidized and that the oxygen atom of the resulting cysteic acid side chain is ligated to the heme iron. The length of the resulting side chain that tethers the heme iron is similar to that of the glutamine and glutamate proximal ligands, suggesting that the proximal ligand may contribute to peroxidase catalysis by other means.

In CCP, Asp 235 was mutated to an asparagine to eliminate the strong hydrogen bond between Asp 235 and His 175. D235N CCP formed Compound I at a rate that was 4-fold lower than that of native CCP (Vitello *et al.*, 1992). Mutation of Asp 235 to both an asparagine and an alanine also caused pH-sensitive changes in the coordination state of the heme iron (Vitello *et al.*, 1992; Ferrer *et al.*, 1994). For D235N CCP in nitrate buffer, a hydroxyl group (pKa = 4.4) and the distal histidine (pKa 6.3) are speculated to coordinate to the sixth heme position with increasing pH. At pH 7 an estimated 92% of the D235N mutant has the distal histidine ligated to the heme iron. These studies suggest that the proximal imidazolate ligand modulates the coordination state of the heme but only slightly influences Compound I formation. D235N CCP also displays significantly reduced (>1000 fold) cytochrome c peroxidase activity (Goodin and McRee, 1993). This drastic

drop in activity is probably due to the reorientation of Trp 191 in the mutant and the loss of coupling between the Compound I Trp 191 protein radical and the heme active site. Thus, Asp 235 in CCP appears to assist in the oxidation of cytochrome c, possibly by correctly orienting Trp 191 for optimal electron transfer between the substrate and the oxidized heme of Compound I and Compound II. Correspondingly, D235E CCP, which contains a correctly oriented Trp 191 residue that forms a native-like protein radical, displays 41% of native cytochrome c activity (Goodin and McRee, 1993). This mutant displays a weaker hydrogen bond relative to that observed for native CCP. This finding suggests that the hydrogen bond network between His 175, Asp 235, and Trp 191 controls electron transfer from cytochrome c to the heme molecule of Compound I.

More recently, the proximal imidazole has been removed from CCP through mutagenesis, and the resulting mutant, H175G, displays 1.6% of native cytochrome c activity (McRee *et al.*, 1994). Solution of the crystal structure of this mutant demonstrates the heme iron to be ligated to two water molecules. Exogenous imidazole binds to the proximal cavity created by the H175G mutation with a K_d value of 2.7 mM. Saturating imidazole concentrations improve the peroxidase activity 3 fold over the bis-aquo mutant. The crystal structure of imidazole-bound H175G CCP shows the plane of the imidazole ring to be angled 20° from that of the proximal histidine in the native crystal structure. This variation could account for the inability of imidazole to restore full native activity. As revealed through EPR studies, the protein radical associated with Trp 191 is altered in the H_2O_2-treated, imidazole-bound H175G CCP. Thus, removing the tether between the imidazole and the protein through mutagenesis could sever Trp 191-mediated electron transfer between cytochrome c and the Compound I species of CCP.

These CCP studies suggest that the role of the imidazolate ligand is to maintain a five coordinate heme species by tethering the heme iron. Additionally, the hydrogen bond network between the proximal histidine, aspartate, and tryptophan residues appears to

modulate cytochrome c activity. Exploration of the role that the proximal histidine ligand plays in HRP catalysis is warranted, owing to the differences in the nature of the substrates and Compound I species that distinguish CCP from HRP and other prototypic peroxidases (Chapter 1). The proximal histidine, His 170, was therefore removed from HRP through mutagenesis. The following studies characterize H170A HRP in the presence and absence of imidazole to explore the role that the proximal ligand plays in HRP catalysis.

MATERIALS & METHODS

Assaying Guaiacol and ABTS Activities. Guaiacol and ABTS activities were monitored spectrophotometrically at 20°C. H170A HRP was initially incubated with imidazole (0.5 - 50 mM) for 2 hr at 20°C. In assaying guaiacol activity, the incubated enzyme was diluted into assay buffer containing 5 mM guaiacol in 20 mM Na_2HPO_4, pH 6.0, giving a final enzyme concentration of 0.94 μM in 1 ml volume. Hydrogen peroxide (0.5 mM final concentration) was added to initiate the reaction and guaiacol consumption was monitored at 470 nm (ε_{470}= 2.75 cm^{-1} mM^{-1}) (Chapter 4). ABTS activity was measured with the same amount of enzyme in 1 ml of buffer containing 5 mM ABTS in 20 mM NaOAc, pH 5.0. Hydrogen peroxide (0.5 mM final concentration) was added to initiate the reaction, and formation of the ABTS cation radical was monitored at 414 nm (ε_{414}= 36 cm^{-1} mM^{-1}) (Childs and Bardsley, 1975).

Determination of Binding Constant for Imidazole Binding to H170A HRP. The K_d for imidazole binding was determined spectrophotometrically. In a 400 μl volume, imidazole (5, 14, 23, 32, 41, 50, and 59 mM, pH 6.0) was pre-incubated with 7 μM H170A HRP in 20 mM Na_2HPO_4 pH 6.0. The difference spectrum (300-550 nm) between imidazole-bound and imidazole-free H170A HRP was obtained by subtracting the imidazole-free H170A HRP spectrum from the spectrum generated when imidazole-bound

H170A HRP was scanned against a reference cuvette containing the corresponding amount of imidazole in buffer.

Determination of the pH Profile for Guaiacol and ABTS Activities. Guaiacol and ABTS activities of native-, rWT-, and H170A-HRP were assayed at pH 4-10 and 20°C. Buffers were prepared at 25 mM concentrations and included HOAc/NaOAc (4-5.5), NaH_2PO_4/Na_2HPO_4 (6-8), and $HBO_3/Na_2B_4O_7$ (8.5-10). NaCl was added to maintain constant ionic strength (0.1 M). The buffers of varying pH were mixed with either guaiacol or ABTS, giving a final substrate concentration of 5 mM. Enzyme (1 nM native- or rWT-HRP, or 0.95 μM H170A HRP) was added to 1 ml of assay buffer. H170A HRP (0. 95 μM), incubated for 2 hr with 10 mM imidazole, was also assayed. Hydrogen peroxide (0.5 mM final concentration) was added to initiate the reaction. Guaiacol consumption and ABTS cation radical production were monitored spectrally as described above.

Steady State Kinetics of ABTS Oxidation. The ABTS assay described above was also used to determine the rate constants for both Compound I formation and substrate oxidation. ABTS oxidation was assayed using varying levels of hydrogen peroxide and ABTS as outlined in Table 6.1. The HRP peroxidase cycle is typically characterized by a

Table 6.1: Enzyme, ABTS, and H_2O_2 concentrations used in the analysis of steady state kinetics. H170A HRP was assayed in the absence and presence of 25 mM imidazole (Im).

Enzyme	[Enzyme] (nM)	[ABTS] (mM)	[H_2O_2] (mM)
WT-HRP	1.0	0.1 - 1.0	0.025 - 0.250
rWT-HRP	1.0	0.1 - 1.0	0.025 - 0.250
H170A	191	0.01 - 0.10	8.5 - 85.0
H170A + Im	95	0.2 - 2.0	0.025 - 0.250

modified version of the ping pong kinetic equation, where v = -d[AH]/dt = -d[ABTS]/dt (Equation 6.1). Normally k_3 is ~40 fold lower than k_2 so that equation 6.1 simplifies to equation 6.2. A similar equation fits ABTS oxidation catalyzed by native HRP (Smith *et al.*, 1992b). This equation includes k_u, a first order rate constant that describes product release. Equation 6.3 was used to determine values for k_1, k_3, and k_u using measured velocities of ABTS production.

$$2[HRP]_o/v = ((k_2+k_3)/(k_2k_3))(1/[ABTS]) + (1/k_1)(1/[H_2O_2]) \quad \text{(Eq. 6.1)}$$

$$2[HRP]_o/v = (1/k_3)(1/[ABTS]) + (1/k_1)(1/[H_2O_2]) \quad \text{(Eq. 6.2)}$$

$$2[HRP]_o/v = (1/k_3)(1/[ABTS]) + (1/k_1)(1/[H_2O_2]) + (1/k_u) \quad \text{(Eq. 6.3)}$$

RESULTS

H170A HRP Spectral Characterization. The Soret and visible absorptions displayed by H170A HRP vary markedly from that of the native enzyme and are sensitive to pH (Figure 6.2; Table 6.2). At pH 5, 6, and 7, the Soret band of H170A HRP has a λ_{max} at 412, 414, and 414 nm, respectively. This is red-shifted by 9-13 nm from the rWT HRP Soret absorption observed within this pH range. The visible region is also altered, displaying significant α/ß bands at pH 5-7. This suggests that a significant portion of the heme contains two strong axial ligands. At pH 4, the α/ß bands in the H170A HRP spectrum are diminished and charge transfer bands appear, bearing closer resemblance to native HRP and suggesting that at this pH the mutant is predominantly high spin. The Soret band is also blue-shifted from that found in the spectrum at neutral pH and displays a λ_{max} at 370 nm.

Upon addition of 25 mM imidazole, the spectrum of H170A HRP does not change significantly. The shoulder at 370 nm is reduced, resulting in a sharpening of the Soret band. The intensity of the α/ß bands also increases slightly (Figure 6.3).

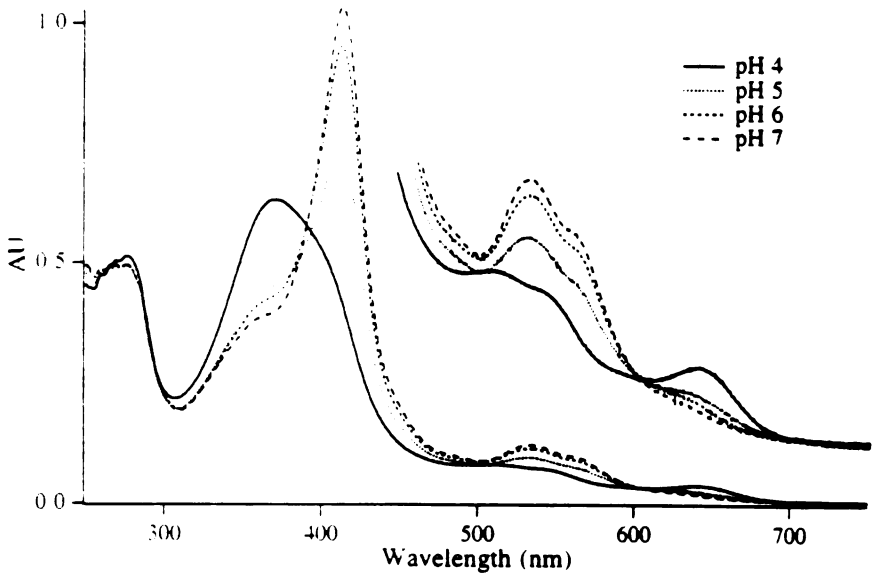

Figure 6.2: pH-Dependent absorption spectra for H170A HRP. Prior to obtaining the following spectra, (10 μM) H170A HRP was incubated overnight in 100 mM acetate buffer (pH 4) or 100 mM phosphate buffer (pH 5, 6, and 7).

Table 6.2: Spectral values describing the Soret, α/ß, and charge transfer bands for rWT- and H170A-HRP as they are influenced by pH.

Enzyme	pH	Soret (nm)	α/ß (nm)	CT1/CT2 (nm)
rWT	4	406	-	503/641
"	5	403	-	503/641
"	6	403	-	503/641
"	7	403	-	503/641
H170A	4	370 (399 sh)	-	512 (545 sh)/641
"	5	412	564 (sh)/532	641
"	6	414	564 (sh)/533	-
"	7	414	563 (sh)/534	-

Determination of Binding Constant for Imidazole. Increasing the imidazole concentration from 5 to 59 mM causes the spectral changes seen in the difference spectra in Figure 6.3. The addition of imidazole sharpens the Soret band, with a λ_{max} at 414 nm. The changes in absorption between 372 nm and 414 nm and the corresponding imidazole concentrations were fit to Equation 6.4 to calculate a dissociation constant. The resulting K_d value was 22.1 ± 4.2 mM.

$$\frac{\Delta A}{\Delta A_{max}} = \frac{[S]}{(K_d + [S])} \qquad \text{(Eqn 6.4)}$$

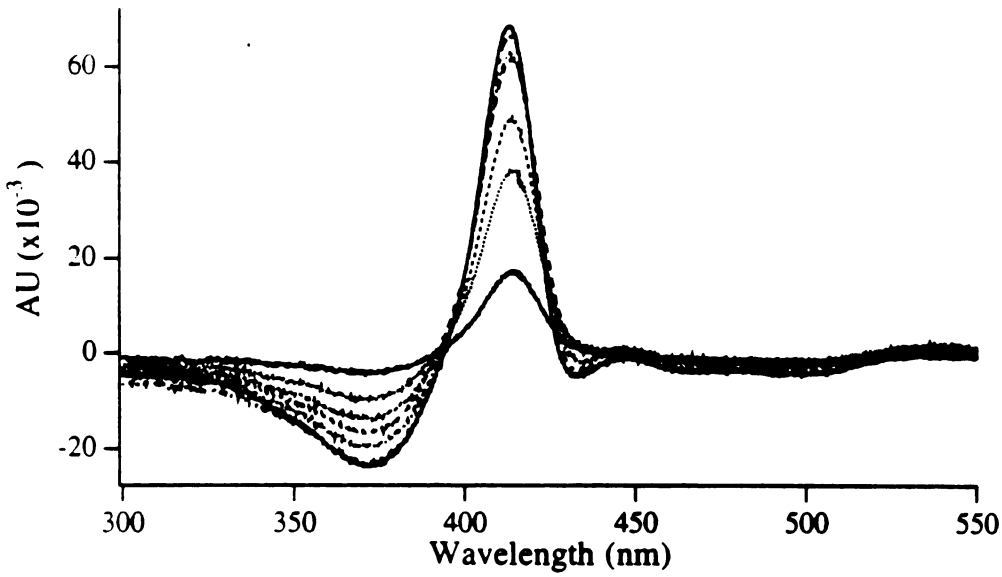

Figure 6.3: Difference spectra obtained for imidazole-bound versus imidazole-free H170A HRP. The plotted spectra correspond to 5, 14, 23, 32, 41, 50, and 59 mM imidazole.

Imidazole Rescue of Guaiacol and ABTS Activities. H170A HRP has optimal activity when stored and incubated at pH 6.0. This activity is significantly less than that of the native enzyme. H170A HRP displays 0.003% of the guaiacol activity and 0.004% of the ABTS activity of rWT HRP.

H170A HRP was pre-incubated with imidazole prior to taking an aliquot for activity assay. The rescued activity increased in a time-dependent manner and began to level off after 40 min (Figure 6.4). Consequently, the proximal mutant was incubated with imidazole for 2 hr prior to the activity assay. Dilution of the rescued enzyme into assay

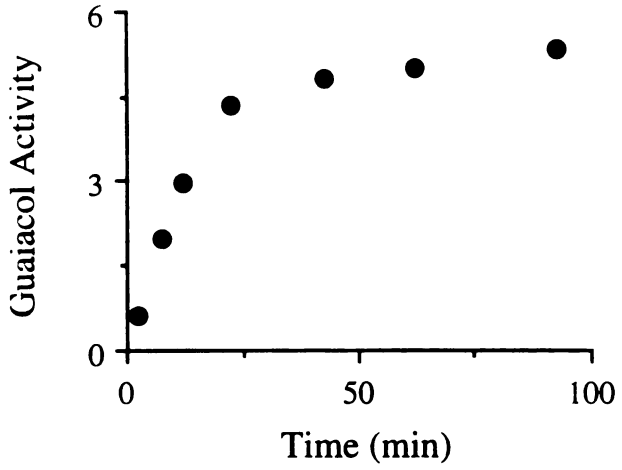

Figure 6.4: Time-dependent rescue of the H170A HRP activity promoted by pre-incubation with 16 mM imidazole. The units describing guaiacol activity are mol $s^{-1}mol^{-1}$. The assay solution contained 0.5 μM H170A HRP in 20 mM Na_2HPO_4 (pH 7.0). H_2O_2 (0.5 mM) was added to initiate the reaction.

buffer containing the same imidazole concentration as the pre-incubation medium displayed activity that was equivalent to activity measured in assay buffer lacking imidazole. This suggested that the off rate for imidazole binding was slow relative to the time scale of the assay. Given these observations, imidazole was pre-incubated with the mutant for 2 hr prior to the assay and imidazole was excluded from the assay buffer. Conducting the assay in this manner was advantageous in two ways. The enzyme was diluted immediately prior to the assay, which avoids incubating the proximal mutant at dilute concentrations under which the proximal mutant appears to be unstable (< 1 μM). Additionally, the high

imidazole concentrations required for H170A HRP to bind imidazole are diluted in the assay mixture and are therefore less likely to bring about the enhancement of activity observed earlier with native HRP (Kuo and Fridovich, 1988).

Increasing the imidazole concentration that is incubated with H170A HRP rescues peroxidase activity in a saturable manner (Figure 6.5). The resulting hyperbolic trend matches that observed for the absorption differences exhibited with the binding of

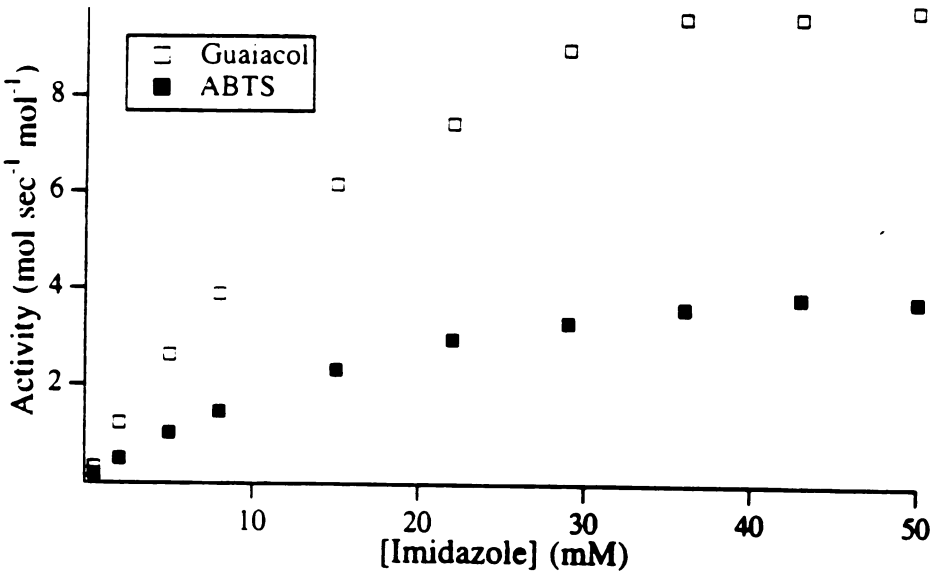

Figure 6.5: Influence of imidazole on ABTS and guaiacol activities.

imidazole by H170A HRP. Fitting the data in Figure 6.5 to the Michaelis Menten equation (Equation 6.5) yields 23.9 mM and 24.4 mM as the K_m values for imidazole with regard to

$$\frac{v}{V_{max}} = \frac{[S]}{(Km + [S])} \qquad \text{(Eqn 6.5)}$$

guaiacol and ABTS activities, respectively. These values are markedly similar to the K_d value obtained earlier (K_d = 22.1 mM), which suggests that the enhanced activity is caused by the bound imidazole. V_{max} values were also determined from the data that is presented

in Figure 6.5 and showed the rescued H170A HRP to display 0.8% of the guaiacol activity and 0.5% of the ABTS activity of rWT HRP. Saturating imidazole concentrations, thus, improve guaiacol activity 260 fold and ABTS activity 125 fold over the activities of H170A HRP alone.

pH Profile of H170A HRP in the Absence and Presence of Imidazole. The pH profiles of guaiacol and ABTS activities were determined for H170A HRP (Figure 6.6). In assaying both activities, this mutant displays a novel pH profile that is restored to that of the native enzyme when H170A HRP is rescued by imidazole. Based on activities measured at their respective pH optima, rWT HRP guaiacol activity is 320 fold greater and ABTS activity is 280 fold greater than the activity of H170A HRP rescued by 10 mM imidazole.

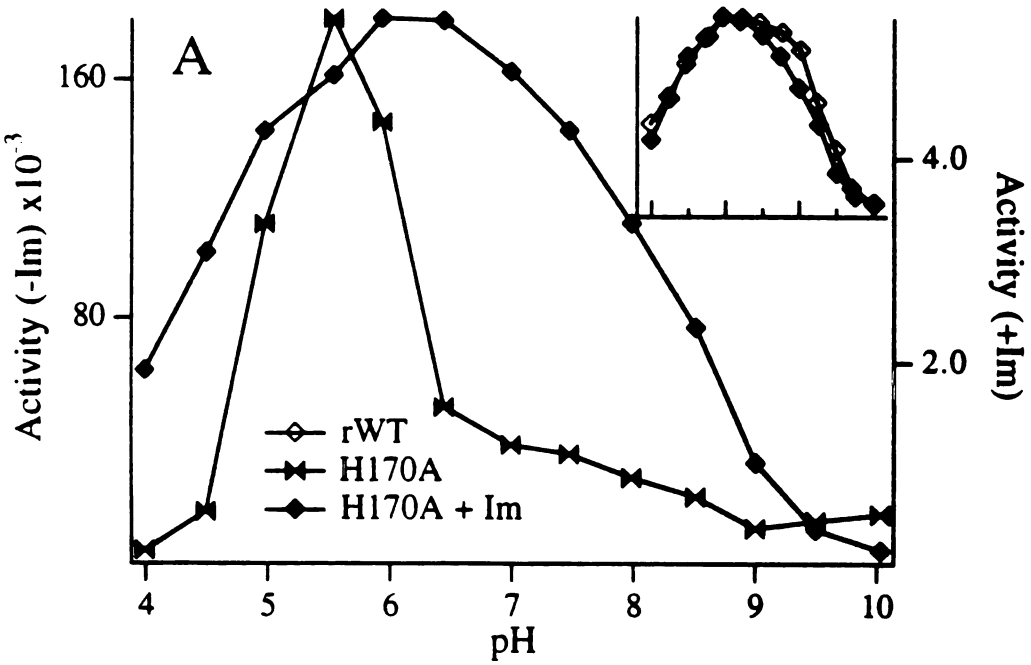

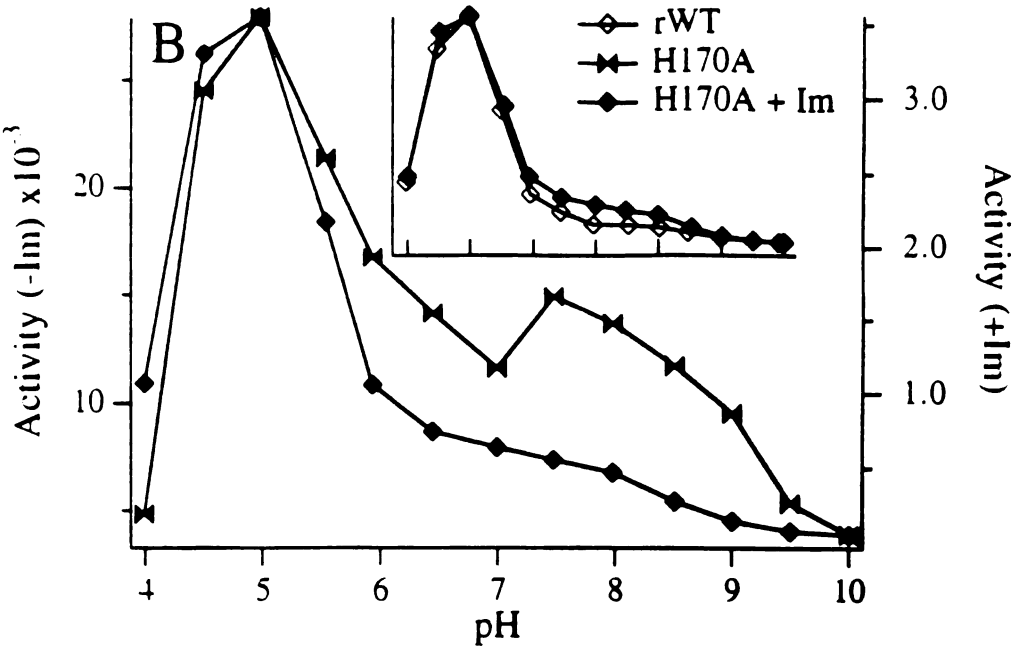

Figure 6.6: pH profiles of guaiacol (A) and ABTS (B) activities as catalyzed by H170A HRP in the absence and presence of imidazole (10 mM). The inset shows imidazole-rescued activity versus rWT HRP activity. rWT activity is scaled to match that of imidazole-rescued H170A HRP.

Steady State Kinetics Performed With the ABTS Assay. The Compound I and Compound II species can typically be obtained by the addition of 1 equivalent of hydrogen peroxide, followed by one equivalent of ferrocyanide. The addition of a second equivalent of ferrocyanide regenerates the resting state. This means of generating Compound I and Compound II species for H170A HRP, in the absence or presence of imidazole, failed to generate the typical spectra characteristic of these species. The addition of excess peroxide (100 equivalents) caused the Soret band to decrease; however, this decrease occurred with destruction of the heme, as suggested by the failure to recover Soret absorbance upon adding the reducing agent ferrocyanide. Presumably, Compound I and Compound II species are formed since substrate oxidation occurs. The inability to detect these species suggests that they may decay quickly to the resting state. In lieu of measuring Compound I

formation directly, a steady state kinetics approach was implemented to obtain rate constants for Compound I formation and for substrate oxidation.

In accordance with equation 6.3, the reciprocal of a range of measured velocities was linearly related to the reciprocal of the ABTS concentration (Figure 6.7A). Varying the peroxide concentration yields a series of approximately parallel lines. From this series of

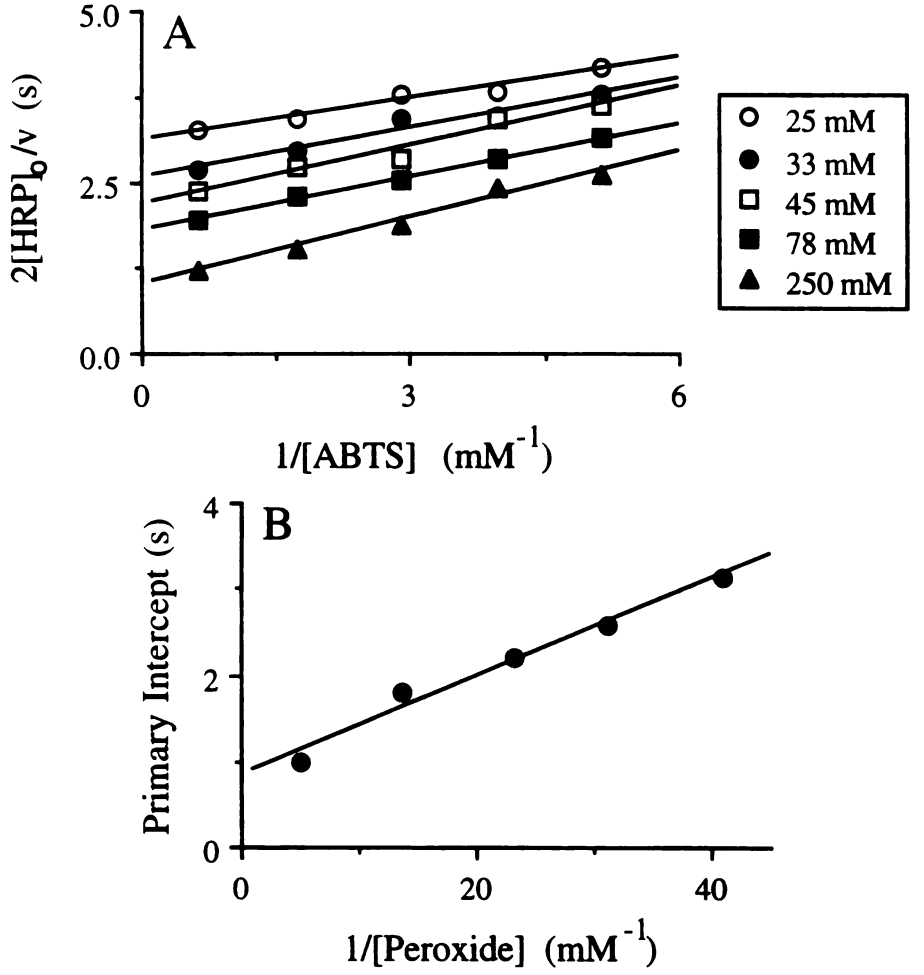

Figure 6.7: Steady state kinetic analysis of ABTS oxidation. The primary plot (A) illustrates the data measured for imidazole-rescued H170A HRP activity and was used to determine k_3. Each line was generated by employing the peroxide concentration indicated in the legend. The secondary plot (B) was generated to determine k_1 and k_u for imidazole-rescued H170A HRP.

lines, the reciprocal values of the slopes were averaged to obtain k_3. The y-intercepts obtained from this plot were plotted versus the reciprocal of the peroxide concentration (Figure 6.7B). The reciprocal of the slope of this secondary plot gave k_1, and the reciprocal of the y-intercept of this secondary plot gave k_u. Similar plots were obtained for native-, rWT, and H42A-HRP. The resulting values are shown in Table 6.3. The high

Table 6.3: Kinetic rate constants determined by analysis of steady state kinetics for ABTS oxidation. Each protein was analyzed twice, and the reported error shows the variation between these two values.

Enzyme	k_1 ($M^{-1}s^{-1}$)	k_3 ($M^{-1}s^{-1}$)	k_u (s^{-1})
WT	4.7 (± 0.0) x 10^6	7.2 (± 0.4) x 10^5	3.4 (± 0.0) x 10^2
rWT	4.4 (± 0.2) x 10^6	8.2 (± 0.1) x 10^5	4.1 (± 1.1) x 10^2
H170A	1.6 (± 1.2) x 10^1	3.0 (± 3.4) x 10^4	4.4 (± 0.4) x 10^{-1}
H170A + Im	2.4 (± 0.9) x 10^4	4.8 (± 1.4) x 10^3	1.6 (± 0.5) x 10^0

error reported for H170A is due to the need to assay small ABTS concentrations because the mutant was extremely sensitive to inhibition at higher ABTS concentrations. A random order type of inhibition at elevated ABTS levels has been reported for native HRP (Childs and Bardsley, 1975). The most notable change observed in Table 6.3 is the decrease in k_1 for H170A HRP, which is 5 orders of magnitude lower than the value calculated for native- and rWT-HRP. The presence of 25 mM imidazole, which half-saturates the enzyme, partially rescues Compound I formation, increasing k_1 1000-fold relative to the value for the mutant alone. The value of k_3, as reported in Table 6.3, assumes that reduction of Compound II is rate limiting. This assumption may not be valid given the anomalous

behavior of this mutant (inability to see stable Compound I or Compound II species). Whether the value obtained represents k_2, k_3, or a combination of both, $(k_2 + k_3)/(k_2k_3)$, it is clear that substrate turnover is modestly influenced by removal of the proximal ligand. The addition of imidazole did not rescue the ability of H170A HRP to oxidize ABTS, but rather slightly retarded ABTS oxidation. It is possible that oxidation of the imidazole ligand competes with ABTS oxidation, lowering k_3 for imidazole-rescued H170A HRP. Differences in k_u also exist between rWT HRP and the H170A mutant. Product dissociation is slower for H170A HRP, both in the absence or presence of imidazole, than it is for the wild-type proteins. This is may be due to the existence of structural differences between the mutant and native enzymes.

DISCUSSION

Removal of the proximal ligand in HRP through mutagenesis generates a protein that is spectrally and kinetically distinct from the native enzyme. The spectral differences, manifested by the appearance of α/ß bands in the visible region of the H170A HRP spectrum, implicate a change in the coordination state. The strength of these α/ß bands at pH 5-7 predicts that H170A HRP exists predominantly as a low spin species. Preliminary resonance Raman studies performed on the ferric enzyme also indicate that this mutant is predominantly low spin at pH 6.0 and that a histidine is coordinated to the heme iron as indicated by an iron-nitrogen stretch that is characteristic of this structure (data not shown). Given that the mutant protein lacks the proximal histidine, these studies suggest that the distal histidine coordinates to the heme iron as it is the only histidine that is proximal to the iron atom. Coordination of the distal histidine to the heme iron within H170A HRP is reminiscent of the Asp 235 CCP mutants (Vitello *et al.*, 1992; Ferrer *et al.*, 1994). The coordination state of the heme iron within these mutants was similarly sensitive to pH. Weaker acidic conditions (pKa = 6.3) remove the distal histidine ligand in the Asp 235

CCP mutants relative to removing the distal ligand in H170A HRP. This suggests that His 52 ligates less easily to the heme iron within CCP than does His 42 in H170A HRP. The differing readiness of the distal histidine to coordinate to the heme iron in HRP versus CCP may be explained by differences in their respective heme pockets. Phe 41 abuts the distal histidine in HRP. Its counterpart in CCP, Trp 51, is bulkier and may obstruct ligation of the distal histidine to the heme iron. This is consistent with the W51F CCP mutant which is predominantly six coordinate at neutral pH. This reasoning may also explain why coordination of the distal histidine is not observed for H175G CCP, which retains the distal tryptophan (McRee *et al.*, 1994).

The identity of the proximal iron ligand in H170A HRP is less definitive. The spectral studies indicate that H170A HRP is largely low spin. This suggests that the proximal ligand is relatively electron donating, ruling out ligation of a water molecule to the proximal axial position. Asp 247 in HRP could, however, serve to deprotonate a water molecule in the proximal cavity, promoting the ligation of a hydroxide molecule. The addition of exogenous imidazole to H170A HRP displaces the unidentified proximal ligand, as shown by a new imidazole-iron stretch in the resonance Raman spectrum (Lohr, preliminary data). Imidazole-ligated H170A HRP also retains some degree of coordination to the distal histidine, as indicated by the significant presence of the nitrogen-iron stretch discussed above. In view of the fact that the imidazole-bound mutant is predominantly low spin, it is likely that the majority of the imidazole-bound enzyme is largely bis ligated with His 42 and the exogenous imidazole coordinating to the distal and proximal axial positions, respectively.

The K_d value for imidazole binding, 22 mM, is high considering that dissociation of imidazole should be deterred by coordination to the heme iron. However, the time-dependent stimulation of activity observed when imidazole is incubated with H170A HRP suggests that the proximal cavity, created by the H170A mutation, may be partially buried.

This is consistent with NMR studies which demonstrate that the $N_{\delta 1}H$ proton of His 170 in HRP does not rapidly exchange with the solvent (La Mar and de Ropp, 1979). The binding constant describing imidazole binding to H170A HRP is 8 fold higher than that reported for H175G CCP (McRee *et al.*, 1994). The weaker ability of H170A HRP to bind imidazole may reflect differences in the size of the cavity that remains in the presence of an alanine side chain versus that of a glycine. Alternatively, the differences between the heme pocket of HRP and CCP may offer disparate accessibility or binding of imidazole to this cavity.

In a manner that parallels the concentration-dependent spectral changes observed with the binding of imidazole, H170A HRP activity is rescued by exogenous imidazole in a saturable manner. Full activity is not restored, however, and the maximum activities obtained are calculated to be 125-fold and 200-fold lower than those of rWT HRP for guaiacol and ABTS, respectively. Imidazole does, however, fully restore the native pH profiles for guaiacol and ABTS oxidation. The pH profile of the native enzyme is predominantly governed by either the reduction of Compound I or Compound II at low pH values and by Compound II reduction at neutral to high pH values (Marnett *et al.*, 1986). These reactions are largely influenced by ionization of the distal histidine. For H170A HRP, the drastic changes observed in the pH-dependence of these activities suggests that the proximal imidazole ligand influences either the native pH profile or causes a change in the kinetics of peroxidase cycling. The finding that the addition of imidazole to H170A HRP fully restores both substrate pH profiles indicates that the protein environment surrounding the heme has not changed drastically with removal of the heme tether. It also appears that the exogenous imidazole is not solvent accessible, since decreasing the pH below 7 would cause significant protonation of the imidazole with a concomitant decrease in the propensity to ligate the heme. Coordination of the proximal histidine in myoglobin increases the acidity of the imidazole NH proton by ~4 pKa units (Morishima *et al.*, 1980).

The steady state kinetics analysis of ABTS oxidation illustrates that the most notable effect of the H170A mutation is to reduce the rate of Compound I formation by five orders of magnitude. The addition of exogenous imidazole improves k_1 of H170A HRP 1000-fold. The proximal ligand is postulated to assist Compound I formation by 1) providing a heme tether to pull the iron out of the plane of the heme, promoting the maintenance a 5 coordinate heme species and 2) by donating electron density to the heme iron to promote heterolytic cleavage of the O-O bond. Since the addition of imidazole to H170A HRP does not drastically increase the amount of 5 coordinate high spin species, the 1000 fold improvement in the rate of Compound I formation can probably be attributed to promotion of heterolytic cleavage by the exogenous imidazole.

The ability of the proximal ligand to donate electron density to the heme iron is postulated to stabilize higher oxidation states, like Compound I and Compound II. Thus we might anticipate exogenous imidazole to influence the rate of reduction of both Compound I and Compound II. For H170A HRP, the substrate turnover rates for the imidazole-free and imidazole-bound enzyme are comparable. This suggests that the proximal ligand plays an insignificant role in substrate turnover despite its gross effect on Compound I formation. This minor role played by the proximal ligand in stabilizing Compound I and Compound II is consistent with kinetic studies performed on D235N CCP, which show that Compound I stability is essentially not influenced by removing the imidazolate character of the proximal histidine ligand. The findings of the present work also agree with the proximal ligand CCP mutants (H175Q and H175E) which produced Compound I species that were comparatively stable to that of native CCP.

Interestingly, k_1, k_3, and k_u are all reduced 200 fold for the rescued H170A HRP relative to the native enzyme. The likelihood that each rate constant would be reduced to the same extent is suspicious considering that these three steps are mechanistically distinct. An intriguing possibility is that the predominance of the six-coordinate form renders the

majority (99.5%) of the protein inactive. This could explain the inability to detect Compound I and Compound II species spectrally since the dominant six coordinate species would mask the minor levels of Compound I and Compound II formed. Regardless of the interpretation of these data, the predominance of the six coordinate species for H170A HRP in the presence and absence of imidazole suggests that an additional role of the proximal ligand is to maintain the five coordinate heme. Presumably this is provided by the tether to the C_α backbone since exogenous imidazole does not deter coordination to the sixth heme position. Collectively, these studies suggest that the role of the proximal ligand is to promote heterolytic cleavage and to provide a tether to the heme iron to deter coordination of the distal histidine.

CONCLUSIONS

Removal of the proximal ligand of HRP through mutagenesis deters Compound I formation and, to a lesser extent, decreases substrate oxidation. These reactions are likely to be similarly inhibited by the predominant six coordinate nature of H170A HRP. Coordination of the distal histidine to the iron would effectively inhibit peroxidase activity by tying up the nitrogen atom that deprotonates peroxide and by impeding the coordination of the peroxide anion to the iron atom. Exogenous imidazole, unlike the normal His 170 ligand, does not deter the coordination of the distal histidine to the heme iron. Thus one role of the proximal ligand is to provide a heme tether to maintain a five coordinate heme. Exogenous imidazole can, however, rescue the peroxidase activity of H170A HRP principally by accelerating Compound I formation. The electron density donated to the heme iron by the strongly-ligating imidazole presumably fosters heterolytic cleavage of the dioxygen bond of the iron peroxide complex.

Although the role of Asp 247 in HRP was not directly addressed in this study, the prevalence of a six coordinate heme in the Asp 235 CCP mutants suggests that this highly

conserved hydrogen bond acceptor is required to prevent coordination of solvent molecules or amino acid side chains to the sixth heme position. The hydrogen bond between the proximal histidine and the proximal aspartate could function in the maintenance of a five coordinate heme species by 1) strengthening and thus shortening the iron-nitrogen bond and 2) limiting the flexibility of the proximal imidazole, particularly its movement towards the heme iron. As observed for D235N CCP, the imidazolate character provided by the hydrogen bond to the proximal aspartate does not appear to influence Compound I formation significantly. To put these findings into perspective with Compound I formation observed for the CCP proximal histidine mutants, the increasing electron donation to the heme iron provided by glutamine, glutamate, and histidine proximal ligands is not critical for improving the rate of heterolytic cleavage of the dioxygen bond in the formation of Compound I. However, as observed for H170A HRP, the improved electron donation provided by exogenous imidazole versus a water or hydroxyl ligand suggests that the protein ligands do promote heterolytic cleavage. The proximal ligand also plays an important role in tethering the heme iron, thus deterring the formation of six coordinate species. This is especially true for HRP, where the distal histidine is prone to coordinate to the distal axial position.

Chapter 7: Conclusions

Several conserved residues and features distinguish the peroxidase heme pocket from that of other hemoproteins. Correspondingly, these residues and features are postulated to distinguish peroxidase function from that of other hemoproteins. Conserved amino acids found in the heme pocket of fungal and plant peroxidases include histidine, asparagine, arginine, and phenylalanine (tryptophan) residues at the distal heme face and histidine and aspartate residues at the proximal heme face (Figures 1.5, 1.6). Solvent accessibility to the enzyme-bound heme molecule is similar among the fungal and plant peroxidases and is restricted to the δ-*meso* heme edge. Accordingly, classic peroxidase activity, such as the HRP-catalyzed oxidation of guaiacol to phenolic radicals, is characterized by one electron abstraction by this heme edge. HRP also catalyzes the two electron oxidation of thioanisole. This reaction occurs in a mechanistically distinct manner to that of guaiacol oxidation and produces thioanisole sulfoxide in which the oxygen atom derives from the peroxide and thus from the ferryl oxygen of Compound I (Kobayashi *et al.*, 1986). Thioanisole is argued to bind near the ferryl oxygen of Compound I in order to permit oxygen transfer to the sulfur atom. Consistent with this theory, Robert Z. Harris carried out chemical modification and inhibition studies that provide support for the interaction of these two substrates with HRP at differing sites (Harris *et al.*, 1993). Specifically, reconstitution of HRP with δ-*meso*-ethylheme was shown to suppress guaiacol peroxidation but to stimulate thioanisole peroxygenation. Since δ-*meso*-ethylheme-reconstituted HRP binds guaiacol 2.8-fold more avidly than the native enzyme, the ethyl group was proposed to deter electron transfer to the heme edge rather than to hinder guaiacol binding. In agreement with the postulated interaction of thioanisole with the ferryl oxygen, thioanisole sulfoxidation is not suppressed by substitutions which interfere with electron abstraction at the heme edge.

The studies in Chapter 3 compare thioanisole and guaiacol with iodide, a two electron oxidizable substrate, in order to characterize iodide oxidation and to gain insight into the mechanisms of oxidation for the one electron- and two electron-oxidizable substrates. These studies suggest that iodide oxidation occurs at the δ-*meso* heme edge, as demonstrated by the diminished ability of δ-*meso*-ethyl heme-reconstituted HRP to oxidize iodide. The δ-*meso*-ethyl group suppresses iodide and guaiacol activities to similar extents (~20 fold reduction) (Table 3.1). Despite the similar suppression of these activities by the ethyl group, substrate binding, as studied by difference spectroscopy and inhibition studies, supports the existence of differing sites for guaiacol and iodide as bound by the resting state and Compound I species, respectively. NMR studies demonstrate that iodide binds HRP within 10 Å of the heme iron and at an equal distance from the 1- and 8-methyl heme groups (Sakurada *et al.*, 1987). Hence, we predict iodide binds near the δ-*meso* heme edge and between the 1- and 8-methyl groups. This site differs from that which binds phenolic compounds, which is proximal to the δ-*meso* heme edge within 5 Å of the 8 methyl group (Sakurada *et al.*, 1986; Veitch, 1995). Difference spectroscopy and inhibition studies also demonstrate that iodide binds independently of thioanisole (Figures 3.7, 3.8, 3.9). Thus, these three substrates interact with the heme in differing manners. Guaiacol is oxidized by one electron, which is abstracted by the heme edge. Thioanisole is sulfoxygenated, presumably at a site near the heme iron, by transfer of the Compound I ferryl oxygen. Iodide, like guaiacol, is oxidized near the δ-*meso* heme edge, suggesting that iodide oxidation also occurs through electron abstraction by the heme edge. The finding that two different substrate binding sites exist near the δ-*meso* heme edge suggests that varying orbital overlap between the substrate and the heme molecule may yield varying heme reactivity. This may explain why Compound II is not detected in the steady state turnover of iodide but is detected in the steady state turnover of guaiacol. The data obtained for iodide oxidation, however, do not exclude a mechanism involving transfer of the ferryl

oxygen to the substrate. Iodide binding near the plane of the heme at the distal heme face may permit sufficient interaction between the iodide and the ferryl oxygen to allow oxygen transfer. Further characterization of the iodide binding site may elucidate the location of this substrate relative to the distal heme face, revealing whether oxygen transfer is actually possible. The characterization of iodide oxidation and its relationship to that of guaiacol and thioanisole suggests, that despite the limited accessibility of substrates to the heme molecule within peroxidases, subtle differences in substrate binding provide for different heme reactivities.

Less subtle differences in heme accessibility are observed in comparing classes of hemoproteins and are postulated to control their respective functions. Chemical modification of P450s by phenyldiazene predominantly produces an iron-phenyl complex, whereas similar treatment of peroxidases yields heme edge modifications (Ortiz de Montellano, 1995). These contrasting modifications support crystallographic studies which show that the heme iron is accessible in the P450s but relatively inaccessible in the peroxidases (Li and Poulos, 1994). Thus, the varying reactivities displayed by these two classes of hemoproteins have been reconciled by postulating that the ferryl oxygen is accessible and readily transferred in the P450s but is shielded from transfer in the peroxidases. The distal histidine, phenylalanine (tryptophan), and arginine residues of peroxidases provide the primary barrier that shields the heme iron on the distal heme face. To promote peroxygenase activity, the distal histidine and phenylalanine residues within HRP were mutated to smaller inert residues (alanine and valine). These mutations were expected to create sufficient space on the distal heme face to make the ferryl oxygen accessible to the substrate. All of these individual mutants--F41A, H42A, and H42V--displayed improved peroxygenase activity relative to native and rWT HRP (Table 4.3). Relative to the native enzyme, F41A HRP exhibited thioanisole and styrene peroxygenase activities which were increased by 100-fold and > 10-fold, respectively. These improved

peryoxygenase activities suggest that accessibility to the Compound I ferryl oxygen is, in fact, improved in the F41A mutant. However, the inability to form an iron-phenyl complex in the reaction of F41A HRP with phenyldiazene suggests that access to the heme iron is still restricted in the F41A mutant. The His 42 mutants display markedly improved heme iron accessibility, as manifested by the formation of iron-phenyl complexes in the reaction of these mutants with phenyldiazene (Figure 4.13). Correspondingly, the distal histidine mutants also display improved peroxygenase activities relative to those for the wild-type proteins. Nevertheless, the rate of F41A HRP-catalyzed thioanisole sulfoxidation is ~10-fold faster than those determined for H42A- and H42V-HRP, although F41A HRP-catalyzed styrene epoxidation is ~3-fold reduced from that for the distal histidine mutants (Table 4.3). The weaker ability of the distal histidine mutants to oxidize thioanisole, relative to F41A HRP, is probably due to the fact that Compound I formation becomes partially rate limiting for the His 42 mutants. This is consistent with the 2-3 fold decrease in the rate of thioanisole sulfoxidation when the H42A- and H42V-HRP-catalyzed reactions were assayed with a five-fold lower concentration of peroxide. The intrinsically slower rate of styrene epoxidation, relative to that of thioanisole sulfoxidation, is less likely to be limited by the slow rate of Compound I formation of the distal histidine mutants. Thus, the distal histidine mutants which display greater accessibility to the heme iron relative to F41A HRP exhibit improved peroxygenase activity provided that Compound I formation is not rate limiting. This suggests that improved HRP peroxygenase activity may be promoted by retaining the distal histidine in the heme pocket while removing protein bulk in the vicinity of the heme iron. This might be accomplished by generating a double mutant, F41H/H42A, which would retain the distal histidine as well as the distal cavity created by the H42A mutation.

In addition to exhibiting peroxygenase activity, F41A HRP catalyzes guaiacol peroxidation at a rate that is comparable to that displayed by the native enzyme. F41A HRP

also exhibits Compound I and Compound II species that are formed and reduced in a native-like manner. In contrast, the distal histidine mutants display rates for guaiacol peroxidation that are reduced by five orders of magnitude from that of the native enzyme (Table 4.3). This decreased peroxidase activity parallels the 10^6-fold decrease in the rate of H42A- and H42V-HRP Compound I formation (Table 4.1). The Compound I species for the distal histidine mutants are reduced to Compound II by ferrocyanide at a rate that is decreased 5-fold from that observed for reduction of the native Compound I species (Table 4.2). The rate of reduction of Compound II to the resting state species, however, appears to be increased for the distal histidine mutants relative to the native enzyme. The reduction of Compound II is normally rate limiting for the native enzyme, allowing for the detection of Compound II in the reduction of Compound I to the resting state. However, Compound II is not observed in the reduction of Compound I to the resting state for the distal histidine mutants, suggesting that the reduction of Compound II is faster than that of Compound I (Figure 4.5). Thus, these studies demonstrate that removal of the distal imidazole group by the H42A and H42V mutations predominantly impedes Compound I formation, but has little deterring influence on the reduction of Compound I and Compound II. Thus, rapid peroxidase turnover depends on rapid Compound I formation, and Compound I formation is largely determined by the distal histidine.

Compound I formation and peroxidase activity exhibited by H42A HRP can be rescued by exogenous imidazole. Imidazoles substituted at the 2 position do not coordinate to the sixth heme coordination site and are most effective at rescuing H42A HRP peroxidase activity (Figure 5.2). 2-Methyl- and 1,2-dimethylimidazole bind H42A HRP weakly (~3 M). Support for the binding of these imidazoles in the cavity created by the H42A mutation is provided by the 14-fold improvement in the binding of 1,2-dimethylimidazole when it binds to cyanide-ligated H42A HRP versus the native ferric enzyme. Cyanide ligates to the sixth iron coordination site, which lies within the distal

cavity in H42A HRP. Hydrogen bonding between the nitrogen atom of the ligated cyanide and the distal histidine occurs in the native enzyme, and analogous hydrogen bonding between the H42A HRP-ligated cyanide and the exogenous imidazole could enhance the binding of 1,2-dimethylimidazole. Imidazole rescues the rate-limiting formation of Compound I for H42A HRP. The unprotonated form of the imidazole is most effective at rescuing H42A HRP, as revealed by the pH profile for guaiacol oxidation (Figure 5.4). This suggests that the imidazole principally functions in deprotonating peroxide, as this is the only step that requires a base in the mechanism of Compound I formation. A range of 1-methyl-2-substituted imidazoles of varying pKa values was assayed to determine their ability to promote H42A HRP Compound I formation. The results of this Brønsted analysis support the acquisition of 60% of a positive charge on the imidazole in the transition state in the peroxide deprotonation step of H42A HRP Compound I formation (Figure 5.10). This suggests that in the transition state the peroxide proton is 60% transferred to the rescuing imidazole. Given that this deprotonation event is likely to take place proximal to the heme iron in order for the ferric peroxide complex to form, the iron-oxygen bond is probably also partially formed in the transition state (Figure 5.13).

The overall inefficiency of imidazole in rescuing the H42A HRP peroxidase activity highlights the advantage of tethering this general acid/base catalytic residue to the C_α backbone. An effective 30 M concentration of imidazole is needed to fully restore H42A HRP guaiacol activity (Table 5.1). In the native enzyme, movement of the distal histidine is also restricted by a distal asparagine (Asn 70 in HRP). This residue hydrogen bonds to the $N_{\delta 1}$ nitrogen atom of the distal histidine. This interaction restricts rotation of the C_β-C_γ bond of the distal histidine and may also influence the basicity of the imidazole group. Consistent with these theories, N70V HRP forms Compound I at a rate that is 25-fold lower than that of the native enzyme (Nagano *et al.*, 1995). Imidazole-rescued H42A HRP provides a system with which to investigate the influence that this distal asparagine has on

the distal histidine. Exogenous imidazole bound by H42A HRP appears not to hydrogen bond to Asn 70, as suggested by the similar affinity that the mutant exhibits for 2-methyl- and 1,2-dimethylimidazoles. Perhaps a hydrogen bond that mimics that between His 42 and Asn 70 could be provided for exogenous imidazole by mutating Asn 70 to an aspartate, glutamate, or glutamine residue. Comparing the ability of imidazole to rescue the resulting H42A/N70D-, H42A/N70E-, and H42A/N70Q-HRP mutants with its ability to rescue H42A HRP may further elucidate the function of the distal asparagine.

The proximal histidine ligand, which is characteristic of peroxidases, is postulated to maintain the five coordinate heme species of the resting state enzyme which allows unhindered attack by the peroxide anion on the heme iron. The fifth heme ligand is also postulated to promote the heterolytic cleavage of the dioxygen bond of the ferric peroxide intermediate by donating electron density to the heme iron. The function of the proximal histidine ligand (His 170 in HRP) in peroxidase catalysis was probed by characterizing the proximal mutant, H170A HRP. At neutral pH values H170A HRP is predominantly six coordinate low spin as indicated by spectral characterization. Preliminary resonance Raman studies suggest that the distal histidine is coordinated to the sixth heme coordination site, confirming the role that the proximal ligand plays in maintaining a five coordinated heme species. This mutant also exhibits a significantly reduced peroxidase activity that is predominantly influenced by a 10^5-fold decrease in the rate of Compound I formation (Table 6.3). Exogenous imidazole binds to the cavity created by the H170A mutation. Imidazole-bound H170A HRP is still predominantly six coordinate low spin, suggesting that the tethered nature of the proximal imidazole in the native enzyme significantly contributes to the maintenance of a five coordinate heme species. Preliminary resonance Raman studies suggest that exogenous imidazole and the distal histidine coordinate to the heme iron, yielding a bis-ligated heme. Exogenous imidazole is bound within the proximal cavity created by the H170A mutation and is secluded from the solvent, as revealed by its

ability to fully restore the pH profiles for guaiacol and ABTS oxidation (Figure 6.6). Imidazole bound to the proximal cavity within the H170A mutant increases the rate of Compound I formation 1000-fold relative to that in the absence of imidazole (Table 6.3). The imidazole ligand presumably accelerates Compound I formation by donating electron density to the heme iron which promotes heterolytic cleavage of the dioxygen bond of the ferric peroxide complex. These studies suggest that the proximal histidine supports peroxidase cycling, predominantly by promoting Compound I formation through the maintenance of a five coordinate heme species and in donating electron density to the heme iron. This system also makes possible an examination of the role that imidazolate character plays in heterolytic cleavage. The proximal histidine is hydrogen bonded to a highly conserved aspartate residue (Asp 247 in HRP). This strong hydrogen bond accepting group effectively deprotonates the proximal histidine, producing a proximal ligand which exhibits considerable imidazolate character. Relative to the neutral imidazole, the imidazolate ligand donates increased electron density to the heme iron, as indicated by resonance Raman studies which show that the strength of this hydrogen bond in various peroxidases correlates with an increase in the (Fe^{3+}/Fe^{2+}) reduction potential (Banci *et al.*, 1993). The imidazole used to rescue H170A HRP could be replaced by 4-fluoro- or 4,5-difluoroimidazole to investigate whether improved donation of electron density to the heme iron, such as that promoted by the hydrogen bond between Asp 247 and His 170, increases the rate of Compound I formation.

Collectively, these HRP studies clarify the manner by which peroxidases and hemoproteins, in general, control heme reactivity. The fate of substrate oxidation is largely determined by how the substrate interacts with the heme edge and the ferryl oxygen of Compound I. The protein can modulate the interaction of substrate with the heme molecule by either binding the substrate proximal to the heme or hindering its interaction with the ferryl species. The distal peroxidase residues are part of the barrier that hinders substrate

accessibility to the ferryl oxygen of Compound I. The fast rates of peroxidase turnover are largely promoted by the invariant distal and proximal histidines, both of which accelerate the formation of Compound I. The distal histidine promotes Compound I formation predominantly by deprotonating the peroxide and thus facilitating the formation of the ferric peroxide complex. The proximal histidine maintains a five coordinate heme species and transfers electron density to the heme iron, thus promoting heterolytic cleavage of the dioxygen bond of the ferric peroxide complex.

References

Adachi, S., Nagano, S., Ishimori, K., Watanabe, Y. and Morishima, I. (1993) Roles of proximal ligand in heme proteins: replacement of proximal histidine of human myoglobin with cysteine and tyrosine by site-directed mutagenesis as models for P-450, chloroperoxidase, and catalase, *Biochemistry* 32, 241-252.

Adediran, S. A. and Dunford, H. B. (1983) Structure of horseradish peroxidase Compound I, *Eur. J. Biochem.* 132, 147-150.

Allentoff, A. J., Bolton, J. L., Wilks, A., Thompson, J. A. and Ortiz de Montellano, P. R. (1992) Heterolygic versus homolytic peroxide bond cleavage by sperm whale myoglobin and myoglobin mutants, *J. Am. Chem. Soc.* 114, 9744-9749.

Araiso, T., Miyoshi, K. and Yamazaki, I. (1976) Mechanisms of electron transfer from sulfite to horseradish peroxidase-hydroperoxide compounds, *Biochemistry* 15, 3059-3063.

Araiso, T. and Dunford, H. B. (1980) Horseradish peroxidase. XLI. Complex formation with nitrate and its effect upon Compound I formation, *Biochem. Biophys. Res. Comm.* 94, 1177-1182.

Araiso, T. and Dunford, H. B. (1981) Horseradish peroxidase. Complex formation with anions and hydrocyanic acid, *J. Biol. Chem.* 256, 10099-10104.

Ashley, P. L. and Griffin, B. W. (1981) Chloroperoxidase-catalyzed halogenation of antipyrine, a drug substrate of liver microsomal cytochrome P-450, *Arch. Biochem. Biophys.* 210, 167-178.

Aswad, D. W. (1994) *Deamidation of isoaspartate formation in peptides and proteins.* CRC Press, Boca Raton, FL.

Ator, M. A. and Ortiz de Montellano, P. R. (1987) Protein control of prosthetic heme reactivity. Reaction of substrates with the heme edge of horseradish peroxidase, *J. Biol. Chem.* 262, 1542-1551.

Ator, M. A., David, S. K. and Ortiz de Montellano, P. R. (1987) Structure and catalytic mechanism of horseradish peroxidase. Regiospecific *meso* alkylation of the prosthetic heme group by alkylhydrazines, *J. Biol. Chem.* 14954-14960.

Bach, A. N. and Chodat, R., (1903) Untersuchungen über die rolle der peroxyde in der chemie der lebenden zelle. IV. Über peroxydase, *Ber.* 36, 600.

Bagger, S. and Williams, R. J. P. (1971) Intermediates in the reaction beteen hydrogen peroxide and horseradish peroxidase, *Acta Chem. Scand.* 25, 976-982.

Banci, L., Bertini, I., Turano, P., Tien, M. and Kirk, T. K. (1991) Proton NMR investigation into the basis for the relatively high redox potential of lignin peroxidase, *Proc. Natl. Acad. Sci. U. S. A.* 88, 6956-6960.

Banci, L., Bertini, I., Kuan, I., Tien, M., Turano, P. and Vila, A. J. (1993) NMR investigation of isotopically labeled cyanide derivatives of lignin peroxidase and manganese peroxidase, *Biochemistry* 32, 13483-13489.

Barr, D. P., Shah, M. M., Grover, T. A. and Aust, S. D. (1992) Production of hydroxyl radical by lignin peroxidase from *Phanerochaetechrysosporium*, *Arch. Biochem. Biophys.* 298, 480-485.

Baunsgaard, L., Dalbøge, H., Houen, G., Rasmussen, M. and Welinder, K. G. (1993) Amino acid sequence of *Coprinus macrorhizus* peroxidase and cDNA sequence encoding *Coprinus cinereus* peroxidase. A new family of fungal peroxidases, *Eur. J. Biochem.* 213, 605-611.

Baynton, K. J., Bewtra, J. K., Biswas, N. and Taylor, K. E. (1994) Inactivation of horseradish peroxidase by phenol and hydrogen peroxide: a kinetic investigation, *Biochim. Biophys. Acta* 1206, 272-278.

Bhattacharyya, D. K., Bandyopadhyay, U. and Banerjee, R. K. (1992) Chemical and kinetic evidence for an essential histidine in horseradish peroxidase for iodide oxidation, *J. Biol. Chem.* 267, 9800-9804.

Bhattacharyya, D. K., Bandyopadhyay, U. and Banerjee, R. K. (1993) Chemical and kinetic evidence for an essential histidine residue in the electron transfer from aromatic donor to horseradish peroxidase Compound I, *J. Biol. Chem.* 268, 22292-22298.

Blumberg, W. E., Peisach, J., Wittenberg, B. A. and Wittenberg, J. B. (1968) The electronic structure of protoheme proteins. I. An electron paramagnetic resonance and optical study of horseradish peroxidase and its derivatives, *J. Biol. Chem.* 243, 1854-1862.

Bolton, W. and Perutz, M. F. (1970) Three dimensional fourier synthesis of horse deoxyhaemoglobin at 2.8 Angstrom units resolution, *Nature* 228, 551-552.

Bosshard, H. R., Anni, H. and Yonetani, T. (1991) Yeast cytochrome c peroxidase, *Peroxidases in Chemistry and Biology, Vol II*, (Everse, J., Everse, K. E., and Grisham, M. B. Eds.) Boca Raton, FL., CRC Press, Inc. p 51-84.

Bradford, M. M. (1976) A rapid and sensitive method for the quantitation of microgram quantities of protein utilizing the principle of protein-dye binding, *Anal. Biochem.* 72, 248-254.

Brill, A. S. and Sandberg, H. E. (1968) Spectral studies of iron coordination in oxidized compounds of hemoproteins. Difference spectroscopy below 250 millimicrons, *Biochemistry* 7, 4254-4260.

Buffard, D., Breda, C., van Huystee, R. B., Asemota, O., Pierre, M., Ha, D. B. D. and Esnault, R. (1990) Molecular cloning of complementary DNAs encoding two cationic peroxidases from cultivated peanut cells, *Proc. Natl. Acad. Sci U. S. A.* 87, 8874-8878.

Butters, T. D. and Hughes, R. C. (1981) Isolation and characterization of mosquito cell membrane glycoproteins. *Biochim. Biophys. Acta* 640, 655-671.

Butters, T. D., Hughes, R. C. and Vischer, P. (1981) Steps in the biosynthesis of mosquito cell membrane glycoproteins and the effects of tunicamycin. *Biochim. Biophys. Acta* 640, 672-686.

Campa, A. (1991) Biological roles of plant peroxidases: known and potential function, *Peroxidases in Chemistry and Biology, Vol II*, (Everse, J., Everse, K. E., and Grisham, M. B. Eds.) Boca Raton, FL., CRC Press, Inc. p 26-50.

Chance, B. (1949a) The properties of the enzyme-substrate compounds of peroxidase and peroxides. I. The spectra of the primary and secondary complexes, *Arch. Biochem. Biophys.* 21, 416-430.

Chance, B. (1949b) The properties of the enzyme-substrate compounds of horse-radish and lacto-peroxidase, *Science* 109, 204-208.

Chance, B. (1950) Reaction of ferrocytochrome-c with peroxidases and peroxides, *Fed. Proc. Fed. Amer. Soc. Exp. Biol.* 9, 160.

Chance, B. (1952) The spectra of the enzyme-substrate complexes of catalase and peroxidase, *Arch. Biochem. Biophys.* 41, 404-415.

Chance, B., Ericinska, M., Wilson, D. F., Dutton, P. L. and Lee, C. P. (1970) in *Structure and function of oxidative-reduction enzymes* (Akeson, A. and Ehrenberg, A., Eds.) Pergamon Press, Oxford.

Chance, B., Powers, L., Ching, Y., Poulos, T. L., Schonbaum, G. R., Yamazaki, I. and Paul, K. G. (1984) X-ray absorption studies of intermediates in peroxidase activity, *Arch. Biochem. Biophys.* 235, 596-611.

Childs, R. E. and Bardsley, W. G. (1975) The steady-state kinetics of peroxidase with 2,2'-azino-di-(3-ethyl-benzthiazoline-6-sulphonic acid) as chromogen, *Biochem. J.* 145, 93-103.

Choudhury, K., Sundaramoorthy, M., Hickman, A., Yonetani, T., Woehl, E., Dunn, M. F. and Poulos T. L. (1994) Role of the proximal ligand in peroxidas catalysis - crystallographic, kinetic, and spectral studies of cytochrome c peroxidase proximal ligand mutants, *J. Biol. Chem.* 269, 20239-20249.

Colclough, N. and Smith J. L. (1994) A mechanistic study of the oxidation of phenols in aqueous solution by oxoiron(IV) tetra(N-methylpyridyl)porphyrins. A model for horseradish peroxidase Compound II?, *J. Chem. Soc. Perkin Trans. II* 28, 1139-1149.

Critchlow, J. E. and Dunford, H. B., (1972) Studies on horseradish peroxidase. IX. Kinetics of the oxidation of *p*-cresol by Compound II, *J. Biol. Chem.* 247, 3703-3713.

Dalton, D. A. (1991) Ascorbate peroxidase, in *Peroxidases in Chemistry and Biology, Vol II*, (Everse, J., Everse, K. E., and Grisham, M. B. Eds.) Boca Raton, FL., CRC Press, Inc. p 139-153.

DePillis, G. D. and Ortiz de Montellano, P. R. (1989) Substrate oxidation by the heme *Coprinus macrorhizus* peroxidase with hydrazines and sodium azide, *Biochemistry* 28, 7947-7952.

DePillis, G. D., Sishta, B. P., Mauk, A. G. and Ortiz de Montellano, P. R. (1991) Small substrates and cytochrome c are oxidized at different sites of cytochrome c peroxidase, *J. Biol. Chem.* 266, 19334-19341.

Doeff, M. M. and Sweigert, D. A. (1982) Hydrogen bonding in metalloporphyrin reactions. Reaction of (tetraphenylporphinato)iron(III) chloride and N-methylimidazole *Inorg. Chem.* 21, 3699-3705.

Doerge, D. R. (1986) Oxygenation of organosulfur compounds by peroxidases: evidence of an electron transfer mechanism for lactoperoxidase, *Arch. Biochem. Biophys.* 244, 678-685.

Dolphin, D., Forman, A., Borg, D. C., Fajer, J. and Felton, R. H. (1974) Compounds I of catalase and horseradish peroxidase: π-cation radicals, *Proc. Natl. Acad. Sci. U. S. A.* 68, 614-618.

Dunford, H. B. and Stillman, J. S. (1976) On the function and mechanism of action of peroxidases, *Coord. Chem Rev.* 19, 187-251.

Dunford, H. B., Hewson, W. D. and Steiner, H., (1978) Horseradish peroxidase. XXIX. Reactions in water and deuterium oxide: cyanide binding, Compound I formation and reactions of Compounds I and II with ferrocyanide, *Can. J. Chem.* 56, 2844-2852.

Dunford, H. B. and Araiso, T. (1979) Horseradish peroxidase. XXXVI. On the difference between peroxidase and metmyoglobin, *Biochem. Biophys. Res. Comm.* 89, 764-768.

Dunford, H. B. (1982) Peroxidases, *Adv. Inorg. Biochem.* 4, 41-68.

Dunford, H. B. and Adeniran, A. J. (1986) Hammett rho sigma correlation for reactions of horseradish peroxidase Compound II with phenols, *Arch. Biochem. Biophys.* 251, 536-542.

Dunford, H. B. (1991) Horseradish peroxidase: structure and kinetic properties, *Peroxidases in Chemistry and Biology, Vol II*, (Everse, J., Everse, K. E., and Grisham, M. B. Eds.) Boca Raton, FL., CRC Press, Inc. p 1-24.

Edmundson, A. B. (1965) Amino acid sepuence of sperm whale myoglobin, *Nature* 205, 883-887.

Edwards S. L., Poulos T. L. and Kraut J. (1984) The crystal structure of fluoride-inhibited cytochrome c peroxidase. *J. Biol. Chem.* 259, 12984-12988.

Erman, J. E. and Vitello, L. B. (1992) Active-site mutations in cytochrome-c peroxidase - a critical role for histidine-52 in the rate of formation of Compound-I, *J. Am. Chem. Soc.* 114, 6592-6593.

Erman, J. E., Vitello, L. B., Miller, M. A., Shaw, A., Brown, K. A. and Kraut, J. (1993) Histidine 52 is a critical residue for rapid formation of cytochrome c peroxidase Compound I, *Biochemistry* 32, 9798-9806.

Everett, A. J. and Minkoff, G. J. (1953) The dissociation constants of some alkyl and acyl hydroperoxides, *Trans. Farraday Soc.* 49, 410-414.

Ferrer, J. C., Turano, P., Banci, L., Bertini, I., Morris, I. K., Smith, K. M., Smith, M. and Mauk, A. G. (1994) Active site coordination chemistry of the cytochrome c peroxidase D235A variant: spectroscopic and functional characterization, *Biochemistry* 33, 7819-7829.

Finzel, B. C., Poulos, T. L. and Kraut, J. (1984) Crystal structure of yeast cytochrome c peroxidase refined at 1.7-Å resolution, *J. Biol. Chem.* 259, 13027-13036.

Fruetel, J. A., Collins, J. R., Camper, D. L., Loew, G. H. and Ortiz de Montellano, P. R. (1992) Calculated and experimental absolute stereochemistry of the styrene and *beta*-methylstyrene epoxides formed by cytochrome-p450(cam), *J. Am. Chem. Soc.* 114, 6987-6993.

Fruetel, J., Chang, Y.-Y., Collins, J., Loew, G. and Ortiz de Montellano, P. R. (1994) Thioanisole sulfoxidation by cytochrome P450(cam) (cyp101) - experimental and calculated absolute stereochemistries, *J. Am. Chem. Soc.* 116, 11643-11648.

Fry, S. C. (1983) Feruloylated pectins from the primary cell wall: their sturcture and possible functions, *Planta* 157, 111-123.

Fry, S. C. (1986) Polymer-bound phenols as natural substrates of peroxidases, *Plant Peroxidases*, Centre de Botanique, Université de Genève, pp 169-182.

Furhop, J. H. and Smith, K. M. (1975) Laboratory methods , In *Porphyrins and metalloproteins*, (Smith, K. M., ed.) Elsevier, Amsterdam, pp. 757-869.

Gennis, R. B. (1991) Some recent advances relating to prokaryotic cytochrome c reductases and cytochrome c oxidases, *Biochim. Biophys. Acta* 1058, 21-24.

George, P. (1952) The specific reactions of iron in some hemoproteins, *Adv. Catal.* 4, 367-428.

George, P. and Irvine, D. H. (1955) A possible structure for the higher oxidation state of metmyoglobin *Biochem. J.* 60, 596-604.

Gold, M., Wariishi, H. and Valli, K. (1989) Extracellular peroxidases involved in lignin degradation by the white rot basidiomycete *Phanerochaete chrysosporium*, *ACS Symposium on Biocatalysis in Agricultural Biothechnology* Series 389, 127-140.

Goodin, D. B., Davidson, M. G., Roe, J. A., Mauk, A. G. and Smith, M. (1991) Amino acid substitutions at tryptophan-51 of cytochrome c peroxidase: effects on

coordination, species preference for cytochrome c, and electron transfer, *Biochemistry* 30, 4953-4962.

Goodin, D. B. and McRee, D. E. (1993) The Asp-His-Fe triad of cytochrome c peroxidase controls the reduction potential, electronic structure, and coupling of the tryptophan free radical to the heme, *Biochemistry* 32, 3313-3324.

Goodwin, D. C., Aust, S. D. and Grover, T. A. (1995) Evidence for veratryl alcohol as a redox mediator in lignin peroxidase-catalyzed oxidation, *Biochemistry* 34, 5060-5065.

Grimmett, M. R. (1980) Advances in imidazole chemistry, *Adv. Heter. Chem.* 27, 241-323.

Hamberg, M., Svensson, J., Wakabayashi, T. and Samuelsson, B. (1974) Isolation and structure of two prostaglandin endoperoxides that cause platelet aggregation, *Proc. Natl. Acad. Sci. U. S. A.* 71, 345-349.

Harpel, M. R. and Hartman, F. C. (1994) Chemical rescue by exogenous amines of a site-directed mutant of ribulose 1,5-bisphosphate carboxylase/oxygenase that lacks a key lysyl residue, *Biochemistry* 33, 5553-5561.

Harris, R. Z., Newmyer, S. L. and Ortiz de Montellano, P. R. (1993) Horseradish peroxidase-catalyzed two-electron oxidations. Oxidation of iodide, thioanisoles, and phenols at distinct sites, *J. Biol. Chem.* 268, 1637-1645.

Harrison, J. E. and Schultz, J. (1976) Studies on the chlorinating activity of myeloperoxidase, *J. Biol. Chem.* 251, 1371-1374.

Harthill, J. E. and Ashford, D. A. (1992) N-glycosylation of horseradish peroxidase from cell culture, *Biochem. Soc. Trans.* 20, 113S.

Hartmann, C. and Ortiz de Montellano, P. R. (1992) Baculovirus expression and characterization of catalytically active horseradish peroxidase, *Arch. Biochem. Biophys.* 296, 1-12.

Hashimoto, S., Tatsuno, Y. and Kitagawa, T. (1986) Resonance Raman evidence for oxygen exchange between the Fe(IV) = O heme and bulk water during enzymic catalysis of horseradish peroxidase and its relation with the heme-linked ionization, *Proc. Natl. Acad. Sci. U.S.A.* 83, 2417-2421.

Hoffman, B. M., Natan, M. J., Nocek, J. M. and Wallin, S. A. (1991) Long-range electron transfer within metal-substituted protein complexes, *Struct. Bonding* 75, 85-108.

Hosoya, T., Sakurada, J., Kurokawa, C., Toyoda, R. and Nakamura, S. (1989) Interaction of aromatic donor molecules with lactoperoxidase probed by optical difference spectra, *Biochemistry* 28, 2639-2644.

Houseman, A.. L. P., Doan, P. E., Goodin, D. B. and Hoffman, B. M. (1993) Comprehensive explanation of the anomalous EPR spectra of wild-type and mutant cytochrome c peroxidase compound ES, *Biochemistry* 32, 4430-4443.

Hsieh, P. and Robbins, P. W. (1984) Regulation of asparagine-linked oligosaccharide processing. Oligosaccharide processing in *Aedes albopictus* mosquito cells, *J. Biol. Chem.* 259, 2375-2382.

Ishida, A., Ono, K. and Matsusaka, T. (1985) Cell wall-associated peroxidase in cultured cells of liverwort *Marchantia polymorpha L.*, changes of peroxidase level and its localization in the cell wall, *Plant Cell Rep.* 4, 54-57.

Job, D. and Dunford, H. B. (1976) Substituent effect on the oxidation of phenols and aromatic amines by horseradish peroxidase Compound I, *Eur. J. Biochem.* 66, 607-614.

Johnson, K. R. and Nauseef, W. N. (1991) Molecular biology of myeloperoxidase, *Peroxidases in Chemistry and Biology, Vol I*, (Everse, J., Everse, K. E., and Grisham, M. B. Eds.) Boca Raton, FL., CRC Press, Inc. p 63-81.

Jonen, H. G., Werringloer, J., Prough, R. A. and Estabrook, R. W. (1982) The reaction of phenylhydrazine with microsomal cytochrome P-450. Catalysis of heme modification, *J. Biol. Chem.* 257, 4404-4411.

Keilin, D. and Hartree, E. F. (1951) Purification of horseradish peroxidase and comparison of its properties with those of catalase and methaemoglobin, *Biochem. J.* 49, 88-106.

Kim, K. L., Kang, D. S., Vitello, L. B. and Erman, J. E. (1990) Cytochrome c peroxidase catalyzed oxidation of ferrocytochrome c by hydrogen peroxide: ionic strength dependence of the steady-state rate parameters, *Biochemistry* 29, 9150-9159.

Klebanoff, S. J. (1991) Myeloperoxidase: occurrence and biological function, *Peroxidases in Chemistry and Biology, Vol I*, (Everse, J., Everse, K. E., and Grisham, M. B. Eds.) Boca Raton, FL., CRC Press, Inc. p 1-35.

Kobayashi, S., Nakano, M, Goto, T., Kimura, T. and Schaap, A. P. (1986) An evidence of peroxidase-dependent oxygen transfer from hydrogen peroxide to sulfides, *Biochem. Biophys. Res. Commun.* 135, 166-171.

Kobayashi, S., Nakano, M., Kimura, T. and Schaap, A. P. (1987) On the mechanism of the peroxidase-catalyzed oxygen-transfer reaction, *Biochemistry* 26, 5019-5022.

Kornfeld, R. and Kornfeld, S. (1985) Assembly of asparagine-linked oligosaccharides, *Ann. Rev. Biochem.* 54: 631-664.

Kunishima, N., Fukuyama, K., Matsubara, H., Hatanaka, H., Shibano, Y. and Amachi, T. (1994) Crystal structure of the fungal peroxidase from *Arthromyces ramosus* at 1.9 Å resolution. Structural comparisons with the lignin and cytochrome c peroxidases, *J. Mol. Biol.* 235, 331-344.

Kuo, C. and Fridovich, I. (1988) Stimulation of the activity of horseradish peroxidase by nitrogenous compounds, *J. Biol. Chem.* 263, 3811-3817.

Ladner, R. C., Heidner, E. J. and Perutz, M. F. (1977) The structure of horse methaemoglobin at 2.0 Å resolution, *J. Mol. Biol.* 114, 385-414.

La Mar, G. N. and de Ropp, J. S. (1979) Assignment of exchangeable proximal histidine resonances in high-spin ferric hemoproteins: substrate binding in horseradish peroxidase, *Biochem. Biophys. Res. Commun.* 90, 36-41.

La Mar, G. N., Hernandez, G. and de Ropp, J. S. (1992) H^1 NMR investigation of the influence of interacting sites on the dynamics and thermodynamics of substrate and ligand binding to horseradish peroxidase, *Biochemistry* 31, 9158-9168.

Li, H. and Poulos, T. L. (1994) Structural variation in heme enzymes: a comparative analysis of peroxidase and P450 crystal structures, *Structure* 2, 461-464.

Loew, G. H., Du, P. and Smith, A. T. (1995) Homology modelling of horseradish peroxidase coupled to two-dimensional NMR spectral assignments, *Biochem. Soc. Trans.* 23, 250-256.

Makino, R., Uno, T., Nishimura, Y., Iizuka, T., Tsuboi, M. and Ishimura, Y. (1986) Coordination structures and reactivities of Compound II in iron and manganese horseradish peroxidases. A resonance Raman study, *J. Biol. Chem.* 261, 8376-8382.

Marklund, S. (1973) Mechanisms of the irreversible inactivation of horseradish peroxidase caused by hydroxymethylhydroperoxide, *Arch. Biochem. Biophys.* 154, 614-622.

Maltempo, M. M., Ohlsson, P. -I., Paul, K. -G., Petersson, L. and Ehrenberg, A. (1979) Electron paramagnetic resonance analyses of horseradish peroxidase in situ and after purification, *Biochemistry* 18, 2935-2941.

Marnett, L. J., Weller, P. A. and Battista, J. R. (1986) Comparison of the peroxidase activity of hemeproteins and cytochrome P450, In *Cytochrome P-450* (P. R. Ortiz de Montellano, Ed.) Plenum Press, New York, pp. 29-76.

Mauk, M. R. and Girotti, A. W. (1973) Photooxidation of the protoporphyrin-apomyoglobin complex, *Biochemistry* 12, 3187-3193.

Mauk, M. R. and Girotti, A. W. (1974) The protoporphyrin-apoperoxidase complex. Photooxidation studies, *Biochemistry* 13, 1757-1763.

McCarthy, M. B. and White, R. E. (1983) Functional differences between peroxidase Compound I and the cytochrome P-450 reactive oxygen intermediate, *J. Biol. Chem.* 258, 9153-9158.

McLendon, G. (1991) Control of biological electron transport via molecular recognition and binding: the "velcro" model, *Struct. Bonding* 75, 159-174.

McRee, D. E., Jensen, G. M., Fitzgerald, M. M., Siegel, H. A. and Goodin, D. B. (1994) Construction of a bisaquo heme enzyme and binding by exogenous ligands, *Proc. Natl. Acad. Sci. USA.* 91, 12847-12851.

Miller, R. D., Lee, V. Y. and Moylan, C. R. (1994) Substituted azole derivatives as nonlinear optical chromophores, *Chem. Mater.* 6, 1023-1032.

Miller, A. M., Vitello, L. and Erman, J. E. (1995a) Regulation of interprotein electron transfer by Trp 191 of cytochrome c peroxidase, *Biochemistry* 34, 12048-12058.

Miller, V. P., Goodin, D. B., Friedman, A. E., Hartmann, C. and Ortiz de Montellano, P. R. (1995b) Horseradish peroxidase Phe172-->Tyr mutant. Sequential formation of Compound I with a porphyrin radical cation and a protein radical, *J. Biol. Chem.* 270, 18413-18419.

Mittler, R. and Zilinskas, B. A. (1991) Purification and characterization of pea cytosolic ascorbate peroxidase, *Plant Physiol.* 97, 962-968.

Modi, S., Behere, D. V. and Mitra, S. (1991) Horseradish peroxidase catalyzed oxidation of thiocyanate by hydrogen peroxide: comparison with lactoperoxidase-catalysed oxidation and role of distal histidine, *Biochimica et Biophysica Acta* 1080, 45-50.

Morikis D., Champion P. M., Springer B. A., Egebey K. D. and Sligar, S. G. (1990) Resonance Raman studies of iron spin and axial coordination in distal pocket mutants of ferric myoglobin, *J. Biol. Chem.* 265, 12143-12145.

Morishima, I. and Ogawa, S. (1979) Nuclear magnetic resonance studies of hemoproteins. Binding of aromatic donor molecules to horseradish peroxidase, *J. Biol. Chem.* 254, 2814-2820.

Morishima, I., Neya, S. and Yonezawa, T. (1980) Proton NMR study of hemoproteins. Ionization and orientation of iron-bound imidazole in methemoglobin and metmyoblobin, *Biochim. Biophys. Acta* 621, 218-226.

Morrison, M. and Schonbaum, G. R. (1976) Peroxidase-catalyzed halogenation, *Ann. Rev. Biochem.* 45, 861-888.

Moss, T. H., Ehrenberg, A. and Bearden, A. J. (1969) Mossbauer spectroscopic evidence for the electronic configuration of iron in horseradish peroxidase and its peroxide derivatives, *Biochemistry* 8, 4159-4162.

Nagano, S., Tanaka, M., Watanabe, Y. and Morishima, I. (1995) Putative hydrogen bond network in the heme distal site of horseradish peroxidase, *Biochem. Biophys. Res. Commun.* 207, 417-423.

Nakajima, R. and Yamazaki, I. (1980) The conversion of horseradish peroxidase C to a verdohemoprotein by a hydroperoxide derived enzymatically from indole-3-acetic acid and by *m*-nitroperoxybenzoic acid, *J. Biol. Chem.* 255, 2067-2071.

Newmyer, S. L. and Ortiz de Montellano, P. R. (1995) Horseradish peroxidase His-42 --> Ala, His-42 --> Val, and Phe-41 --> Ala mutants. Histidine catalysis and control of substrate access to the heme iron, *J. Biol. Chem.* 270, 19430-19438.

Nicholls, P. (1962) The oxidation of cytochrome c by horseradish peroxidase, *Biochem. J.* 84, 68P.

Northrup, S. H., Boles, J. O. and Reynolds, J. C. L. (1988) Brownian dynamics of cytochrome c and cytochrome c peroxidase association, *Science* 24, 67-70.

Nunez, J. and Pommier, J. (1982) Formation of thyroid hormones, *Vitam. Horm.* 39, 175-229.

Oertling, W. A. and Babcock, G. T. (1988) Time-resolved and static resonance Raman spectroscopy of horseradish peroxidase intermediates, *Biochemistry* 27, 3331-3338.

Ogura, T. and Kitigawa, T. (1987) Device for simultaneous measurements of transient Raman and absorption spectra of enzymic reactions: application to Compound I of horseradish peroxidase, *J. Am. Chem. Soc.* 109, 2177-2179.

Ortiz de Montellano, P. R. and Kerr, D. E. (1983) Inactivation of catalase by phenylhydrazine. Formation of a stable aryl-iron heme complex, *J. Biol. Chem.* 258, 10558-10563.

Ortiz de Montellano, P. R. (1987) Control of the catalytic activity of prosthetic heme by the structure of hemoproteins, *Accts. Chem. Res.* 20, 289-294.

Ortiz de Montellano, P. R. (1995) Arylhydrazines as probes of hemoprotein structure and function, *Biochemie* 77, 581-593.

Patterson, W. R. and Poulos, R. L. (1995) Crystal structure of recombinant pea cytosolic ascorbate peroxidase, *Biochemistry* 34, 4331-4341.

Patterson, W. R., Poulos, T. L. and Goodin, D. B. (1995) Identification of a porphyrin pi cation radical in ascorbate peroxidase Compound I, *Biochemistry* 34, 4342-4345.

Paul, K. G. and Ohlsson, P. I. (1978) Equilibria between horseradish peroxidase and aromatic donors, *Acta Chem. Scand. B32*, 395-405.

Peisach, J. and Blumberg, W. E. (1972), in *Structure and Function of Oxidation-Reduction Enzymes*, (Akeson, A., and Ehrenberg, A., Ed.) New York, N. Y., Academic Press, p 191.

Pelletier, H. and Kraut, F. (1992) Crystal structure of a complex between electron transfer partners, cytochrome c peroxidase and cytochrome c, *Science* 258, 1748-1755.

Penner-Hahn, F. E., Eble, K. S., McMurry, T. J., Renner, M., Balch, A. L., Groves, J. T., Dawson, J. H. and Hodgson, K. O. (1986) Structural characterization of horseradish peroxidase using EXAFS spectroscopy. Evidence for Fe=O ligation in Compounds I and II, *J. Am. Chem. Soc.* 108, 7819-7825.

Pettigrew, G. W. and Moore, G. R. (1987) *Cytochrome c: biological aspects*, Springer-Verlag, Berlin.

Pérez, U. and Dunford, H. B. (1990a) Spectral studies on the oxidation of organic sulfides (thioanisoles) by horseradish peroxidase Compounds I and II, *Biochim. Biophys. Acta* 1038, 98-104.

Pérez, U. and Dunford, H. B. (1990b) Transient-state kinetics of the reactions of 1-methoxy-4-(methylthio)benzene with horseradish peroxidase Compounds I and II, *Biochemistry* 29, 2757-2763.

Perona, J. J., Hedstrom, L., Wagner, R. L., Rutter, W. J., Craik, C. S. and Fletterick, R. J. (1994) Exogenous acetate reconstitutes the enzymatic activity of trypsin Asp189Ser, *Biochemistry* 33, 3252-3259.

Piontek, P., Glumoff, T. and Winterhalter, K. (1993) Low pH crystal structure of glycosylated lignin peroxidase from *Phanerochaete chrysosporium* at 2.5 Å resolution, *Febs Lett.* 315, 119-124.

Poulos, T. L., Freer, S. T., Alden, R. A., Edwards, S. L., Skogland, U., Takio, K., Eriksson, B., Xuong, N., Yonetani, T. and Kraut, J. (1980) The crystal structure of cytochrome c peroxidase, *J. Biol. Chem.* 255, 575-580.

Poulos, T. L. and Kraut, J. (1980) The stereochemistry of peroxidase catalysis, *J. Biol. Chem.* 255, 8199-8205.

Poulos, T. L., Edwards, S. L., Wariishi, H. and Gold, M. H. (1993) Crystallographic refinement of lignin peroxidase at 2 Å, *J. Biol. Chem.* 268, 4429-4440.

Raag, R., Swanson, B. S., Poulos, T. L. and Ortiz de Montellano, P. R. (1990) Formation, crystal structure, and rearrangement of a cytochrome P-450cam iron-phenyl complex, *Biochemistry* 29, 8119-8126.

Rao, S. I., Wilks, A. and Ortiz de Montellano, P. R. (1993) The roles of His-64, Tyr-103, Tyr-146, and Tyr-151 in the epoxidation of styrene and ß-methylstyrene by recombinant sperm whale myoglobin, *J. Biol. Chem.* 268, 803-809.

Reese, C. B. and Zhang, P. Z. (1993) Phosphotriester approach to the synthesis of oligonucleotides: a reappraisal, *J. Chem. Soc., Perkin Trans. I* 19, 2291-2301.

Ringe, D., Petsko, G. A., Kerr, D. E. and Ortiz de Montellano, P. R. (1984) Reaction of myoglobin with phenylhydrazine: a molecular doorstop, *Biochemistry* 23, 2-4.

Roe, J. A. and Goodin, D. B. (1993) Enhanced oxidation of aniline derivatives by two mutants of cytochrome c peroxidase at tryptophan 51, *J. Biol. Chem.* 268, 20037-20045.

Roman, R. and Dunford, H. B. (1972) pH dependence of the oxidation of iodide by Compound I of horseradish peroxidase, *Biochemistry* 11, 2076-2082.

Roman, R. and Dunford, H. B. (1973) Studies on horseradish peroxidase. XII. A kinetic study of the oxidation of sulfite and nitrite by Compounds I and II, *Can. J. Chem.* 51, 588-596.

Sakurada, J., Takahashi, S. and Hosoya, T. (1986) Nuclear magnetic resonance studies on the spatial relationship of aromatic donor molecules to the heme iron of horseradish peroxidase, *J. Biol. Chem.* 261, 9657-9662.

Sakurada, J., Takahashi, S. and Hosoya, T. (1987) Proton nuclear magnetic resonance studies on the iodide binding by horseradish peroxidase, *J. Biol. Chem.* 262, 4007-4010.

Sanders, S. A., Bray, R. C. and Smith, A. T. (1994) pH-dependent properties of a mutant horseradish peroxidase isoenzyme C in which Arg38 has been replaced with lysine, *Eur. J. Biochem.* 224, 1029-1037.

Schonbaum, G. R., Welinder, K. G. and Smillie, L. B. (1971) In, *Probes of Structure and Function of Macromolecules and Membranes, Vol. II* (Chance, B., Yonetani, T., and Mildvan, A. S., Ed.) New York, N. Y., Academic Press, p 533.

Schonbaum, G. R. and Lo, S. (1972) Interaction of peroxidases with aromatic peracids and alkyl peroxides. Product analysis, *J. Biol. Chem.* 247, 3353-3360.

Schonbaum, G. R. (1973) New complexes of peroxidases with hydroxamic acids, hydrazides, and amides, *J. Biol. Chem.* 248, 502-511.

Segel, I. (1976) In, *Biochemical Calculations*: *How to solve mathematical problems in general biochemistry*, 2nd Ed., (by Segel, I.) New York, N. Y., Wiley, pp 252-262.

Shah, M. M. and Aust, S. D. (1993) Iodide as the mediator for the reductive reactions of peroxidases, *J. Biol. Chem.* 268, 8503-8506.

Shannon, L. M., Kay, E. and Lew, J. Y. (1966) Peroxidase isozymes from horseradish roots. I. Isolation and physical properties, *J. Biol. Chem.* 241, 2166-2172.

Shoemaker, H. E. (1990) On the chemistry of lignin biodegradation, *Rev. Trav. Chim. Pays-Bas* 109, 255-272.

Sitter, A. J., Reczek, C. M. and Terner, J. (1985) Heme-linked ionization of horseradish peroxidase Compound II monitored by the resonance Raman Fe(IV)=O stretching vibration, *J. Biol. Chem.* 260, 7515-7522.

Sivaraja, M., Goodin, D. B., Smith, M. and Hoffman, B. M. (1989) Identification by ENDOR of Trp191 as the free-radical site in cytochrome c peroxidase compound ES, *Science* 245, 738-740.

Smith, A. T., Santama, N., Dacey, S., Edwards, M., Bry, R. C., Thorneley, R. N. R. and Burke, J. F. (1990) Expression of a synthetic gene for horseradish peroxidase C in *Escherichia coli* and folding and activation of the recombinant enzyme with Ca^{2+} and heme, *J. Biol. Chem.* 265, 13335-13343.

Smith, A. T., Sanders, S. A., Greschik, H., Thorneley, R. N., Burke, J. F. and Bray, R. C. (1992a) Probing the mechanism of horseradish peroxidase by site-directed mutagenesis, *Biochem. Soc. Trans.* 20, 340-345.

Smith A. T., Sanders, S. A., Thorneley, R. N. F., Burke, J. F. and Bray, R. R. C. (1992b) Characterisation of a haem active-site mutant of horseradish peroxidase, Phe41-Val, with altered reactivity towards hydrogen peroxide and reducing substrates, *Eur. J. Biochem.* 207, 507-519.

Smulevich, G., Miller, M. A., Kraut, J. and Spiro, T. G. (1991) Conformational change and histidine control of heme chemistry in cytochrome c peroxidase: resonance Raman evidence from Leu-52 and Gly-181 mutants of cytochrome c peroxidase, *Biochemistry* 30, 9546-9558.

Stein, P., Mitchell, M. and Spiro, T. G. (1980) H-bond and deprotonation effects on the resonance Raman iron-imidazole mode in deoxyhemoglobin models: Implications for hemoglobin cooperativity, *J. Am. Chem. Soc.* 102, 7795-7797.

Swanson, B. A. and Ortiz de Montellano, P. R. (1991) Structure and absolute stereochemistry of the 4 N-phenylprotoporphyrin-IX regioisomers isolated from phenylhydrazine-treated myoglobin, *J. Am. Chem. Soc.* 113, 8146-8153.

Sundaramoorthy, M., Kishi, K., Gold, M. H. and Poulos, T. L. (1994) The crystal structure of manganese peroxidase from *Phanerochaete chrysosporium* at 2.06-Å resolution, *J. Biol. Chem.* 269, 32759-32767.

Takeuchi, Y., Kirk, K. L. and Cohen, L. A. (1978) Adjacent lone pair (ALP) effects in heteroaromatic systems. 2. Isotope exchange of ring hydrogens in nitro- and fluoroimidazoles, *J. Org. Chem.* 43, 3570-3578.

Tams, J. W. and Welinder, K. G. (1995) Mild chemical deglycosylation of horseradish peroxidase yields a fully active, homogeneous enzyme, *Anal. Biochem.* 228, 48-55.

Tenhunen, R. (1968) The enzymatic conversion of heme to bilirubin by microsomal heme oxygenase, *Proc. Natl. Acad. Sci. U. S. A.* 61, 748-755.

Teraoka, J. and Kitagawa, T. (1981) Structural implication of the heme-linked ionization of horseradish peroxidase probed by the Fe-histidine stretching Raman line, *J. Biol. Chem.* 256, 3969-3977.

Thanabal, V., de Ropp, J. S. and LaMar, G. N., (1988) A nuclear Overhauser effect study of the heme crevice in the resting state and Compound I of horseradish peroxidase: evidence for cation radical delocalization to the proximal histidine, *J. Am. Chem. Soc.* 110, 3027-3035.

Thomas, E. L., Bozeman, P. M. and Learn, D. B. (1991) *Peroxidases in Chemistry and Biology, Vol I*, (Everse, J., Everse, K. E., and Grisham, M. B. Eds.) Boca Raton, FL., CRC Press, Inc. p 123-142.

Tondreau, G. A. and Sweigert, D. A. (1984) Hydrogen bonding in metalloporphyrin reactions. Reaction of (tetraphenylporphinato)iron(III) chloride and imidazole, *Inorg. Chem.* 23, 1060-1065.

Toney, M. D. and Kirsch, J. F. (1989) Direct Brønsted analysis of the restoration of activity to a mutant enzyme by exogenous amines, *Science* 243, 1485-1488.

Traylor, T. G. and Popovitz-Biro, R. (1988) Hydrogen bonding to the proximal imidazole in heme protein model compounds: Effects upon oxygen binding and peroxidase activity, *J. Am. Chem. Soc.* 110, 239-243.

van Huystee, R. B. (1991) Molecular aspects and biological functions of peanut peroxidase, *Peroxidases in Chemistry and Biology, Vol II*, (Everse, J., Everse, K. E., and Grisham, M. B. Eds.) Boca Raton, FL., CRC Press, Inc. p 155-170.

Vitello, L. B., Erman, J. E., Miller, M. A., Mauro, J. M. and Kraut, J. (1992) Effect of Asp-235-->Asn substitution on the absorption spectrum and hydrogen peroxide reactivity of cytochrome c peroxidase, *Biochemistry* 31, 11524-11535.

Veitch, N. C. (1995) Aromatic donor molecule binding sites of haem peroxidases, *Biochem. Soc. Trans.* 23, 232-240.

Vuc-Pavlovic, S. and Siderer, Y. (1977) Probing axial ligands in ferric haemoproteins: an ESR study of myoglobin and horseradish peroxidase in $H_2{}^{17}O$, *Biochem. Biophys. Res. Commun.* 79, 885-889.

Walker, F. A., Lo, M-. W. and Ree, M. T. (1976) Electronic effects in transition metal porphyrins. The reactions of imidazoles and pyridines with a series of *para*-substituted tetraphenylporphyrin complexes of chloroiron (III), *J. Am. Chem. Soc.* 98, 5552-5560.

Wilks, A. and Ortiz de Montellano, P. R. (1992) Intramolecular translocation of the protein radical formed in the reaction of recombinant sperm whale myoglobin with H_2O_2, *J. Biol. Chem.* 267, 8827-8833.

Wilks, A., Sun, J., Loehr, T. M. and Ortiz de Montellano, P. R. (1995) Heme oxygenase His25ala mutant - Replacement of the proximal histidine iron ligand by exogenous bases restores catalytic activity, *J. Amer. Chem. Soc.* 117, 2925-2926.

Welinder, K. G. and Mazza, G. (1977) Amino-acid sequences of heme-linked, histidine-containing peptides of five peroxidases from horseradish and turnip, *Eur. J. Biochem.* 73, 353-358.

Welinder, K. G. (1985) Plant peroxidases. Their primary, secondary and tertiary relation to cytochrome c peroxidase, *Eur. J. Biochem.* 151, 497-504.

Welinder, K. G. (1992a) Superfamily of plant, fungal and bacterial peroxidases, *Curr. Opin. Struc. Biol.* 2, 388-393.

Welinder, K. G. (1992b) Plant peroxidases: structure-function relationships, *Plant Peroxidases 1980-1990* (Penel, C., Gaspar, T. and Greppin, H., Eds.) Geneva, University of Geneva, p 1-24.

Yamada, H. and Yamazaki, I. (1974) Proton balance in conversions between five oxidation-reduction states of horseradish peroxidase, *Arch. Biochem. Biophys.* 165, 728-738.

Yamazaki, I. and Yokota, K. (1973) Oxidation states of peroxidase, *Mol. Cell. Biochem.* 2, 39-52.

Yonetani, T. and Ray, G. S. (1965) Studies on cytochrome c peroxidase. I. Purification and some properties, *J. Biol. Chem.* 240, 4503-4514.

Yonetani, T. and Schleyer, H. (1966) Studies on cytochrome c peroxidase. VII. Electron paramagnetic resonance absorptions of the enzyme and complex ES in dissolved and crystalline forms. *J. Biol. Chem.* 241, 3240-3243.

Yonetani, T. (1976) In,*The Enzymes Vol. 13* (P. D. Boyer, Ed.) Academic Press, New York, pp. 345-362.

Zeng, J. and Fenna, R. E. (1992) X-ray crystal structure of canine myeloperoxidase at 3 Å resolution, *J. Mol. Biol.* 226, 185-207.